



LUND UNIVERSITY

Dangerous Proteins and Where to Find Them- Structural and functional studies of bacterial and viral proteins interacting with human immune receptors in health and disease

Uzuncayir, Sibel

2022

Document Version:

Publisher's PDF, also known as Version of record

[Link to publication](#)

Citation for published version (APA):

Uzuncayir, S. (2022). *Dangerous Proteins and Where to Find Them- Structural and functional studies of bacterial and viral proteins interacting with human immune receptors in health and disease*. [Doctoral Thesis (compilation), Department of Experimental Medical Science]. Lund University, Faculty of Medicine.

Total number of authors:

1

General rights

Unless other specific re-use rights are stated the following general rights apply:

Copyright and moral rights for the publications made accessible in the public portal are retained by the authors and/or other copyright owners and it is a condition of accessing publications that users recognise and abide by the legal requirements associated with these rights.

- Users may download and print one copy of any publication from the public portal for the purpose of private study or research.
- You may not further distribute the material or use it for any profit-making activity or commercial gain
- You may freely distribute the URL identifying the publication in the public portal

Read more about Creative commons licenses: <https://creativecommons.org/licenses/>

Take down policy

If you believe that this document breaches copyright please contact us providing details, and we will remove access to the work immediately and investigate your claim.

LUND UNIVERSITY

PO Box 117
221 00 Lund
+46 46-222 00 00

Dangerous Proteins and Where to Find Them

Sibel Uzunçayır



LUND
UNIVERSITY

DOCTORAL DISSERTATION

by due permission of the Faculty of Medicine, Lund University, Sweden.

To be defended at I1345, BMC, Lund.

April 28, 2022 at 13:00.

Faculty opponent

Professor E. Yvonne Jones
University of Oxford, England

Organization LUND UNIVERSITY Author: Sibel Uzunçayır	Document name Doctoral Dissertation	
	Date of issue April 28, 2022	
	Sponsoring organization Diabetesfonden, Novo Nordisk Fonden, Vetenskapsrådet	
Title and subtitle: Dangerous proteins and where to find them- Structural and functional studies of bacterial and viral protein interacting with human immune receptors in health and disease		
Abstract <p>Bacteria and viruses are threats to human that evolved strategies to bypass the immune system and can cause massive damage. Understanding these strategies and elucidating pathogen interacting partners within the human immune system will pave the way for discovery of new medicines and increase human well-being.</p> <p>Superantigens (SAGs) are toxins that induce a massive immune response, causing sever diseases. The bacteria <i>Staphylococcus aureus</i> produces staphylococcal enterotoxins (SEs) that are the focus of this thesis. In human, SEs are presented by major histocompatibility complex II (MHCII) to T cell receptors (TCRs), located on T cells, leading to clonal expansion of respective T cells and an overactivation of the immune system. This T cell skewing, that is one of the hallmarks for superantigens, has also been seen for the corona virus. The spike protein that is on the surface of the corona virus, partly structurally resembles a superantigen and its superantigenic character must be analysed to further understand disease development.</p> <p>In this thesis, I will describe and discuss my structural and functional data of superantigens, and the superantigen-like spike protein interacting with human immune receptors and put them into context with the current knowledge of the immune system and try to highlight their implication in disease development in human.</p> <p>My work has resulted in new findings within the field of superantigen biology. Firstly, the SEs, SEA and SEH, were shown to interact with $\gamma\delta$ T cells from human peripheral blood in an indirect mechanism utilizing monocytes and $\alpha\beta$ T cells. Moreover, SEA was shown to bind $\gamma\delta$ TCR (Vγ9δ2) directly in a protein interaction experiment. The biological outcome of this interaction is still unknown. Secondly, the interaction of SEA, SEE and SEH with the human cytokine receptor gp130 is further analysed. It was shown that their binding affinity differs and that they do not bind rodent gp130, suggesting a different mode of action in human. A computational model of SEA complexed with gp130 was generated. Taken together, our data supported by previous experiments indicates that the SEA-gp130 interaction might have implications in emesis. Finally, the spike glycoprotein in SARS-CoV-2 was shown to have superantigenic character, because of its sequential and structural similarity with SEB. Here, we show that specific TRBV of TCRs bind presumably the NTD/RBD domain of the spike glycoprotein.</p>		
Key words: Superantigen, Immune receptors, T cell receptor, gp130, Spike, structural biology		
Classification system and/or index terms (if any)		
Supplementary bibliographical information		Language: English
ISSN and key title 1652-8220		ISBN 978-91-8021-222-9
Recipient's notes	Number of pages 77	Price
	Security classification	

I, the undersigned, being the copyright owner of the abstract of the above-mentioned dissertation, hereby grant to all reference sources permission to publish and disseminate the abstract of the above-mentioned dissertation.

Signature 

Date 2022-03-23

Dangerous Proteins and Where to Find Them

Structural and Functional Studies of Bacterial and Viral
Proteins Interacting with Human Immune Receptors in
Health and Disease

Sibel Uzunçayır



LUND
UNIVERSITY

Cover photo by Sibel Uzunçayır

Copyright pp 1-77 (Sibel Uzunçayır)

Paper 1 © Wiley Periodicals LLC

Paper 2 © Manuscript

Paper 3 © John Wiley & Sons Ltd

Paper 4 © Manuscript

Lund University
Faculty of Medicine
Department of Experimental Medical Science
Medical Structural Biology

Doctoral Dissertation Series 2022:61

ISBN 978-91-8021-222-9

ISSN 1652-8220

Printed in Sweden by Media-Tryck, Lund University
Lund 2022



Media-Tryck is a Nordic Swan Ecolabel
certified provider of printed material.
Read more about our environmental
work at www.mediatryck.lu.se

MADE IN SWEDEN 

*” One ought to hold on to one’s heart; for if one lets it go,
one soon loses control of the head too.”*

(Friedrich Nietzsche)

Table of Contents

Original articles	8
Abbreviations.....	9
Popular science summary	11
Abstract	13
Introduction	14
The immune system.....	14
The innate immune system.....	15
The adaptive immune system	16
The 'inbetweeners' of the immune system	19
Immune receptors	21
Superantigens	23
Bacterial superantigens.....	24
The three-dimensional structure of superantigens.....	25
Interaction of superantigens with immune receptors	26
Antigen binding versus superantigen binding	26
Superantigen binding to MHCII	26
Superantigens are a special class of T cell activators	28
Superantigen binding to co-stimulatory receptors.....	29
Viral protein with superantigenic character.....	29
Coronavirus disease.....	29
Structure and function of spike glycoprotein.....	30
Novel insights of superantigens interacting with immune receptors	32
Superantigens role in human disease.....	32
Aims	33
Interplay between superantigens and $\gamma\delta$ T cell receptor	34
Indirect mechanism of $\gamma\delta$ T cell activation by superantigens.....	34
Direct binding of chimeric $\gamma\delta$ TCR and SEA.....	37
Interplay between superantigens and cytokine receptor gp130.....	40
Superantigens bind to gp130	40
Structural analysis of SEA-gp130 complex formation.....	42
Superantigens in emesis studies	45

Superantigenic character of spike protein in SARS-CoV-2	46
Spike protein bind to $\alpha\beta$ TCR.....	48
Methodology.....	52
Expression systems of recombinant proteins.....	52
Biochemical and biophysical methods	54
Electron microscopy techniques	55
Concluding remarks and future perspectives	60
Summary	63
References	66
Acknowledgements	76
Paper I-IV.....	78

Original articles

Paper I

Forsberg M. M., Arasa C., Van Zwol W., Uzunçayır S., Schönbichler A., Regenthal P., Schelin J., Lindkvist-Petersson K.; Björkander S. & Sverremark Ekström E.

Activation of human $\gamma\delta$ T cells and NK cells by Staphylococcal enterotoxin requires both monocytes and conventional T cells. *Journal of Leukocyte Biology*

Paper II

Uzunçayır S., Petruk G., Lindkvist-Petersson K.

Expression and purification of human $\gamma\delta$ T cell receptor for activity studies. *Manuscript*

Paper III

Uzunçayır S., Vera-Rodriguez A., Regenthal P., Åbacka H., Emanuelsson C., Bahl C.D., Lindkvist-Petersson K.

Analyses of the complex formation of staphylococcal enterotoxin A and the human gp130 cytokine receptor. *FEBS Letter*

Paper IV

Uzunçayır S., Venskutonyté R., Happonen L., Martinez-Carranza M., Bowman J., Bahl C.D., Lindkvist-Petersson K.

Structural basis for T cell receptor recognition by SARS-CoV-2 glycoprotein. *Manuscript*

Abbreviations

Ag	Antigen
APC	Antigen presenting cell
C	Constant
CD	Cluster of differentiation
CDR	Complementary determining region
CTF	Contrast transfer function
CTL	Cytotoxic T lymphocyte
CTZ	Chemoreceptor trigger zone
Covid	Corona virus disease
D	Domain
EM	Electron microscopy
FBD	Food borne disease
FNIII	Fibronectin type III
FSC	Fourier shell correlation
Gp	Glycoprotein
hACE2	Human angiotensin converting enzyme 2
H/D X	Hydrogen deuterium exchange
HSC	Hematopoietic stem cell
IB	Inclusion body
IFN	Interferon
IL	Interleukin
IL-6R	Interleukin-6 receptor
ITAM	Immunoreceptor tyrosine-based activation motifs
JAK	Janus activated kinase
LIF	Leukemia inhibitory factor

MAIT	Mucosal associated invariant T
NK	Natural killer
NTD	N-terminal domain
PBMC	Peripheral blood mononuclear cell
PDB	Protein data bank
RBD	Receptor binding domain
SAg	Superantigen
SARS	Sever acute respiratory syndrome
SE	Staphylococcal enterotoxin
SFP	Staphylococcal food poisoning
SPR	Surface plasmon resonance
T _c	T cytotoxic
TCR	T cell receptor
T _H	T helper
TNF	Tumour necrosis factor
TRAC TRAV	T cell receptor α constant T cell receptor α variable
TRBC TRBV	T cell receptor β constant T cell receptor β variable
TRGC TRGV	T cell receptor γ constant T cell receptor γ variable
TRDC TRDV	T cell receptor δ constant T cell receptor δ variable
TSST	Toxic shock syndrome toxin
V	Variable
wt	Wild type
XL-MS	Cross-linking mass spectrometry

Popular science summary

Toxins, superantigens, viral and bacterial infection, toxic shock syndrome, food poisoning and corona – all terms leave a ring of danger in people. In this thesis, I will describe my structural and functional data of superantigens, and the spike protein interacting with human immune receptors and put them into context with the current knowledge of the immune system and try to highlight their implication in disease development in human.

Humans have evolved an immune system to protect from threats of the outside world. The immune system is highly adaptable and defends the body against pathogens such as bacteria, viruses, fungi, and parasites. This wide range of potential pathogens requires a complex defence mechanism, meaning a diverse recognition and destruction system. The most important ability of the immune system is to sense pathogenic invaders and distinguish them from the organism's own cells, and eventually destroy them. Many organs, cells, molecules, and pathways are involved and interconnected in the immune system.

However, some bacteria and viruses evolved strategies to bypass the immune system and can cause massive damage in humans. Elucidating their strategy and interacting partner will embed the way for medicine and increase human well-being.

In the field of structural biology, the aim is to visualize the structure of different biological molecules; like proteins to get a deeper insight in their function. After obtaining the structure of proteins and their interacting partners (other proteins, ligands, or chemicals), we get a deeper knowledge of the parts involved in the interaction and ultimately understand more about their signalling in human.

There are three main methods in structural biology to obtain the structure of protein namely X-ray crystallography, cryo-electron microscopy, and nuclear magnetic resonance. Therefore, the proteins are recombinantly produced in the laboratory. Plasmid DNA including the sequence for the protein of interest is transformed into competent *E. coli* cells. These cells are grown in cultures to produce our protein of interest in larger amounts. The protein is then purified from the cells with different biochemical methods. To get a protein complex, the two pure proteins are mixed and then structurally characterized and analysed. Also, other methods are used to describe the protein-protein interaction for example to describe the binding strength

and the interacting parts of the proteins. With this information a computational model of the interacting proteins can be created.

This thesis is about superantigens (toxins) secreted by the bacteria *S. aureus* and their interaction with human proteins and their impact in the immune system and disease progression.

In my main project we are aiming to obtain information of a protein-complex; consisting of a toxin bound to a human receptor, namely glycoprotein 130 (gp130). Toxins are toxic proteins secreted by bacteria and viruses. These can bind to proteins in human and lead for example to food poisoning and toxic shock syndrome (TSS). The biological outcome of this new interaction of the toxin SEA and the human protein gp130 is unknown and needs to be investigated. For this reason, a structural model and information of the interaction of the two proteins are indispensable. Our results show that the toxin SEA might bind to gp130 on mast cells in the gut and might be responsible for inducing vomiting after consumption (Fig. 1).

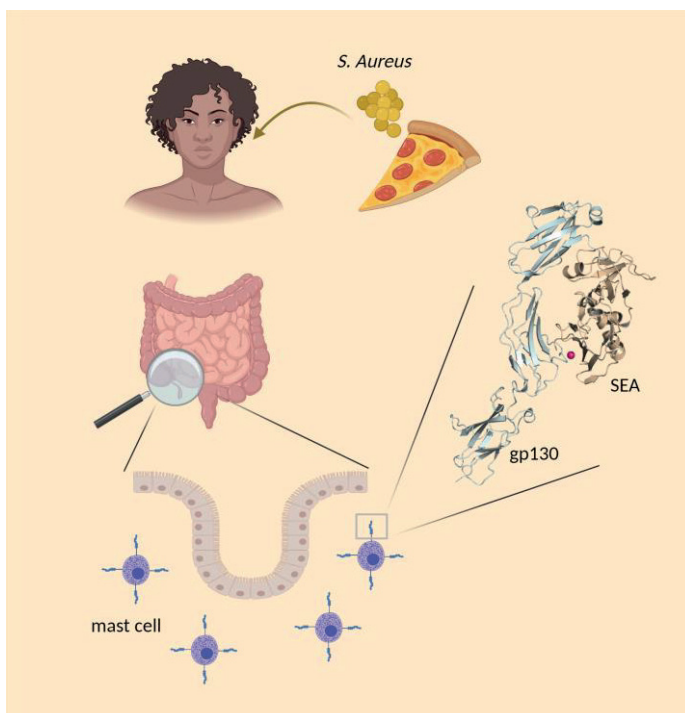


Figure 1: Paper III graphical summary.

Abstract

Bacteria and viruses are threats to human that evolved strategies to bypass the immune system and can cause massive damage. Understanding these strategies and elucidating pathogen interacting partners within the human immune system will pave the way for discovery of new medicines and increase human well-being.

Superantigens (SAGs) are toxins that induce a massive immune response, causing severe diseases. The bacteria *Staphylococcus aureus* produces staphylococcal enterotoxins (SEs) that are the focus of this thesis. In human, SEs are presented by major histocompatibility complex II (MHCII) to T cell receptors (TCRs), located on T cells, leading to clonal expansion of respective T cells and an overactivation of the immune system. This T cell skewing, that is one of the hallmarks for superantigens, has also been seen for the corona virus. The spike protein that is on the surface of the corona virus, partly structurally resembles a superantigen and its superantigenic character must be analysed to further understand disease development.

In this thesis, I will describe and discuss my structural and functional data of superantigens, and the superantigen-like spike protein interacting with human immune receptors and put them into context with the current knowledge of the immune system and try to highlight their implication in disease development in human.

My work has resulted in new findings within the field of superantigen biology. Firstly, the SEs, SEA and SEH, were shown to interact with $\gamma\delta$ T cells from human peripheral blood in an indirect mechanism utilizing monocytes and $\alpha\beta$ T cells. Moreover, SEA was shown to bind $\gamma\delta$ TCR (V γ 9 δ 2) directly in a protein interaction experiment. The biological outcome of this interaction is still unknown. Secondly, the interaction of SEA, SEE and SEH with the human cytokine receptor gp130 is further analysed. It was shown that their binding affinity differs and that they do not bind rodent gp130, suggesting a different mode of action in human. A computational model of SEA complexed with gp130 was generated. Taken together, our data supported by previous experiments indicates that the SEA-gp130 interaction might have implications in emesis. Finally, the spike glycoprotein in SARS-CoV-2 was shown to have superantigenic character, because of its sequential and structural similarity with SEB. Here, we show that specific TRBV of TCRs bind presumably the NTD/RBD domain of the spike glycoprotein.

Introduction

The immune system

The immune system is a complex interactive network of tissues, organs, cells, and soluble components. For a successful immune response, the interaction of many diverse cell types that are dispersed throughout the body is needed. All mature blood cells arise from the hematopoietic stem cell (HSC). The process in which HSC differentiate into mature blood cells is called haematopoiesis (Fig. 2). HSC develop to lymphoid or myeloid progenitors. The immature precursors immune cells develop in the primary lymphoid organs - the bone marrow and the thymus. Almost all immune cells differentiate in the bone marrow, except for T cells that mature in the thymus. Immune cells then travel from primary lymphoid organs to secondary lymphoid organs, including the spleen, lymph nodes, sites in the gut and other mucosal tissue to browse for antigen. The organs are connected via the blood and lymphatic circulation system.

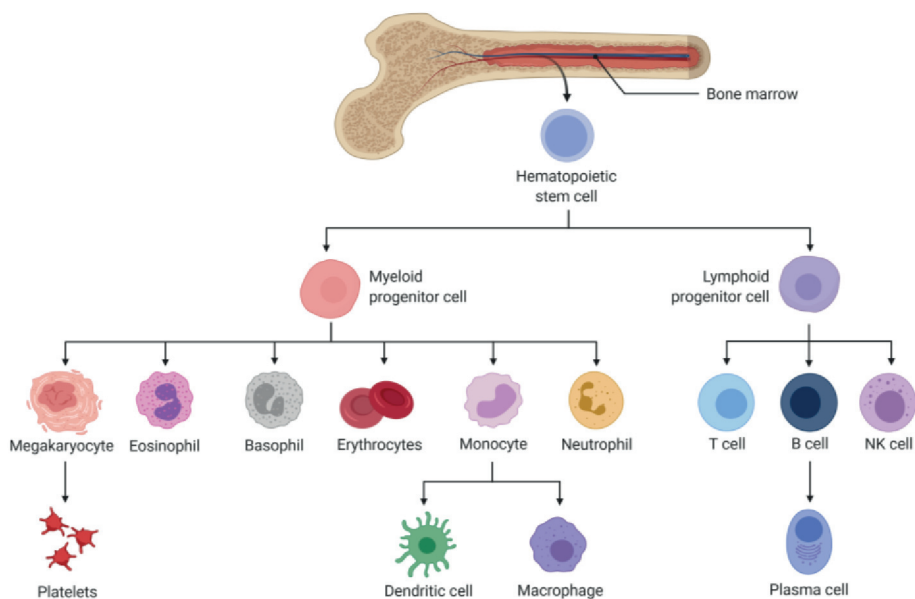


Figure 2: Hematopoiesis.

Mature antigen-specific lymphocytes then differentiate into effector and memory cells. The task of the immune cells is to maintain the protection of the body, by surveillance, detection, and destruction of foreign- and self-threats. The immune response is composed of two interconnected systems: the innate and the adaptive immune system (1).

The innate immune system

The innate immune system is the first line of defence, that is built out of physical and chemical barriers to infection and is comprised of receptors that recognize common antigen structures of many pathogens. Antigens (Ag) are molecules like proteins or peptides that bind to a specific immune receptor and can result in an immune response. There are self (from within the body) and non-self (from external environment) Ags. Here, we mainly focus on foreign Ags introduced from pathogens. The main task of the innate immune system is to prevent infection and to label and eliminate invaders fast. It is evolutionary primitive and inherited. The innate system is not highly specific and is unable to recognize small differences in foreign antigens. It uses different pattern recognition receptors (PRRs) to find PAMPS (pathogen-associated molecular patterns) and characterize the group of the invading pathogens (2). Phagocytic cells can fight the invader locally by secretion of intracellular messenger molecules like cytokines, chemokines, and anti-microbial compounds that induce a biological activity. If the innate immune system is not able to eliminate the pathogen, it switches on the adaptive immune system and transfers information about the invader (3,4).

Antigen presenting cells

Monocytes, macrophages, dendritic cells of the myeloid lineage and the natural killer (NK) cells of the lymphoid lineage form the group of antigens presenting cells (APCs). APCs belong to the innate immune system and are responsible for pathogen clearance and the activation of the adaptive immune system and initiation of the immune response by antigen presentation. All nucleated cells and APCs have surface bound proteins called major histocompatibility (MHC) class I and II, respectively.

MHC proteins are divided into three classes based on their mode of action and localization. MHC class I and II present intracellular and extracellular antigens, respectively. On the contrary, MHCIII is a group of immune proteins with different tasks that comprises cytokines, complement proteins and heat-shock proteins.

MHC class I is expressed on all nucleated cells throughout the body. The expression of MHCI with a self-peptide typically means that the cells is healthy. Whereas the absence of MHCI occurs in infected cells and tumour cells and leads to destruction by NK cells. NK cells function as cell killers. These cells act in two ways: firstly, by attacking cells that lack MHCI and secondly, by binding antibodies, that are specific for viral proteins on the cell surface of infected cells. Once these criteria are identified the NK cell releases granules and induces cell death of its target (1).

The innate and adaptive immune system are tightly intertwined and work together to prevent disease.

The adaptive immune system

The adaptive immune system can distinguish between diverse pathogens. It is composed of highly specialized cells that eliminate pathogens or stop their growth. The main actors of the adaptive immune system are B and T lymphocytes.

Lymphocytes

Lymphocytes are the main cell type active in the adaptive immune response. They represent 20-40 % of circulating white blood cells (leukocytes). They are subdivided into three populations: B lymphocytes (B cells), T lymphocytes (T cells) and innate lymphoid cells (ILCs) that include the natural killer (NK) cells (Fig. 2).

T and B lymphocytes appear identical under the microscope and are therefore distinguished by their surface proteins referred to as CD (cluster of differentiation) proteins. Additionally, they express antigen specific receptors, B cell receptor (BCR) and T cell receptor (TCR) respectively on their surface. The diversity of the B cell and T cell receptors is immense in the body, but on each single cell all antigen-specific receptors are identical in structure and specificity (1).

When B cells and T cells divide, all its progeny will have this identical BCR or TCR. Newly formed B cells and T cells are referred to as naïve. After encountering an antigen, these cells undergo clonal selection, meaning the cells that recognize that specific antigen will proliferate and differentiate into effector cells and memory cells. Effector cells fight pathogens and memory cells persist in the host to respond to re-entering pathogen with the same antigen faster (1).

B lymphocytes

B cells mature in the bone marrow. The BCR is a membrane bound version of an antibody. Upon activation by an antigen, B cells can operate as an antigen presenting cell (APCs). Upon antigen presentation T cells provide B cells then with cytokines that induce differentiation into either memory cells or plasma cells, that can produce antibodies (5).

T lymphocytes

T cells mature in the thymus. They are a diverse group that can be divided depending on the expressed TCR variable chains ($\alpha\beta$ and $\gamma\delta$), the co-receptor and the effector function. Most T cells belong to the conventional $\alpha\beta$ T cells, divided into T helper (T_H) and T cytotoxic (T_C) cells with surface membrane glycoprotein CD4 or CD8, respectively. Unlike B cells, the conventional T cells only recognize antigens bound to the cell membrane protein MHC (6,7).

Naïve $CD4^+$ T_H cells recognize MHC class II peptide complex and become activated, proliferate, and differentiate into different effector T_H cells. These regulate the response to pathogens, by secreting cytokines that activate B cells, T_C cells and macrophages to form an immune defence (8). Naïve $CD8^+$ T_C cells recognize foreign peptides in the cytosol bound to MHC class I, become activated, proliferate, and differentiate into the effector cell cytotoxic T lymphocyte (CTL). CTLs observe the cells in the body and eliminate those displaying non-self-antigen bound to MHCI, like tumour cells and virus infected cells (1,9).

T cell activation

Three signals are required for activation of naïve T cells. Apart from MHC-peptide-TCR complex formation (signal 1) that is stabilized by the co-receptors CD4/CD8, a second co-stimulatory signal through CD28-CD80 (signal 2) is indispensable (10). Signal 1 and 2 initiate a signal cascade that leads to activation of cytokines and transcription factors (signal 3) that then result in T cell proliferation and differentiation into effector cell types (11) (Fig. 3).

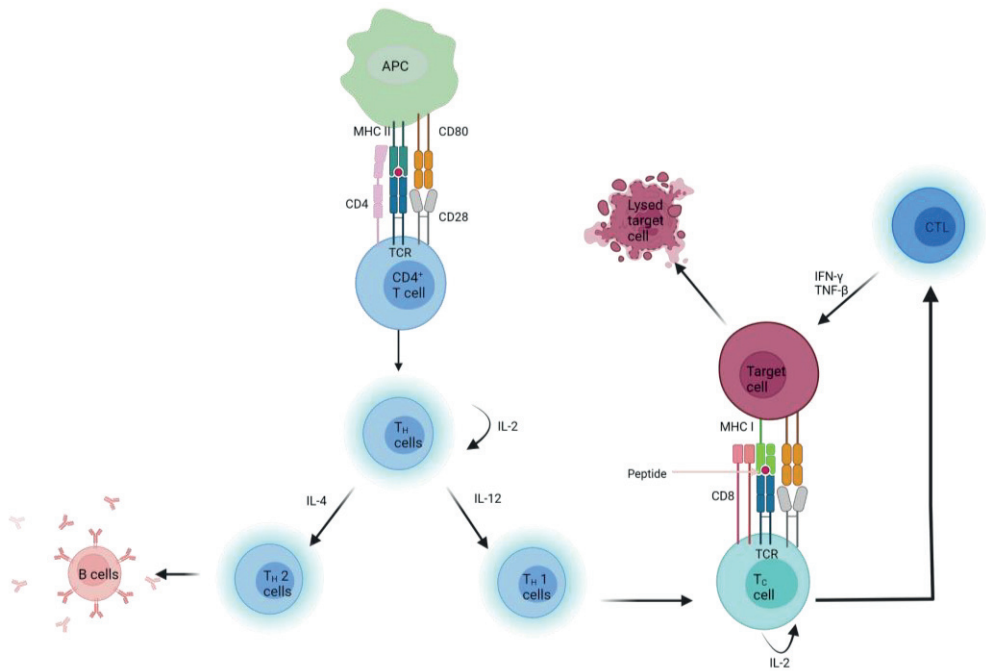


Figure 3: T cell antigen recognition and activation.

A summary of possible adaptive immune cell responses, that are central for this thesis, for different pathogen types like bacteria, viruses and superantigens is shown below (Fig. 4).

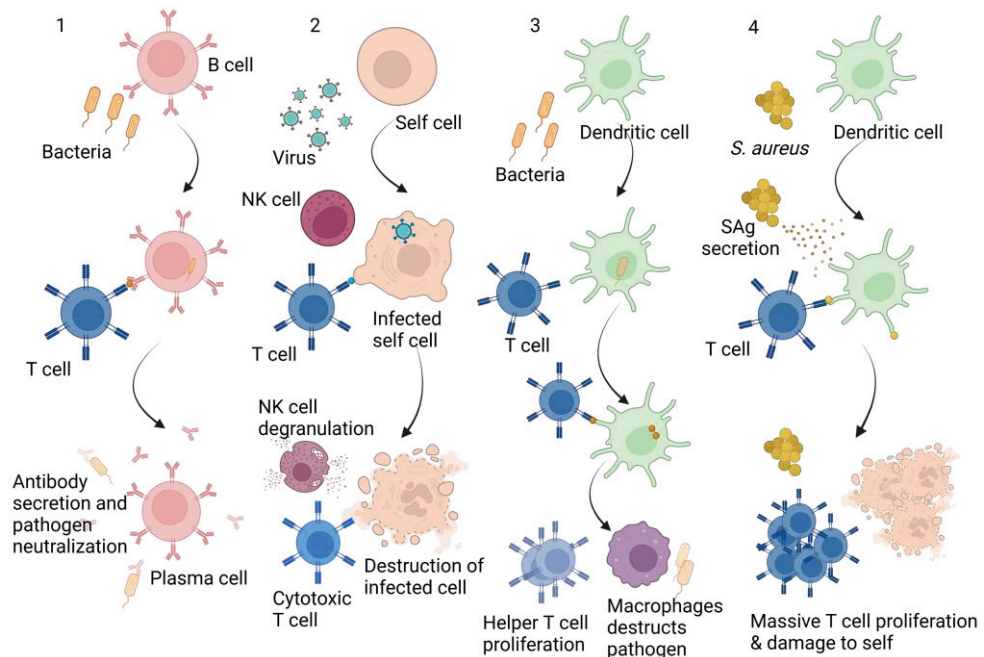


Figure 4: Variety of adaptive immune responses. 1) B cell presents extracellular antigen to T cell. B cell activation and differentiation into plasma cell, followed by secretion of antibodies that neutralize pathogen. 2) Virus infection of self cell. Virus peptide presentation to T cell, that then differentiates into cytotoxic T cell and destroys infected self cell. Furthermore, NK cell degranulates and induces cell death. 3) Pathogen recognition of extracellular bacterium by dendritic cell, followed by T cell recognition, differentiation and proliferation into T helper cell that subsequently secrete cytokines and recruit macrophages for pathogen destruction. 4) *S. aureus* secretes SAGs that bind to dendritic cells and cross-link T cells in antigen independent manner. This leads to overactivation of T cell and a cytokine storm that damages self cells.

The 'inbetweeners' of the immune system

Several cells show characteristics of the innate and adaptive immune and are referred to as innate-like cells (12,13). Unconventional T cells belong to the group of innate-like cells, under them $\gamma\delta$ T cells, mucosal associated invariant T (MAIT) cells and NKT (natural killer T) cells. These reside in peripheral and mucosal tissues and respond to non-peptide antigens such as metabolic derivatives and lipids, that don't have to be necessarily presented by MHC (14). Non-classical peptides can also be presented by alternative MHC-like receptors to $\gamma\delta$ T cells and MAIT cells, respectively (15).

Role of $\gamma\delta$ T cells in the immune system

The $\gamma\delta$ T cells were identified as late as 1984 as a separate T lymphocyte lineage and due to their low representation, they remain the least studied ones. Activation of $\gamma\delta$ T cells results in cytokine production (IFN- γ , TNF- α , IL-17), lysis of infected cells, inflammation, epithelial growth, antigen presentation, B cell help and antibody production (Fig. 5) (16,17).

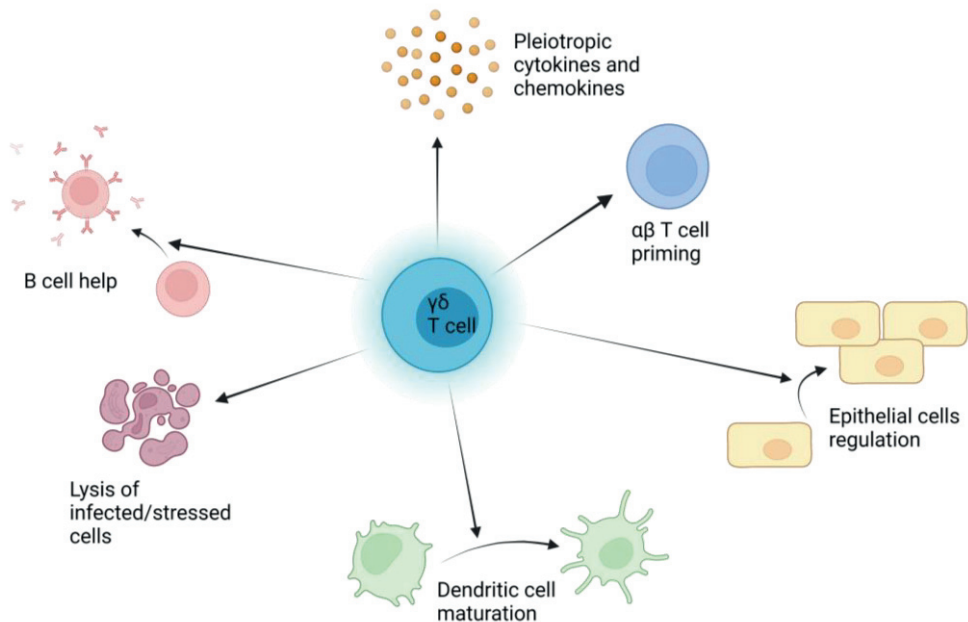


Figure 5: $\gamma\delta$ T cell contribution to immune response (17).

Mast cells

Furthermore, mast cells are described to have a role in the innate as well as in adaptive immunity. Mast cells are derived from monocytes and are found predominantly at the interface between tissue and external environment for example on mucosal surfaces of the lung and the gut, in the skin and around blood vessels. They have an important role including host defence to infection and in allergic reactions, when activated they release a range of mediators like histamines, cytokines, and lipid mediators (18).

Immune receptors

Cells of the immune system have the challenge to interact and respond to a vast number of infectious organisms and toxins over the whole body. These signals are transmitted via a vast number of immune and cytokine receptors into an appropriate cellular response. Here, I will introduce the T cell receptor ($\alpha\beta$ and $\gamma\delta$ TCR) and the cytokine receptor gp130 in more detail, that are known to bind superantigen.

T cell receptors

T cell receptors are antigen specific and are only found on the surface of T lymphocytes. There are two types of TCRs, and both are heterodimers. The majority of TCRs is composed of one α and one β -chain and the other type of TCR has one γ and one δ chain (Fig. 6). Structurally all the TCR chains have two immunoglobulin domains, one variable (V) at the N-term that functions as antigen binding site and one constant domain (C). The distinct chains are held together by a disulphide bridge close to the plasma membrane. The TCR V domains have three complementary determining regions (CDRs) that form the contact to the antigenic complex. Generally, CDR1 and 2 interact with MHC and CDR3 binds the antigen (19,20). The TCR is noncovalently associated with a molecular signal transduction complex CD3 that is in charge to transmit the signal into the cell. After activation, the tyrosine residues of the immune receptor tyrosine activation motif (ITAMs) get phosphorylated and ITAM serves as docking site for adapter proteins (21).

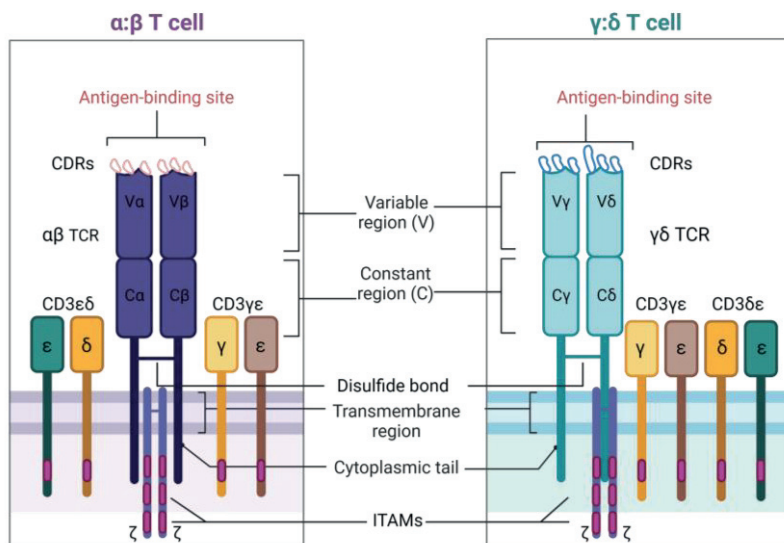


Figure 6: Structural features of both types of T cell receptors (21).

The conventional $\alpha\beta$ T cells are extremely diverse in their antigen specificity. Whereas, the unconventional $\gamma\delta$ T cells have oligoclonal subpopulations in tissue specific locations sharing the same TCR (22). Human peripheral blood for instance has largely variable chain $\gamma 9$ and $\delta 2$ ($V\gamma 9\delta 2$) TCR.

The cytokine receptor gp130

The immune system needs to coordinate immune responses throughout the whole body. The communication between the various immune cells is facilitated by proteins referred to as cytokines. Cytokines regulate inflammation, immunity, and haematopoiesis. Cytokines bind to their receptor on a target cell and can induce a wide variety of biological responses, for example changes in gene expression of adhesion proteins or receptors thus coordinating cell movement, increase or decrease the activity of an enzyme, change its transcription and in turn activate proliferation and differentiation or modulate effector functions. Moreover, cytokines are responsible for cell survival or death. Cytokines are subdivided into six major cytokine families and are named according to their function: interleukin-1, interleukin-17, hematopoietin (class I), interferon (class II), tumour necrosis factor, and chemokine family (1,23).

There are six major families of cytokine receptors. The cellular origins and target cells of this class are extremely diverse, for example they are involved in B and T cell proliferation (IL-2), B cell differentiation and antibody secretion (IL-6) (1).

In this thesis, one relevant class I cytokine receptor is gp130. The common feature of class I cytokine receptors is the four-helix bundle motif important in cytokine binding (24,25). The class I cytokine receptors are comprised of two chains, that are both needed for successful signalling. One α chain that mediates the binding of the cytokine and one of the alternative chains - γ_c , β_c or gp130 that mediate signalling (26). Gp130 is expressed throughout the body. RNA expression level is notably high in the brain, liver, female tissues, heart muscle tissues and in the bone marrow and lymphoid tissues. Gp130 is involved in the regulation of a variety of tissue systems like haematopoiesis, bone metabolism, nervous system, heart, muscle, and adipose tissue. Gp130 recognizes IL-6 (25), IL-11, LIF, OSM, CT-1, CNTF and IL-27 (27,28). Structurally, it consists of one Ig-like domain (D1) and 5 fibronectin like type domains (D2-D6) with a bend between D4 and D5 (Fig. 7). The cytokine binding region is in D2-D3 (29).

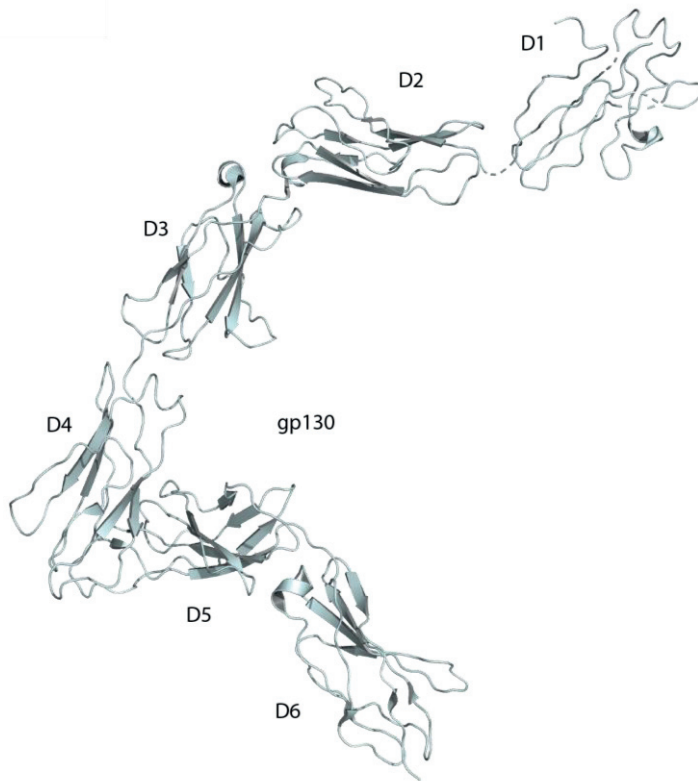


Figure 7: gp130 D1-D6, PDB: 3L5H in cartoon presentation.

Gp130 activates the Jak/STAT signal pathway. Cytokine binding induces receptor dimerization, which activates the associated Jaks resulting in phosphorylation of themselves and the receptor (30–32). The phosphorylated sites and Jaks serve now as docking sites SH2-containing Stats (like Stat3) and other adaptor proteins can bind. This then can activate MAP kinase, PI3K/ Akt and other signal pathways. Phosphorylated STATs dimerize and translocate in the nucleus and regulate gene transcription (31,32).

Superantigens

Superantigens are toxic proteins generated by viruses or bacteria. Endogenous and exogenous superantigens have been identified (33). Endogenous superantigens are cell-membrane proteins generated by viruses that have integrated into mammalian genomes. Exogenous superantigens, are soluble proteins secreted by bacteria and are the focus of this thesis. I work with superantigens secreted by *Staphylococcus*

aureus (*S. aureus*), that generally can be divided into five evolutionary groups (I-V) and have their own distinct way of TCR and MHCII binding (34). Generally, superantigens crosslink TCRs and MHCII in an antigen independent manner and over activate the immune system (35,36). Here, we focus on the classical superantigens secreted by *S. aureus*., that belong to class I and III. These include toxic shock syndrome 1 (TSST-1) in class I and staphylococcal enterotoxins (SEs) A/E/H in class III.

Bacterial infection

Bacteria can enter the body through various routes for example gastrointestinal, respiratory, and urogenital routes or through breaks in skin or mucosal tissue. There are different host defences depending on number of bacteria entering and virulence. If both numbers are low, localized tissue phagocytes of the innate immune system eliminate the intruding bacteria. For pathogens with greater virulence or intracellular bacteria the adaptive immune response is initiated for an antigenic specific response. Then APCs bound to antigen travel from the site of infection to the lymph nodes where B and T cells are activated. These differentiate into effector cells that ideally clear the infection and form memory cells that protect us from reoccurring infections. Extracellular bacteria induce production of antibodies either in neighbouring lymph nodes or in the submucosa of the respiratory and gastrointestinal tracts. Extracellular bacteria trigger an inflammation, which is caused by the presence of immunogenic toxins. These can be either endotoxins that are integral components of the bacterial cell wall or exotoxins that are secreted proteins (1) (Fig. 3/4).

Bacterial superantigens

Staphylococcus aureus (Fig. 8) is a gram-positive bacterial pathogen that produces toxins (37). In 1989, Marrack and Kappler named them superantigens (SAg) due to their ability to activate larger numbers of T cells than regular antigens. *S. aureus* colonizes the skin in 30-50 % of humans (38). Normally, it does not threaten the host but for largely unknown reasons it can become pathogenic (39,40) by secreting superantigen proteins, which can cause diseases like toxic shock syndrome (TSS) (34,41) and food poisoning (42,43). The superantigen family consists of over 40 different toxins. The staphylococcal superantigens include staphylococcal enterotoxins (SE) A-E and G-X (44–47). These toxins share the overall same three-dimensional fold but have slightly varying binding sites on TCR and MHCII and lead to different functions.

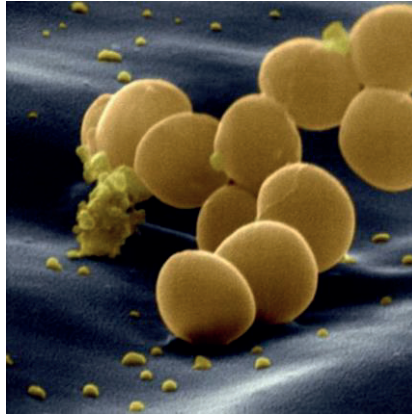


Figure 8: *Staphylococcus aureus*.

The three-dimensional structure of superantigens

Staphylococcal enterotoxins share a similar three-dimensional structure consisting of two domains and have a molecular weight of 19-30 kDa (39). The N-terminal domain forms an oligosaccharide-binding (OB) part, comprised of a β -sandwich (β_1 - β_5), and a short α -helix (α_3). The C-terminal domain is forming a β -grasp motif (β_6 , β_7 , β_9 , β_{10} and β_{12}) packed against three α -helices (α_2 , α_4 and α_5). The first superantigen structure (SEB) was determined in 1992 (48). Since then, many more have been characterized including SEA (49) (Fig. 9), SEE (50) and SEH (51).

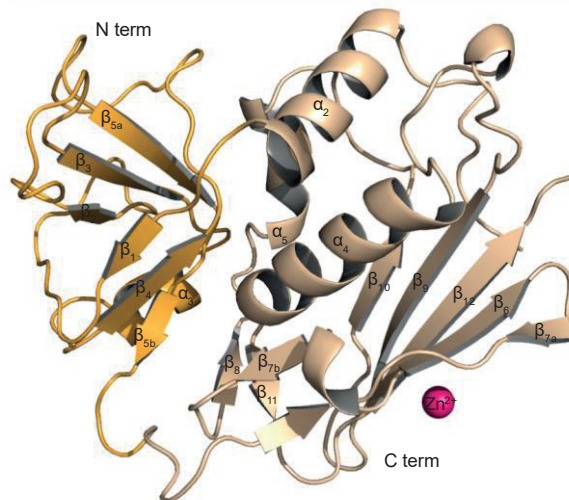


Figure 9: Crystal structure of SEA, PDB: 1SXT (52). N-term (orange) and C-term (wheat) and Zn (pink).

Interaction of superantigens with immune receptors

Cells of the immune system have the challenge to interact and respond to a vast number of infectious organisms and toxins over the whole body. These signals are transmitted through a variety of immune and cytokine receptors into an appropriate cellular response. The conventional and more studied superantigen immune receptors are MHCII (53–59) and the $\alpha\beta$ TCR (50,60–62), apart from that several co-receptors CD28 (63–65) and CD40 (66), LAMA2 (67) and gp130 (68) have been identified to interact with superantigen.

Antigen binding versus superantigen binding

Generally, superantigens bind simultaneously to the α -chain or β -chain of MHCII and specific V β regions of TCRs. V β regions are encoded by 65 different genes in human. Superantigens display a selectivity for one of these V β version, which is expressed by up to 5 % of the T cells. Here, SEH is the only known exception so far, because it binds TCR V α region (59). Superantigens crosslink TCRs and MHCII outside the antigen binding groove and mimic a strong TCR-MHC interaction. Therefore, superantigens bypass the TCR antigen specificity and are able to massively activate T cells and lead to a cytokine storm that can be toxic for the host (35,36,69–71).

Superantigen binding to MHCII

Superantigens only bind to MHCII and not to MHCI (53). Structurally MHCII receptors, HLA-DM, DO, DP, DQ and DR, are heterodimers and have one α - and one β -chain, each with one domain consisting of an α -helix and antiparallel β -sheet (α_1 and β_1) and one immunoglobulin domain (α_2 and β_2). A large β -sheet is formed with the two α -helices on top. The antigenic peptide (at least 13 residues) is bound on top of the β -sheet between the α -helices (Fig. 10) (72).

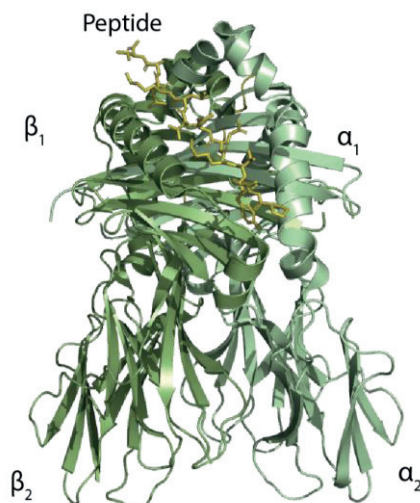


Figure 10: Crystal structure MHCII, PDB: 1DLH

Group III superantigens (including SEA and SEE) have two binding sites on MHCII, one low affinity N-terminal binding site on the α -chain and one high-affinity (nanomolar range) binding site on the β -chain of the MHCII (54,55). From the SAgS discussed here, SEH is an exception and does not bind on the α -chain of MHCII. On SEA, the amino acid residues 44-53 and in particular Phe47 and Leu48 are important for binding to the α -chain at MHCII (59). Superantigens bind to the MHCII β -chain in a Zn-dependent manner via their C-terminal domain, which involves H187, H225 and D227 in SEA and SEE, while in the SEH the zinc ion is coordinated with only two residues H206 and D208. The zinc binding site is completed by H81 on MHCII β -chain (54,58,73).

SEA and SEE bind at two sites of the MHCII, this can lead to cross-linking of two MHCII molecules with a superantigen bound in between (Fig. 11), which is needed for full activity of the superantigen (74,75). In the ternary complex superantigen sites have different functions; in which the N-terminal low affinity binding site is stabilizing TCR binding, and the C-terminal high affinity binding site is important for MHC binding to activate the APC (54).

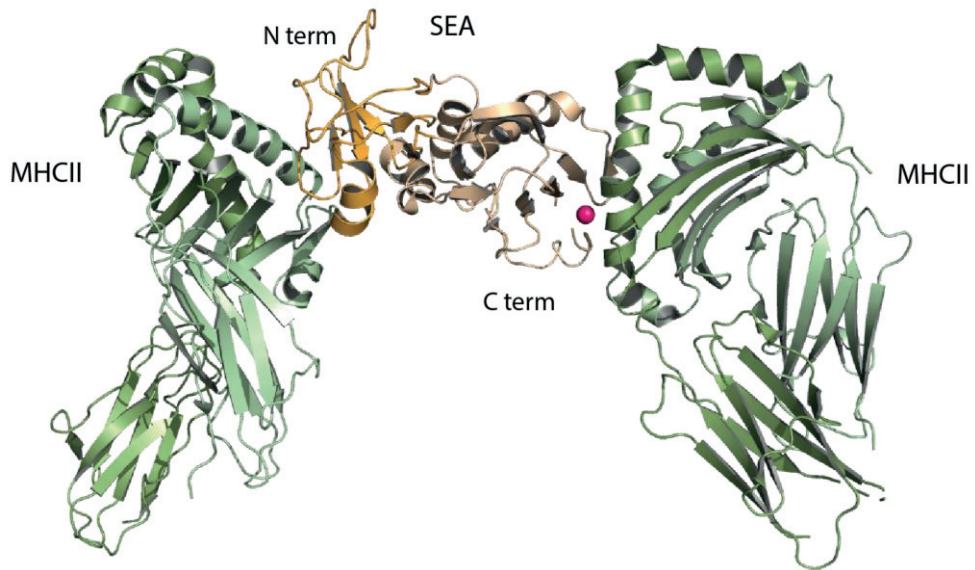


Figure 11: Model of SEA binding two MHCII molecules (green) via its N-term (bright orange) and C-term (wheat). Zn in pink. The model is created in PyMOL with PDB: 1LO5 and 1HXY.

Superantigens are a special class of T cell activators

Superantigen binding to $\alpha\beta$ T cell receptor

The conventional mechanism of $\alpha\beta$ T cell activation is through an antigen that is presented to $\alpha\beta$ TCR by MHC I/ MHCII. Exogenous, classical superantigens (SEA, SEB, SEE etc.) bind in a non-antigen specific way, by cross-linking MHCII and the TCR (Fig. 12) (35,36). Superantigens are not able to bind to MHC I (53).

SAGs generally bind to the β -chain of TCR (50,60–62), except for SEH that mainly binds to the α -chain (59,76,77). They bypass the need for antigen specificity and cause a massive T cell activation and T_H -cell cytokine (IL-2, TNF and IFN- γ) release leading to toxicity.

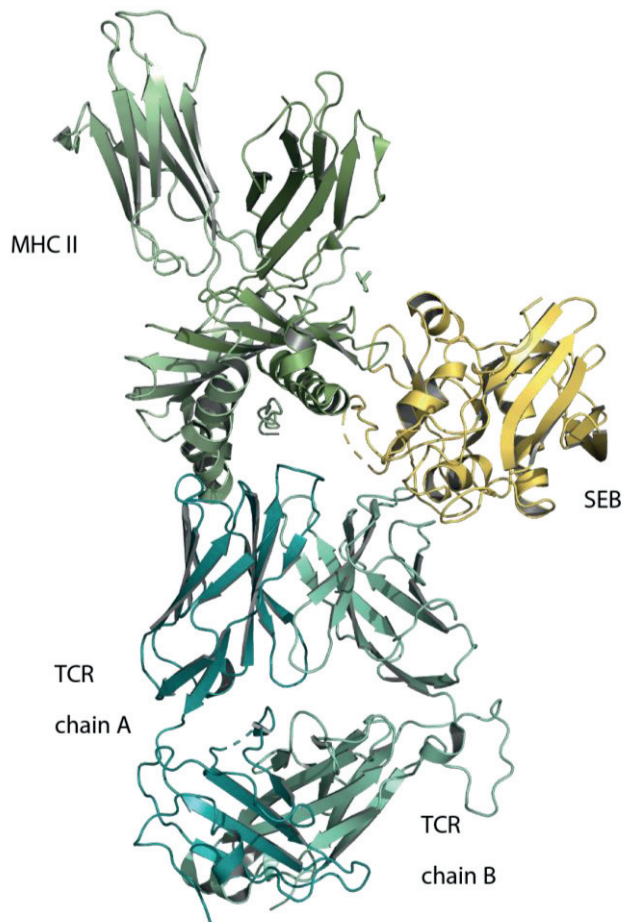


Figure 12: Superantigen binding mode of SEB (yellow) to MHC II (green) and TCR chain α (teal) and chain β (cyan) (adapted (62)).

Superantigen binding to co-stimulatory receptors

For full T cell activation co-stimulatory receptors like CD28 are required (10). This is also true for superantigen mediated T cell activation, since CD28 deficient mice are resistant to toxicity by TSST-1 and SEB (63,64). Early on it was thought that this might be because of the normal requirement of CD28-CD80 interaction for activation, but later direct interaction of CD28 and SEB was shown. The putative binding site on SEB lies in the C-terminal β_7 sheet and the N-terminal α_4 helix, which are thought to interact with CD28 (65).

Furthermore, it was shown that the superantigens TSST-1, SEB and SEC bind CD40. CD40 is a costimulatory protein found on APCs and is required for their activation. It is hypothesized that the SAg CD40 interaction leads to expression of chemokines that in turn disrupt mechanical barriers and facilitate inflammation, which is beneficial for the pathogen (66).

Another receptor that was identified for superantigen binding is the co-receptor LAMA2. Superantigens can trigger TCR signalling by activating an alternative pathway utilizing a G-protein coupled receptor leading to PLC β activation. SEE was shown to bind LAMA2 receptor that is directly linked to GPCR signalling. This path could be relevant for finding treatments against toxic shock syndrome (67).

Viral protein with superantigenic character

A publication by Cheng et al. describing that the spike glycoprotein of the SARS-CoV-2 virus, of the current Coronavirus disease 19 (COVID-19) pandemic, has superantigenic characteristics and sequentially and structurally resemble the superantigen SEB, motivated us to investigate this further (78).

Coronavirus disease

Already in November 2002-May 2003 an outbreak of an atypical form of pneumonia was seen in China, resisting any treatment. The agent was identified as corona virus and the disease called severe acute respiratory syndrome (SARS) and another epidemic later-on called middle eastern respiratory syndrome (MERS) (1). This virus was traced back to its likely origin bats that proposedly mutated and allowed the spread to humans (1). COVID-19 caused by SARS-CoV-2 was declared a pandemic in 2020. It has been observed that in both SARS and MERS, peripheral

blood lymphocytes play a critical role in defence against the infection (79). Both humoral and cellular immunity seem to be involved in COVID-19 patients (80). It is still unclear why some people are asymptomatic, whereas others have long-term effects, or an infection even results in death. Disease severity is based on common characteristics as age and predispositions, whereas the immunological features for disease severity remain largely unknown. Nevertheless, more and more studies are emerging showing that T cells have an important role in pathogenesis of COVID-19 (80–82).

Viral infection

Viruses consist of a nucleic acid segment and a lipo- protein coat and need a host for replication. Most viruses enter the body through the respiratory system, wounds, the urogenital or gastrointestinal tract. Commonly, viruses enter the host cell via a specific cell surface receptor and once inside the cell, the viral replication can start.

Generally, the innate immune response is activated and PAMPS are recognised by PRR expressed on phagocytic cells (1). This can lead to viral RNA degradation, blocking viral replication or activation of NK cells that kill already infected cells. Viruses can be neutralized by antibodies that are specific for viral surface antigens. They are crucial in blocking the spread, by interfering with the binding to or the fusion with the host cell. Furthermore, free virions are eliminated by opsonisation, lysis of the viral envelope and phagocytosis.

Cell mediated immunity is important for already infected cells and viral clearance. Both, $CD4^+$ Th1 cells and $CD8^+$ Tc cells are needed for cell-mediated antiviral defence. Th1 cells produce cytokines, which defend against the virus by inducing an anti-viral state in nearby cells (INF- γ), activating $CD8^+$ cells (IL-2) to kill infected cells and activating NK cells (INF- γ and IL-2). Th1 cells also license APC for cross-presentation to activate naïve $CD8^+$ T cells. Virus specific $CD8^+$ T cells are formed. CTL arises on day 3-4 of infection, peaks on 7-10 and declines over the following weeks/months (1) (Fig. 3/4).

Structure and function of spike glycoprotein

Viruses have formed several strategies to invade the host. SARS-CoV and SARS-CoV-2 both enter the human body by binding to human angiotensin converting enzyme 2 (hACE2) (83). The coronavirus virion is made up four main parts: the nucleocapsid (N), the membrane (M), the envelope (E) and the spike (S) protein (84).

Attachment to the host cell and fusion cells is orchestrated by using its spike glycoprotein that covers the surface of the virus. The spike glycoprotein is a homotrimer. It has a prefusion and post-fusion state. In the prefusion state it consists of two subunits S1 and S2. In the post-fusion state, the spike protein is cleaved into S1 and S2 subunit in the Golgi apparatus of the host cell by furin and then forms two non-covalently associated subunits (84).

The spike protein binds via its receptor-binding domain (RBD) in the S1 subunit to human Angiotensin converting enzyme 2 (hACE2) and the S2 subunit anchors the spike protein in the membrane and mediates membrane fusion that is proteolytically activated by human proteases. This stage is induced by the virus engagement with ACE2 that exposes S2' cleavage site in the S2 subunit. S2' is cleaved by TMPRSS2 leading to endocytosis and pore formation. After immense structural changes in the subunits the viral and cellular membrane are brought together and create a fusion pore that allows the viral genome to reach the host.

The S1 subunit consists of amino-terminal domain (NTD), receptor binding domain (RBD), carboxy-terminal domain 1 and 2 (CTD 1/2) and surrounds subunit 2 that consist of a helix called heptat repeat 1/2 (HR 1/2) towards the viral membrane (Fig. 13). There are two distinct conformations receptor accessible and inaccessible for binding, where the RBD domains are up or down, respectively (84).

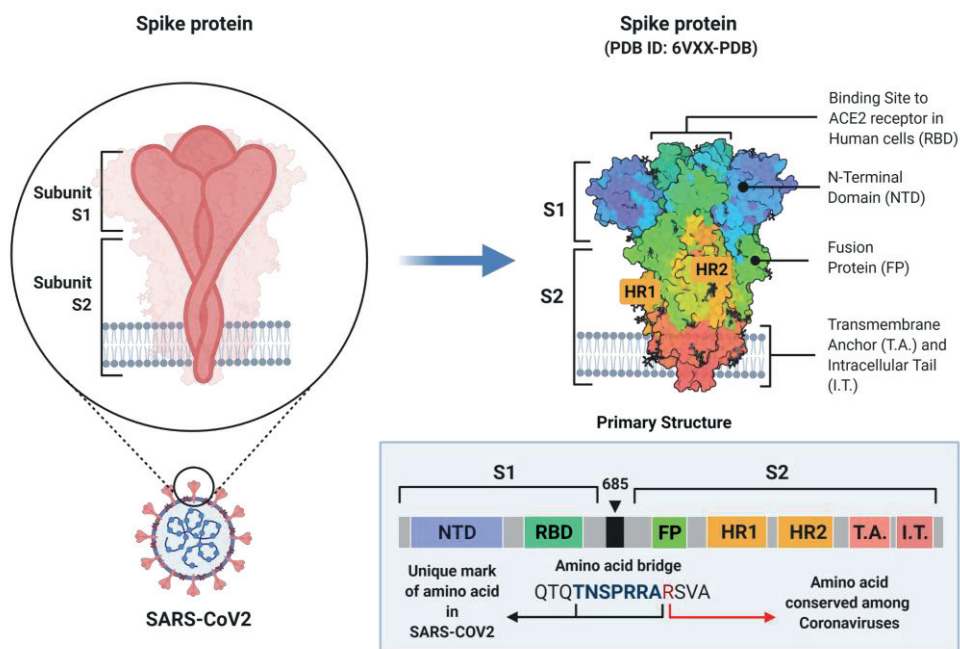


Figure 13: Spike protein domains.

Novel insights of superantigens interacting with immune receptors

Superantigens role in human disease

Superantigens have been implicated for various types of disease including toxic shock syndrome (TSS), infective endocarditis, pneumonia, food poisoning, emesis, and inflammatory skin disease.

Toxic shock syndrome, food poisoning and emesis

Superantigens cause toxic shock syndrome (45) and food poisoning (42). TSS was reported as staphylococcal scarlet fever already in 1927 (37). TSS is characterized by fever, rash and hypotension that than can cause organ failure and lethal shock (34). These patients didn't have detectable bacteria, suggesting the intoxication by bacterial products. Later in 1981, these secreted proteins from *S. aureus* were characterized. These toxins were named superantigens (SAGs) to point out the extensive T cell activation (33). SAGs circumvent regular antigen recognition and activate 5-20 % of all T cells, whereas conventional antigens activate 1/1000 (71). SAGs interact simultaneously with receptors on different cell types and trigger excessive cell proliferation and inflammatory cytokine release. This immense cytokine release is thought to be one of the most dangerous consequences of SAGs, that might lead to organ failure and death (Kotb 1995). Superantigens are already active at concentrations as low as 1 fg/mL, making them extremely potent (36).

The world health organization describes food borne diseases (FBD) as disease of infectious and toxic nature caused by consumption of food or water. Bacteria cause two thirds of FBD outbreaks. Staphylococcal food poisoning (SFP) results from absorption of staphylococcal enterotoxins (SEs) formed in food (43). SFP is characterized by nausea, abdominal pain, vomiting and diarrhoea 2-6 h after consumption of SEs contaminated food (42).

Interestingly, symptoms of TSS and food poisoning are not caused by the superantigen itself, but by over activation of the immune response. Studying these diseases showed at least two different molecular modes of action of superantigens

in the human body that do not seem to be connected. Superantigenicity and emetic activity are both caused by superantigens. Superantigenicity results from superantigens interacting with T cells and activating an enormous amount of them leading to a cytokine storm that might be toxic for the host. Superantigenicity and emetic activity were shown to be mechanistically separated, by using various SEA and SEB variants by site directed mutagenesis inducing either superantigenic T cell proliferation or emesis (85). The mode of action of superantigens leading to emesis is not known yet and therefore needs to be further investigated.

Aims

The overall goal of this thesis was to get structural, mechanistical and biological insight into the complex action of bacterial superantigens in the human body. The specific aims were:

Paper I & II: The role of $\alpha\beta$ T cells in superantigen related disease has been extensively studied, whereas the role of $\gamma\delta$ T cells and its mechanism needs to be further elucidated.

Paper III: Already 20 years ago it was shown that emetic activity was independent from T cells, but another kind of mechanism was not presented yet. Our data combined with literature search suggests that the interaction of superantigens with the cytokine receptor gp130 might play a role in emetic activity.

Paper IV: Furthermore, not only bacterial proteins also viral proteins can lead to superantigenic T cell activation. It was hypothesized that the spike protein in SARS-CoV-2 acts as a superantigen, therefore it was investigated if there is direct binding of the spike glycoprotein to the $\alpha\beta$ T cell receptor.

The results, including cell studies as well as protein-protein interaction studies, described in published papers and manuscripts contribute to a better understanding of superantigens role in human disease (**Paper I-IV**).

Interplay between superantigens and $\gamma\delta$ T cell receptor

Unlike $\alpha\beta$ T cells, $\gamma\delta$ T cells are to the unconventional T cells and make up to 0.5-10 % of cells in the peripheral blood of adults. Interestingly, in foetal development the amount of $\gamma\delta$ T cells is higher than $\alpha\beta$ T cells, suggesting an important role prior birth. The $\gamma\delta$ TCR is not as diverse as the $\alpha\beta$ TCR and it recognizes unconventional antigens (14). They belong to the innate-like immune cells and can join in the early response against bacterial infection. During some bacterial infections the amount of $\gamma\delta$ T cells is upregulated to 50 % of the peripheral blood cells (86). It was shown that $\gamma\delta$ T cells are activated by SEA (87). The mechanism of activation of these unconventional T cells by superantigens is poorly understood. As mentioned before the $\gamma\delta$ T cells can be activated without antigen presentation by MHC. Understanding this underlying mechanism will pave the way to better understanding of superantigen biology and disease development in general.

Indirect mechanism of $\gamma\delta$ T cell activation by superantigens

V γ 9 δ 2 TCR has previously been shown to bind non-peptide antigens and SEA in a distinct manner (87–89). Furthermore, Morita et al. claimed that $\gamma\delta$ T cell expressing V γ 9⁺ TCR proliferate upon SEA recognition (88). $\gamma\delta$ T cells do not require presentation of the antigen by MHCII (90), but several $\gamma\delta$ T cells were reported to bind MHC or MHC like molecules (91–93). However, the mechanism, if and how MHCII or other receptors participate upon activation, is not known yet. Still, Rust and Koning showed that activated T cells can express MHCII and that these cells can present SEA to other T cells and thus may be involved in on-site immune response. An SEA mediated human T cell- T cell interaction has been suggested, where it was shown that TCR $\alpha\beta$ ⁺ T effector cells presented SEA to either TCR $\alpha\beta$ ⁺ T cells and TCR $\gamma\delta$ ⁺ T cells (89). It is still unclear what kind of mechanism of action $\gamma\delta$ TCR and SEA have. Direct or indirect modes of action have been suggested, but direct binding on a protein level was not shown yet. In **Paper I**, an indirect mechanism for the activation of $\gamma\delta$ T cells by SEA, that would utilize monocytes and $\alpha\beta$ T cells in a direct cell to cell manner, has been proposed.

In this study, stimulated peripheral blood mononuclear cells (PBMC) were stained for intracellular cytokine (INF- γ) expression and analysed using flow cytometry. The proportion of INF- γ ⁺ conventional T cells and $\gamma\delta$ T cells were measured after 24 and 48 h of stimulation with SEA, TSST-1 and SEH. Overall, it was observed that SEH induced a weaker response than SEA and TSST-1 (Fig. 14A-B). Subsequently, it was investigated if $\gamma\delta$ T cells activation occurs through a non-canonical receptor, meaning a receptor already known for superantigen interaction like gp130 or $\alpha\beta$ TCR. A co-culture system was set up, in which SE-primed

monocytes were added to isolated $\gamma\delta$ T cells and the intracellular cytokine response was analysed by flow cytometry. Even with monocytes in the $\gamma\delta$ T cell culture, no INF- γ expression was induced. Only by adding conventional CD3⁺ T cells to the co-culture system, activation of $\gamma\delta$ T cells could be observed. This suggests that monocytes as well as conventional T cells are need for activation of $\gamma\delta$ T cells (Fig. 14C). To determine whether cell-to-cell contact was required for activation, $\gamma\delta$ T cells were seeded into membrane transwell plates with SEA stimulated monocytes and total CD3⁺ T cells in the bottom well. No intracellular INF- γ was observed suggesting that physical contact is needed for activation and that surface-expressed co-stimulatory receptors are involved (Fig. 14D). Furthermore, it was observed that $\gamma\delta$ T cells, NK cells and MAIT cells required longer durations of stimulation than conventional T cells that only needed 4 h (Fig. 14E). From this study it was concluded that SEs are able to induce IFN- γ expression in MAIT cells, $\gamma\delta$ T cells and NK cells and require $\alpha\beta$ T cells for activation (**Paper I**).

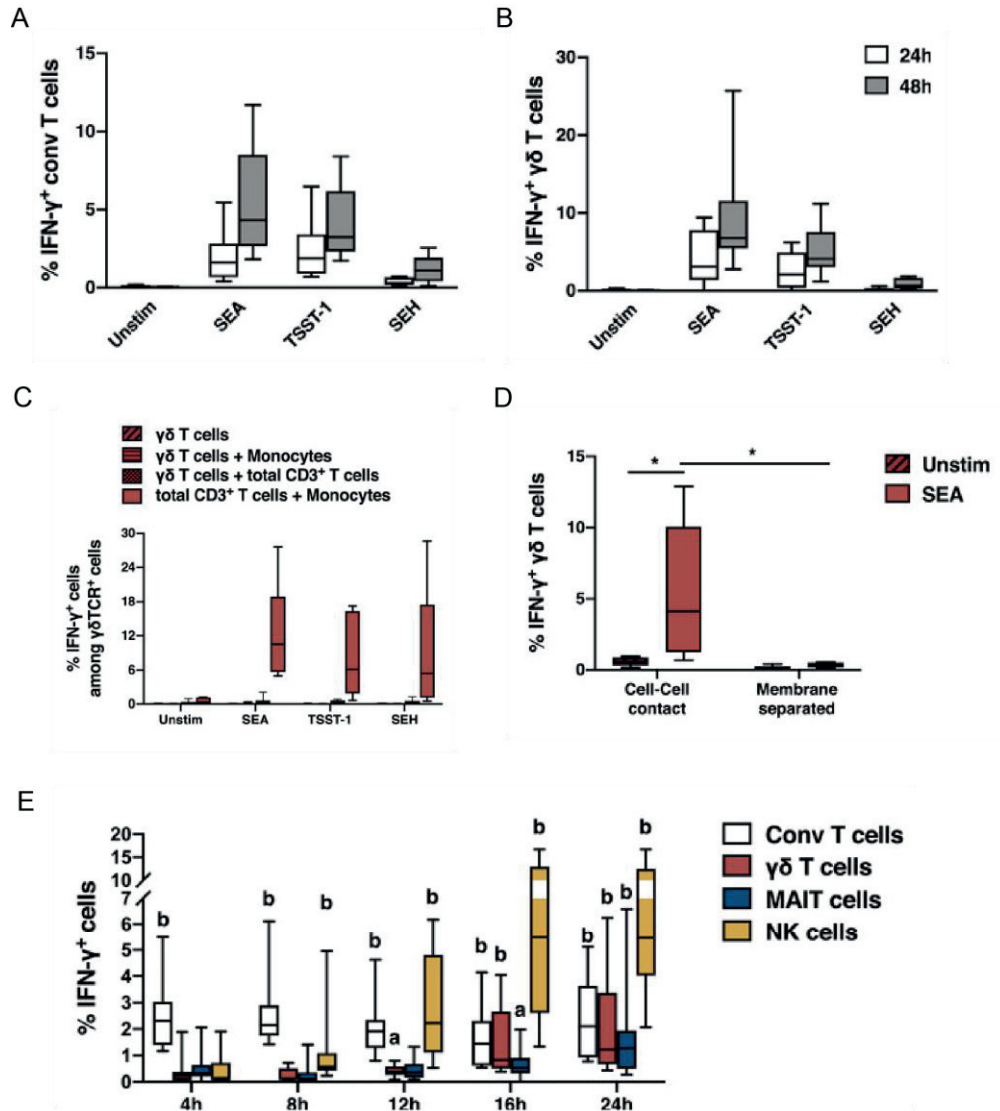


Figure 14: Indirect activation of $\gamma\delta$ T cells by SEs shown by using flow cytometry (**Paper I**). (A-B) Proportion of IFN- γ ⁺ of conventional T cells and $\gamma\delta$ T cells were measured after 24 h and 48 h of stimulation with SEA, TSST-1, SEH. (C-D) Co-culture system shows monocytes as well as conventional T cells are need for activation of $\gamma\delta$ T cells by superantigens in a cell-cell contact manner. (E) Proportion of IFN- γ ⁺ conventional T cells, NK cells and MAIT cells and $\gamma\delta$ T cells were measured after different time points (**Paper I**).

Direct binding of chimeric $\gamma\delta$ TCR and SEA

In **Paper I**, an indirect mode of activation for $\gamma\delta$ T cells by superantigens, relying on the presence of $\alpha\beta$ T cells and monocytes, is proposed. Nevertheless, it does not exclude that SEA potentially could bind directly to $\gamma\delta$ TCR, which was hypothesized before. V γ 9 δ 2 TCR was shown to bind SEA in a distinct manner (87,88). By using different mutations of SEA, it was identified that the α 2 helix of SEA (residues 20-27) is required for $\gamma\delta$ T cell recognition of SEA, especially residue Asn25_{SEA} was crucial for the interaction between SEA and TRGV9 (88). Nevertheless, direct binding on protein level was not shown yet. Being able to study this receptor will clarify their distinct function, shed light into their role in an immune reaction and help to clarify their role in superantigen biology.

In order to facilitate protein-protein interaction and structural studies, sufficient amounts of pure and homogenous $\gamma\delta$ TCR are needed. In **Paper II** we report a protocol to produce chimeric $\gamma\delta$ T cell receptor in *Escherichia coli* periplasm, adapted from the $\alpha\beta$ TCR protocol (94), using the γ 9 δ 2 as representative. This set up will enable biochemical and biophysical studies of $\gamma\delta$ TCRs that require vast amounts of homogeneous material.

Antigen binding takes place in the variable domains of the TCR. For stability reasons a chimeric γ 9 δ 2 construct was created, by fusing the variable domains to the constant domains of the already published $\alpha\beta$ TCR (Fig. 15A), for which the protocol has already been established. The γ 9 δ 2 TCR was successfully expressed and purified with final yields of 8.5 mg at >90 % purity (Fig. 15B). Correct folding and the secondary structure fractionation were demonstrated by CD (Fig. 15C). Interestingly, a higher α -helical content was obtained for the chimeric $\gamma\delta$ TCR than for the $\alpha\beta$ TCR, clearly indicating different structural features in the variable domain, that might explain the difference in binding compared with $\alpha\beta$ TCRs.

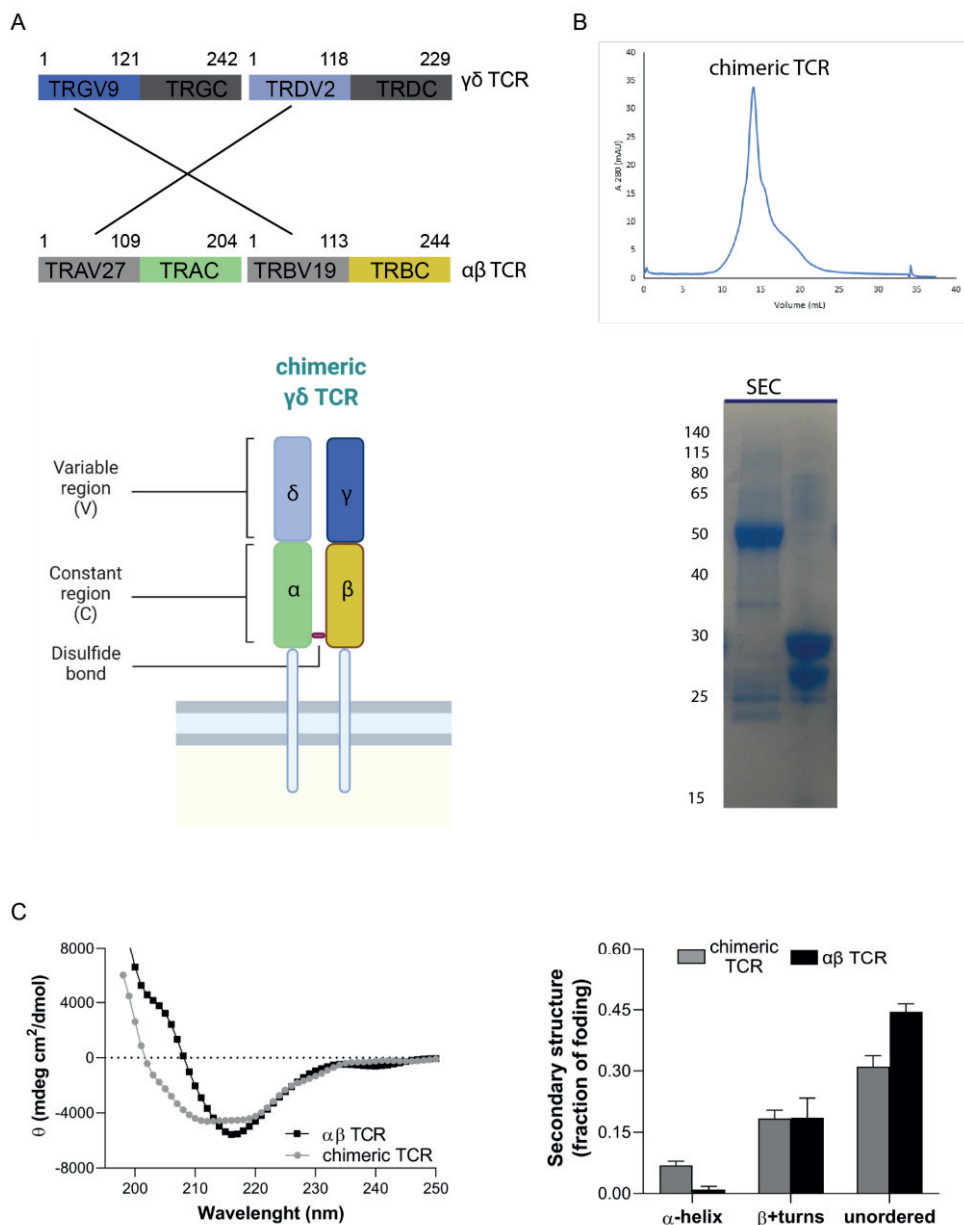


Figure 15: (A) Generation of chimeric TCR construct. Original TCR chain subdivision of amino acids $\gamma\delta$ TCR (TRGV9/TRDV2) with blue (γ) and light blue (δ) highlighted variable domains and $\alpha\beta$ TCR (TRAV27/ TRBV19) with lime (α) and olive (β) highlighted constant domains, forming chimeric TCR with introduced S-S bridge in purple. (B) Purity of chimeric TCR shown by SEC and SDS-PAGE. (C) Analysis of secondary structure of chimeric TCR by CD and comparison with $\alpha\beta$ TCR (**Paper II**).

Furthermore, we show for the first-time complex formation of V γ 9 δ 2 TCR and the superantigen SEA, by using BN-PAGE, validated by using a specific SEA antibody (Fig. 16). To analyse the binding between SEA and $\gamma\delta$ TCR, the two purified proteins were mixed in a molar ratio (1:1, 1:2 or 2:3). Binding of SEA to the $\alpha\beta$ TCR (molar ratio 1:1, 1:2 or 2:3) was used as positive control (**Paper II**).

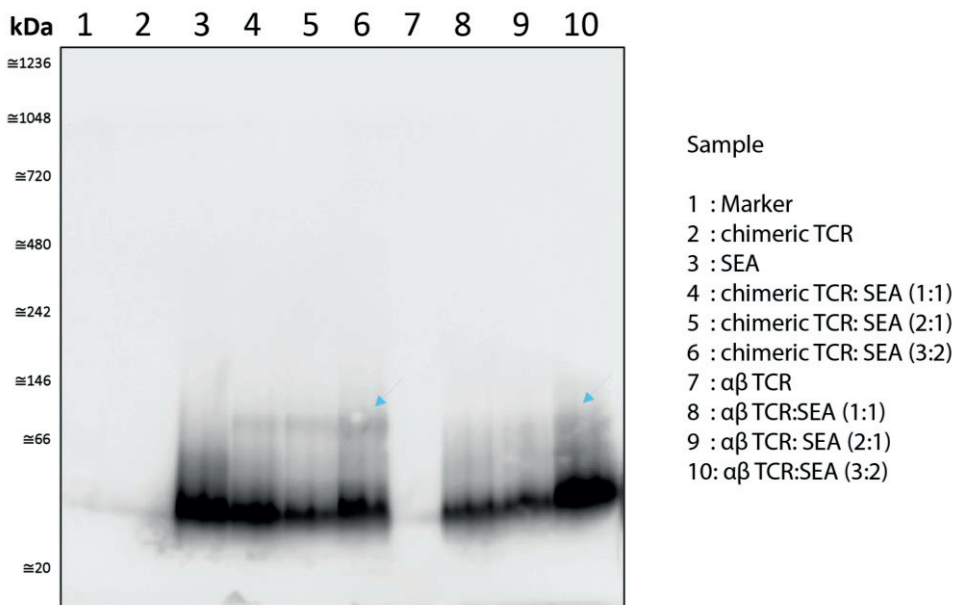


Figure 16: Complex formation of $\gamma\delta$ TCR and SEA shown with native page western blot (α -SEA). SEA: $\gamma\delta$ TCR (left) and SEA: $\alpha\beta$ TCR (right). Proteins were loaded alone in their highest concentration and were also mixed in a molar ratio (1:1, 1:2 or 2:3) and loaded in increasing concentrations (**Paper II**).

Altogether, a protocol to produce pure and active $\gamma\delta$ TCR was established. The availability of large amounts of $\gamma\delta$ TCR will facilitate future experiments to understand the role of $\gamma\delta$ T cells in the immune system and shed light in the mechanism of its interaction of superantigen with this unconventional TCR that is discussed for more than 30 years.

Interplay between superantigens and cytokine receptor gp130

Recently, it was discovered that the superantigens SEA and SEE also can bind to the cytokine binding domain (D1-D3) of human cytokine receptor gp130. It was shown that SEA binds to gp130 using the C-terminal domain, as binding could not be detected with the SEA_{D227A} mutant (68). Also, non-classical superantigens have been identified to bind to gp130 (95). The biological outcome of this interaction is yet to be discovered. In **Paper III** the gp130-SEA binding is analysed in more detail and a structural model is proposed as well as the implication of such interaction in emesis is discussed.

Superantigens bind to gp130

Here, surface plasmon resonance (SPR) is applied to show the binding of the superantigens SEA, SEE and SEH to immobilized human gp130 (hgp130). The highest affinity was seen for SEA ($K_D = 0.5 \mu\text{M}$), slightly lower for SEE ($K_D = 2.7 \mu\text{M}$) and the lowest affinity for SEH ($K_D = 34 \mu\text{M}$) (Fig. 17A-C).

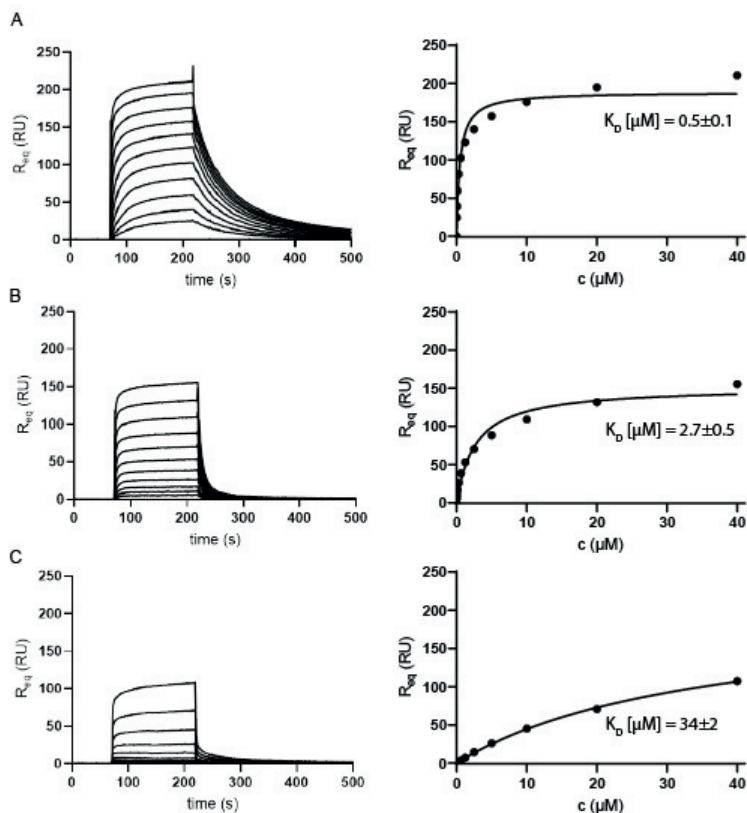


Figure 17: Surface plasmon resonance sensorgrams showing the binding of superantigens to hgp130. A two-fold concentration series of (A) SEA, (B) SEE, and (C) SEH were injected over immobilized human gp130-Fc dimer. The concentrations shown are ranging from 30 nM to 40 μ M. The affinity is calculated via non-linear regression and the standard error is shown (**Paper III**).

The interaction was shown to be zinc dependent (68), which led us to conclude that the different Zn-coordination of SEA and SEH (Fig. 18) could result in lower gp130 affinity.

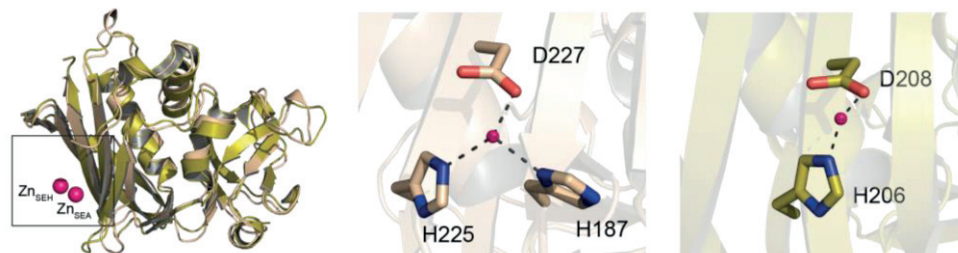


Figure 18: The response units (RU) were recorded and plotted against time (s). SEA (PDB: 1SXT, wheat) and SEH (PDB: 1EWC, gold) structures with the coordinated zinc were overlaid, shown in cartoon representation (left). SEA coordination of zinc (pink) with residues H187, H225 and D227 shown as sticks (middle). SEH coordination of zinc (pink) with residues H206 and D208 shown as sticks (right) (**Paper III**).

Moreover, animal studies were suggested to study the biological outcome for the superantigen-gp130 interaction. Therefore, SPR was used to characterize the binding to rodent gp130. Interestingly, no binding could be seen for mouse and rat gp130 for SEA and SEE, indicating a different mode of action in human (Fig. 19A-F).

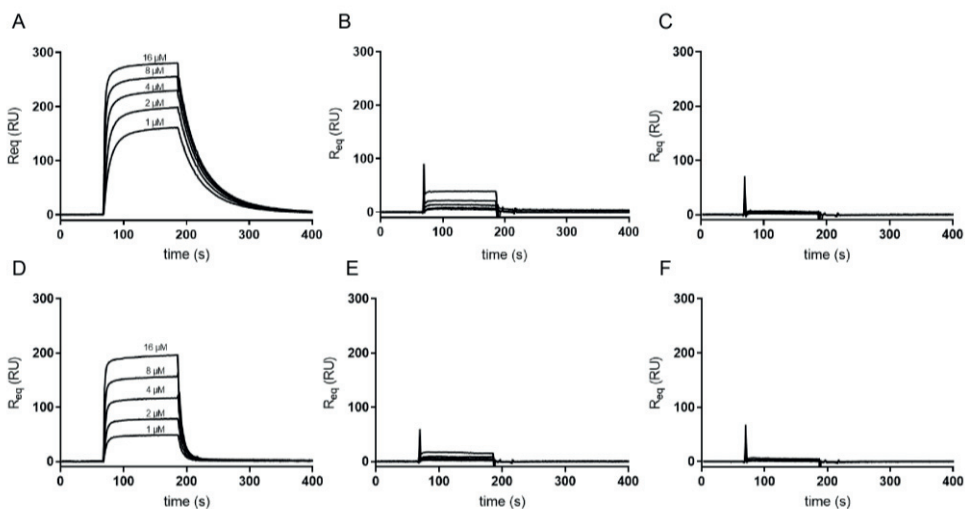


Figure 19: Surface plasmon resonance sensorgrams showing the binding between superantigens (SEA and SEE) and various gp130 variants (human, mouse and rat). A two-fold concentration (1-16 μ M) series of (A-C) SEA and (D-F) SEE were injected over immobilized (A, D) human gp130-Fc dimer, (B, E) mouse gp130-Fc dimer and (C, F) rat gp130-Fc dimer. The response units (RU) were recorded and plotted against time (s) (**Paper III**).

Structural analysis of SEA-gp130 complex formation

To get a better understanding of SEA-hgp130 binding, cross-linking mass spectrometry was applied to identify the residues involved in complex formation. The lysine crosslinker BS3 was used and based on cross-linked residues, for SEA K14 and K79 and for gp130 K29, K139 and K151 (Fig. 20A-C), two likely models of SEA binding to gp130 could be obtained (Fig. 20D-E). The cross-linking results show that SEA interacts with the D1 and D2 domain of human gp130 (**Paper III**).

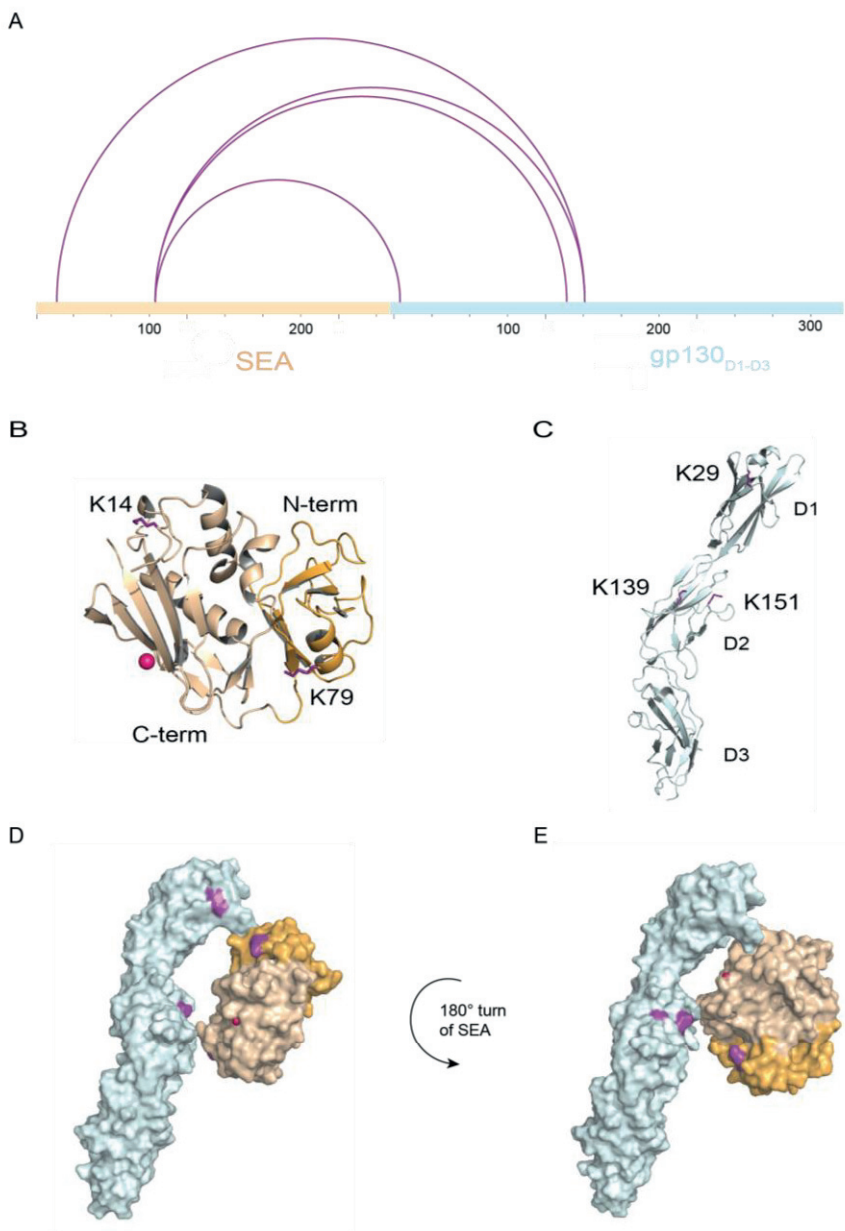


Figure 20: (A) The software xVis was used to visualize the crosslink derived distance restraints (purple lines) of the SEA-gp130 protein complex. A scale for the amino acid-sequence number of SEA and gp130 is displayed. (B) Cartoon representation of SEA, N-terminal domain (orange), C-terminal domain (wheat), Zn²⁺ (magenta) and identified cross-links shown as sticks (purple). (C) Cartoon representation of gp130 D1-D3 (cyan) with identified cross-links shown as sticks (purple). (D-E) Surface representation of two alternative SEA placements created in PyMOL using XL-MS data, varying by a 180 ° vertical turn of SEA. The cross-links with the highest scores are highlighted (purple). SEA is divided into: C-term (wheat) and N-term (orange). (D) Placement A fulfils crosslinks between K79_{SEA} – K29_{gp130} and K14_{SEA} – K151_{gp130} which are shown in purple. (E) Placement B fulfils crosslinks between K79_{SEA} – K139_{gp130} and K151_{SEA} – K151_{gp130} which are shown in purple (**Paper III**).

Computational model of superantigen SEA and gp130

To create a convincing model, the surface plasmon resonance data, the sequence alignments and the cross-linking data were combined, and a computational model was created with Rosetta (Fig. 21A). SEA and human gp130_{D1-D3} interact via D1 and the N-term of SEA involving aa. 47-50 (Fig. 21B) and via H145 in D2 of gp130 and the C-terminal Zn-binding site of SEA involving H187, H225 and D227 (Fig. 21C).

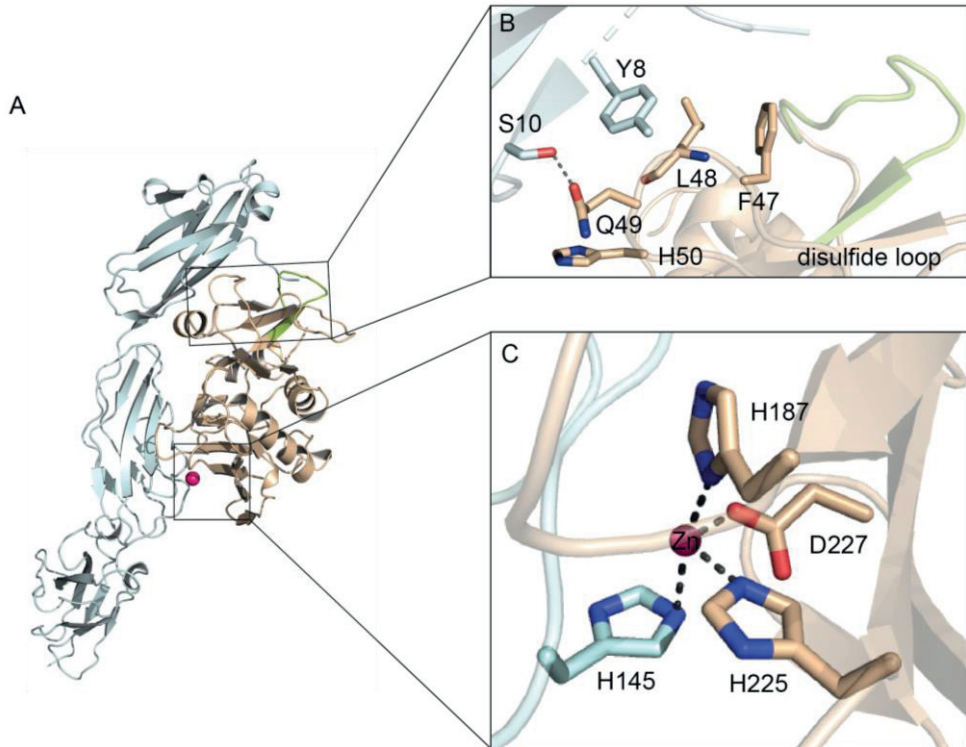


Figure 21: (A) Cartoon representation of Rosetta model of SEA (wheat) and gp130_{D1-D3} (cyan) and Zn²⁺ (magenta). (B, C) Zoom-in of gp130 D1 and D2 binding interfaces with SEA; residues at the binding sites are shown as sticks and the SEA disulfide-containing loop in green, and hydrogen bonds are marked as dotted lines (**Paper III**).

Interestingly, SEA seems to bind D1 and D2 of gp130 in the same way as it crosslinks two MHCII molecules (Fig. 11).

Superantigens in emesis studies

The forceful expulsion of the contents of the stomach via the mouth is termed emesis or vomiting. *Staphylococcal aureus* is known to cause emetic food poisoning. The connection between superantigens and emesis has been discovered but is not yet fully described and understood.

Most recent studies for superantigen induced emesis were conducted in primates, already indicating a variance of action in rodents. One exception is the house musk shrew model for a few studies. The sequence for gp130 of this special mouse is not available but would be very interesting to have for our study. Our surface plasmon resonance data supports the different mode of action in human by showing superantigen (SEA, SEE) binding only to the human gp130 variant and not to mouse and rat gp130 (Fig. 19).

It was shown that SEA binds submucosal mast cells and evokes mast cell degranulation in a house musk shrews (96). Furthermore, it was observed in house musk shrews that intraperitoneal administration lowered the amount of SEA needed 10 times ($ED_{50} = 3 \mu\text{g/kg}$), compared to oral administration (97). This is indicating that the intraperitoneal area is the main region of SEA interaction. The study found that SAGs induce varying responses: while SEA and SEE only require low doses for emetic activity, a higher dose of SEH was needed (97). This might result from the low gp130-SEH affinity that is shown to be 70 times lower affinity than the interaction with SEA (Fig. 17).

Another study used marmosets as a primate model for emetic activity and showed that SEA induces histamine release from submucosal mast cells in the gastrointestinal tract and that histamine contributes to the SEA-induced vomiting reflex (98). Notably, a vomiting response was significantly reduced via intravenous injection compared with peroral administration of SEA, indicating that the binding is in the GI tract. This might imply that SEA does not act directly on the chemoreceptor trigger zone (CTZ) (98). CTZ is an area in the brainstem that receives signals from hormones or other molecules and then communicates with the vomiting centre to initiate vomiting.

It was shown that the emetic response was induced via an unknown receptor that is independent from MHCII (85). We speculate that gp130 might be the unknown receptor. Gp130 is expressed on mast cells and the sequence identity of human gp130 and marmoset gp130 is 95 %. Interestingly, our structural model (Fig. 21) shows that the most important residues for SEA binding, the residues S10 and H145, are conserved in human and marmoset, whereas in mouse and rat they are not. Computational alanine scanning confirmed the importance of these residues for complex formation (**Paper III**).

Furthermore, it was shown in experimental studies that the disulphide loop and residues F47, L48 and C106 on SEA are important for emetic activity (85,99). Also, in our model, the SEA disulfide loop is packing against gp130 and further stabilizing the complex (Fig. 21A-B). Also, it is known that upon substitution of D227A on SEA there is no binding to gp130 and no emetic activity (68,100). D227 is one of the Zn coordinating residues on SEA that is important for complex formation (Fig. 21C). All in all, these results indicate that the gp130-SEA complex formation might lead to emetic activity in primates and humans. This further highlight, why mouse and rat aren't commonly used as models for emetic activity.

Based on our data and literature search we hypothesize that the superantigen bind to gp130 on mast cells in the gut and induce emesis in human and primates.

Superantigenic character of spike protein in SARS-CoV-2

Recently, Cheng et al. published a computational study describing that the spike glycoprotein of the SARS-CoV-2 virus has superantigenic characteristics and sequentially and structurally resemble the superantigen SEB (78). This finding motivated us to investigate the topic further. This computational based publication also speculated on a direct interaction of the spike glycoprotein with the human $\alpha\beta$ TCR, but it was not experimentally shown (78). Many more publications followed that suggested an important role for T cells in COVID-19 disease (82,101,102). Worldwide combined efforts in research of the virus led to the development of several vaccines that all utilize the spike glycoprotein as functional basis.

Vaccines

Protective immunity can be achieved by passive or active immunization. Passive immunization is the administration of antibodies and provides only temporary protection. Whereas active immunization can be achieved by natural exposure to the live pathogen followed by recovery or can be acquired artificially by vaccination. Ideally, in active immunization would engage antigen-specific lymphocytes, generate memory cells, and provide immunity. The most common corona virus vaccines in Europe are either mRNA-, viral vector-, or protein subunit vaccines. mRNA vaccines (Pfizer-BioNTech and Moderna) use genetically engineered RNA to generate a protein that creates an immune response. Viral-vector vaccines consist of genes that encode antigens of a pathogen and are introduced into a safe carrier (virus), that functions as a vector and then replicates in the vaccinated host

producing the gene product to generate an immune response (Astra-Zeneca, Johnson & Johnson). Subunit vaccines only use purified macromolecules derived from the pathogen, in this case the spike protein and generate an immune response (Novavax) (103).

B cell and T cell immunity

One major research question circled around the lasting duration of immunity by vaccination. Important key players for humoral and cellular immunity are antibodies, B cells and CD4⁺ and CD8⁺ T cells. Understanding the adaptive immune response to SARS-CoV-2 is not only important for vaccine development, but also for understanding the pathogenesis and calibration measures of pandemic control.

Immune memory after infection was investigated to deepen the knowledge of protection against reinfection, disease risk and vaccine efficacy. The result was a wide heterogeneity in the adaptive immune response of recovering people. Memory B-cells, antibodies, CD4⁺ and CD8⁺ T cells were observed after infection, and immune memory was observed in 90 % of the people in the case study after up to 8 months of infection. In general, it was observed that antibodies and CD8⁺ T cells declined, CD4⁺ T cells stayed stable and memory B cells increased after a few months (80).

Another study confirmed that SARS-CoV-2 specific CD8⁺ and CD4⁺ T cells were identified in convalescent patients. Furthermore, CD4⁺ T cells that are specific in SARS-CoV-2 were also found in 40-60 % of unexposed patients, suggesting a possibility for cross-reactive T cell recognition (82). T cell responses have been associated with reduced disease and might be important for disease control and resolution after primary infection (81). Increased number of SARS-CoV-2 specific T cell, but no humoral response was observed further highlighting the role of T cells in disease clearance (102). It was clearly shown that SARS-CoV-2 induce remodelling of peripheral lymphocytes and shuffling of adaptive immune response repertoires. Characterization and variations in cell composition showed a more robust humoral and T memory response in severe patients (101). SARS-CoV-2 epitopes (mainly of spike protein) are recognized by a diverse repertoire of human T cell receptors (82). The T cell response, with identified TCRs might be a useful biomarker for surveying antiviral immunity. Among others, TRBV7-9 was shown to be of high usage for SARS-CoV-2 epitope YLQ (102).

Spike protein bind to $\alpha\beta$ TCR

In **Paper IV** we analysed if the spike glycoprotein directly interacts with human $\alpha\beta$ TCR and structurally characterised the interaction.

The surface plasmon resonance data shows that the spike glycoprotein specifically binds to TRAV22/TRBV7-9 and TRAV26-2/TRBV7-9. We observe binding for two different TCRs with TRBV7-9 but no binding for TRAV22/TRBV11-2 (Fig. 22A-C). Taken together, the TRBV7-9 is crucial for binding to spike glycoprotein. Nevertheless, the alpha chain seems to have some impact for binding, indicated by the observed higher RU values for TRAV26-2/TRBV7-9 than for TRAV22/TRBV7-9 (Fig. 22A-B).

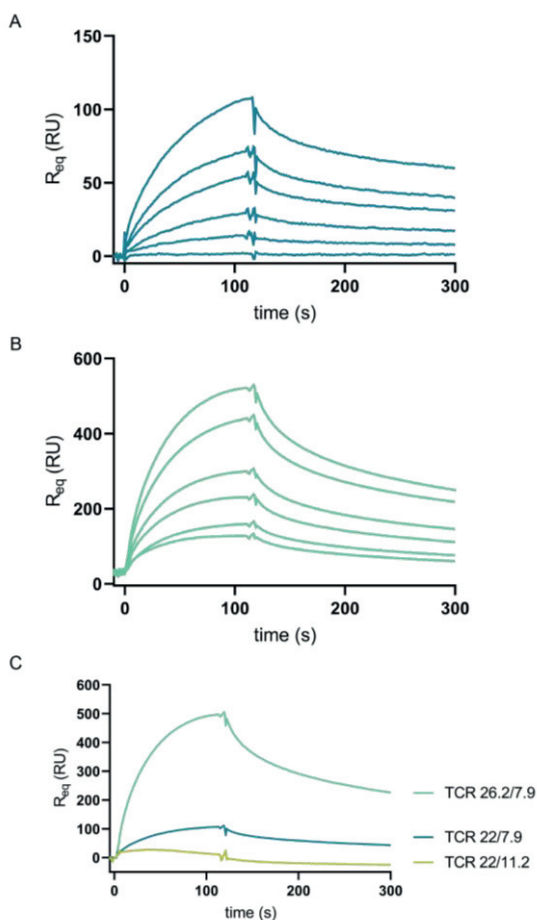


Figure 22: Surface plasmon resonance sensograms (A) TCR (22/7-9), (B) TCR (26-2/7-9) as analyte and spike glycoprotein as ligand. (C) Highest concentration (5 μ M) of 3 tested TCRs shows that specific TRBV7-9 is needed for spike interaction (**Paper IV**).

To get a three-dimensional structure of the spike glycoprotein-TCR (TRAV22/TRBV7-9) complex, negative staining and initial cryo-EM screening was conducted. Negative staining is used to pre-assess the sample quality. In the negative staining EM images, particles resembling the expected shape of the spike protein were visible, as well as smaller particles in the vicinity of the NTD/ RBD region of the spike protein (Fig. 23).

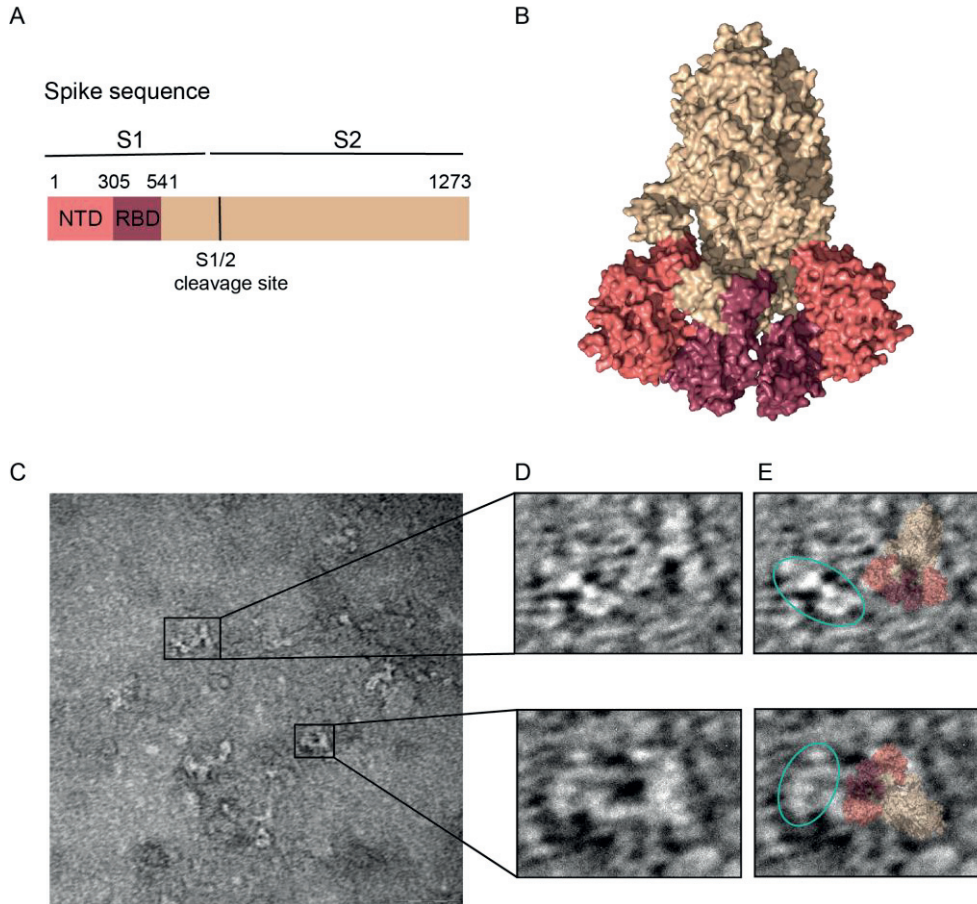


Figure 23: Negative staining showing well dispersed single particles. (A-B) Sequence and structure in surface presentation with highlighted NTD (salmon) and RBD (raspberry) domain. (C-E) Negative stain with zoom in and fitted structure of spike glycoprotein (**Paper IV**).

Next, the spike glycoprotein-TCR sample was subjected to cryo-EM and a dataset collected. The spike protein was clearly visible in selected 2D classes and data processing resulted in a model of 3.5 Å resolution. The resulting cryo-EM map

showed additional density at the NTD/RBD domains; however, the quality of the density was not good enough to conclude if this was bound TCR molecule.

To identify the regions of interaction on TCR and spike glycoprotein crosslinking-mass spectrometry (XL-MS) was applied. The lysine cross-linker BS21 was used, and all obtained cross-links are shown (Fig. 24A-B). Crosslinks in TCRs were identified in the β chain for both TCRs (TRAV22/TRBV7-9 and TRAV26-2/TRBV7-9), that were shown before to bind to the spike protein (Fig. 22), and in the α chain for TRAV22 (Fig. 24C-D). As assumed before, almost all crosslinks were in the NTD/ RBD domain of the spike glycoprotein (Fig. 24E-F).

In line with our results, Shoumuradova et al. showed that antigen-specific T cells were increased in healthy donors and convalescent patients. Immunogenic T cell epitopes are suggested to play a role in SARS-CoV-2 immune response and potential targets of T cell reactivity were investigated. Especially, TRBV7-9 was shown to be of high usage for SARS-CoV-2 epitope YLQ (102), that is in the RBD domain located close to the our detected crosslinks, further supporting our hypothesis of binding. More biochemical experiments and a three-dimensional structure are needed to verify these observations of this interaction that could be immensely important for the understanding of COVID-19 disease progression.

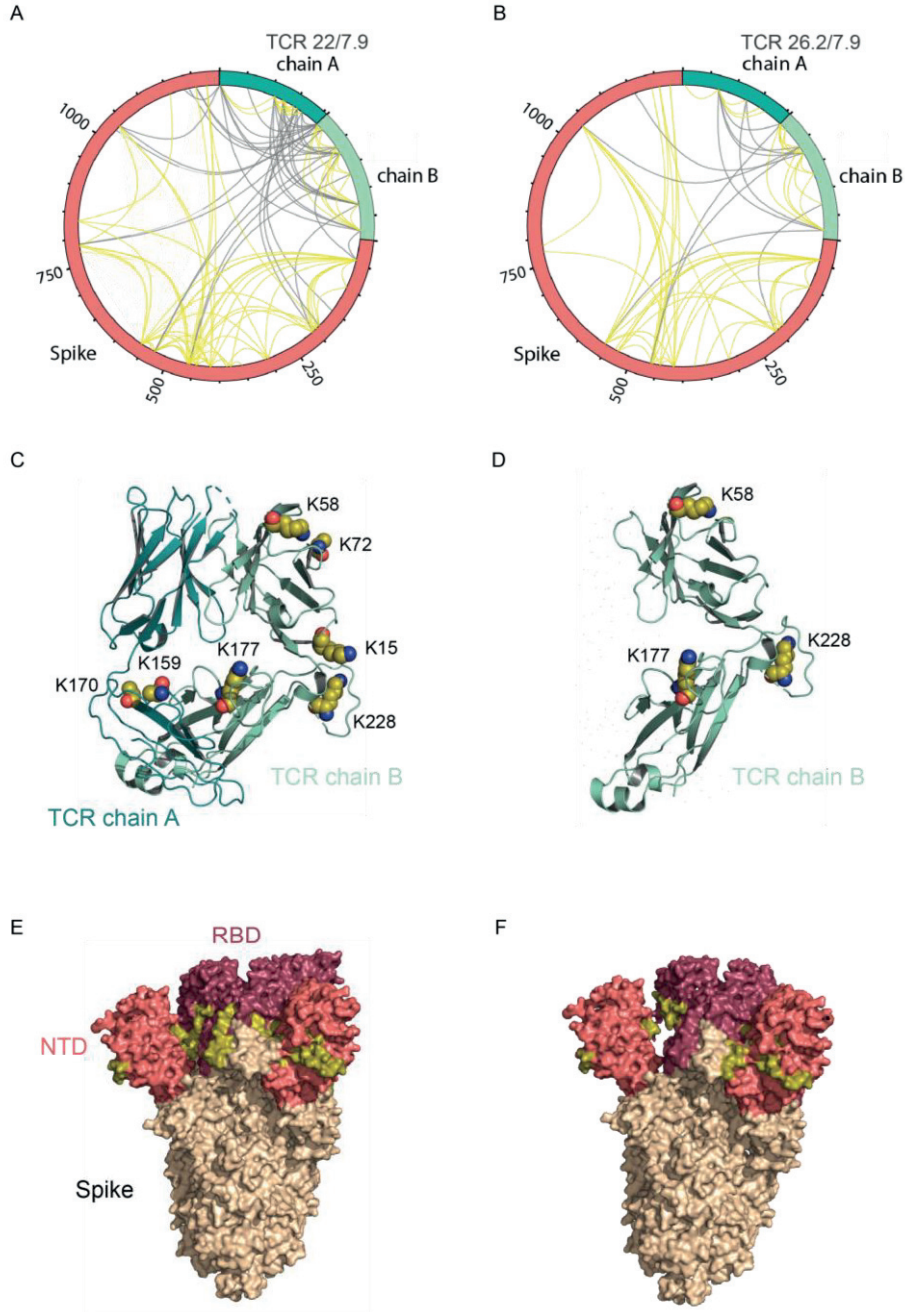


Figure 24: (A-B) Schematic presentation of all intra- (yellow) and interprotein crosslinks of both TCRs with spike protein created in Xvis. (C-D) Cartoon presentation of TCRs (PDB: 4UDT) with identified inter crosslinking lysines residues shown as spheres (yellow). (E-F) Spike protein (PDB: 6VXX) in surface presentation with highlighted crosslinking regions (yellow) in NTD (salmon) and RBD (raspberry) (**Paper IV**).

Methodology

My thesis focuses on studies of the protein-protein interaction (PPI) of toxins and human receptors. The proteins were recombinantly expressed, and by using a combination of biochemical and biophysical approaches their interaction was characterized (**Paper I-IV**). Here, a new chimeric $\gamma\delta$ TCR was produced and the interaction with superantigen SEA is shown but needs to be further characterized (**Paper II**). Furthermore, by combining sequential, structural, chemical, and biophysical data, a computational model was created for the gp130-SEA complex (**Paper III**). Moreover, direct binding between spike glycoprotein and $\alpha\beta$ TCR is shown, interacting domains and residues are indicated and initial cryo-EM data for the spike glycoprotein and human TCR interaction is provided (**Paper IV**).

Here, I will briefly describe the purification of the proteins, the methods to study protein-protein interaction and electron microscopical methods for structural studies, describe alternative methods and highlight advantages and disadvantages.

Expression systems of recombinant proteins

For all the studies the production of the protein is the starting point. There are prokaryotic and eukaryotic production systems. Four main expression systems for proteins exist: *E. coli*, yeast, insect cells and mammalian cells. All these systems have advantages and disadvantages and depending on the protein of interest, already published protocols and future experiments the best strategy is chosen.

Expression in E. coli

The expression in *E. coli* is the fastest and most inexpensive way to purify proteins. Therefore, superantigens (SEA, SEE and SEH) and the TCRs were expressed in *E. coli*. Notably, superantigens were expressed without a purification tag in the periplasm of *E. coli* separated from the host proteins in the cytoplasm. This has the advantage that after using a hypotonic osmotic shock followed by mechanical disruption, the protein sample is rather pure already in the initial purification steps. Furthermore, the cleavage of the tag that is normally performed ON is not needed. After an ion-exchange chromatography step (separation of molecules based on charge), followed by a size-exclusion chromatography step (separation of molecules based on size) the superantigen protein is purified.

TCRs were expressed as inclusion bodies (IBs) in the cytoplasm to ensure very high expression levels and purity. Nevertheless, IBs must be refolded afterwards. The refolding of proteins can be troublesome and is therefore described in more detail below.

Refolding proteins

On one hand, the refolding of proteins is time taking and has a quite low recovery of bioactive protein. On the other hand, IBs once purified can be stored for a very long time. Inclusion bodies are densely packed denatured proteins that can be refolded into their bioactive form (Fig. 25). Therefore, IBs are solubilized with a high concentration of reducing agent (DTT), along with denaturants such as urea (step 4-6). Solubilized proteins are refolded by slowly removing the denaturant, here by dialysis and by adding oxidizing agent (step 7). A two-step purification (step 8-10) is required to obtain purified refolded TCR, an ion-exchange step and one size-exclusion chromatography.

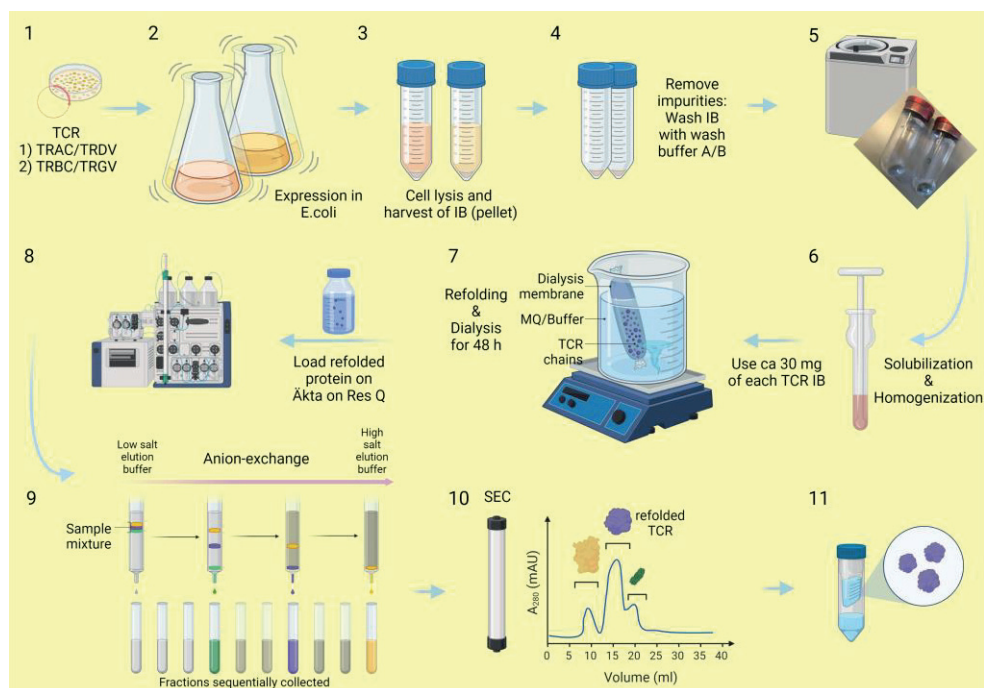


Figure 25: Expression, refolding and purification of TCR (Paper II).

Expression in insect cells

If the protein production in *E. coli* is not successful, another expression system like yeast, insect cells or mammalian cells is chosen. These expression systems can be better for human proteins with post-translational modifications. We used insect cells, because of an already available publication describing the expression of gp130 in insect cells (104). In general, working with insect cells is more expensive and time consuming than with *E. coli*. Here, the glycoprotein130 (gp130_{D1-D3}) was expressed in *Spodoptera frugiperda* (*Sf9*) insect cells using baculovirus expression system. There are two ways of generating recombinant baculovirus, either by homologous recombination or site-specific transposition. Here, homologous recombination was used. Shortly, the gene of interest is cloned into a transfer vector. The next step is the co-transfection, in which a baculovirus is added together with the transfer vector to the insect cells. A high-titre recombinant virus stock is produced that can then be used for infection of large-scale insect cell cultures.

Biochemical and biophysical methods

Antibody based biochemical and biophysical methods are used to show the protein-protein interaction of $\gamma\delta$ TCR with SEA, gp130 with SEA/ SEE/ SEH and LIF, and several TCRs with the spike glycoprotein. Here, I will describe the methods used for the studies of PPI and highlight their main advantages and disadvantages.

Biochemical method

Blue native (BN)-PAGE is a non-denaturing gel that is used to analyse the proteins in their folded state. The electrophoretic mobility depends on the size, but also on the shape of the protein. Coomassie brilliant blue provides the negative charge to the protein to move through the gel. In **Paper II** the complex formation of $\gamma\delta$ TCR and $\alpha\beta$ TCR with the superantigen SEA was shown via BN-PAGE followed by western blotting. Different protein ratios were used to optimally show the seemingly weak interaction of $\gamma\delta$ TCR and SEA.

Biophysical methods

One drawback of biochemical antigen-antibody reactions for PPI is that weak protein interactions are harder to detect, and furthermore unspecific binding can lead to false-positive interactions. Therefore, complementary biophysical methods such as microscale thermophoresis (MST), surface plasmon resonance (SPR), hydrogen-deuterium exchange (H/D X) and cross-linking mass spectrometry (XL-MS) are applied. Here, SPR and XL-MS were used to show binding of gp130 with SEA/ SEE/ SEH and LIF, and several TCRs with the spike glycoprotein.

To study the binding of proteins SPR and MST can be applied. SPR uses the optical phenomenon of surface plasmon resonance and signal detection depends on the

mass concentration of proteins on the chip. One protein is immobilised on the chip and serves as a ligand protein, while the analyte-protein flows over the surface. When binding occurs, there is a shift of the resonance angle, and a response is registered. To set up a functioning SPR experiment several milligrams of the analyte protein are needed whereas the amount for the ligand is normally lower. Another disadvantage can be that the commonly used amino coupling of the ligand on a chip (using EDC/NHS) leads to multiple capturing sites, that might occasionally hide the binding site, whereas a tag specific capturing leads to more concise capturing and binding. Another method to study protein interactions is MST. In MST, the protein does not need to be immobilized or captured. Instead, one of the interacting proteins needs to be labelled, but less protein is consumed in general. One advantage of SPR is that it is label free, so that the protein does not have to be labelled and nothing else is introduced in the binding study. Shortly, in MST an infrared laser introduces a microscopic temperature gradient. In MST one protein is labelled and the change of fluorescence is observed based on the two following effects. Temperature related intensity change (TRIC), that depends on the fluorophores microenvironment that is changed during binding and thermophoresis (movement of the molecule in the temperature gradient) are detected. The MST signal is plotted against the ligand concentration, from which the binding affinity can be estimated. Nevertheless, no kinetic information (association and dissociation rate) can be obtained with MST, whereas with SPR kinetic information can be obtained.

To analyse the interacting protein regions in more detail XL-MS or H/D X can be used. XL-MS is used to simultaneously capture the protein-protein interaction in their native environment and uncover their physical interaction contacts. It is widely used for structural prediction and integrative modelling. Shortly, lysine crosslinker is used to form covalent bonds within and between the two proteins. Next, the proteins are digested, and the resulting peptide mix is separated and analysed via LC-MS/MS and crosslinked peptides are identified. Another way of showing interaction sites of proteins is H/D X, in which hydrogen bonds are replaced with deuterium on surface accessible sites. Single proteins and the putative complex are compared to highlight change in surface accessibility. Both methods require relatively low amounts of protein.

Electron microscopy techniques

Here, we applied negative-staining transmission electron-microscopy to pre-analyse the sample quality of the produced proteins and get an initial picture of the particles of the $\gamma\delta$ TCR (**Paper II**) and spike glycoprotein with $\alpha\beta$ TCR (**Paper IV**). After that single particle cryo-electron microscopy was used to get a three-dimensional structure of near atomic resolution of the spike glycoprotein with $\alpha\beta$ TCR (**Paper IV**). The workflow of TEM and cryo-EM sample processing is shown below, as

well as initial results for data processing of spike glycoprotein with $\alpha\beta$ TCR (**Paper IV**).

Negative-staining TEM

Negative staining is applied to prepare biological specimen to image by TEM. The protein samples are embedded in heavy metal salt, in this case uranyl acetate, to scatter electrons more strongly than those in regular biological molecules and therefore increase the contrast between the stain and the sample. So, thereby the background is stained, and the specimen is visible (Fig. 26). Negative staining is a useful tool for a quick assessment of homogeneity and particle distribution of the protein sample prior cryo-EM screening (105). Furthermore, the images of negatively stained samples can be classified and reconstituted using data processing software's. However, due to preferred orientation and crystals that are formed by the heavy metal, only low resolution of the reconstituted map of approximately 20 Å is reached (106).

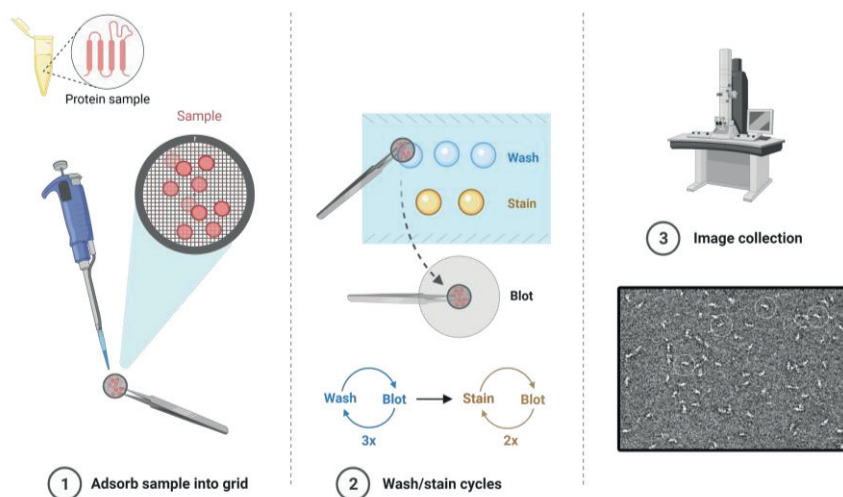


Figure 26: Negative-stain transmission electron microscopy.

Single particle cryo-EM

After the resolution revolution, cryo-EM became an indispensable method for the three-dimensional structural determination of biomolecules. Now near atomic resolution is reached, by a combination of improvements in hardware and software of cryo-EM and improved molecular biological techniques (107). Here, cryo-EM was used to visualize the complex formation of the spike glycoprotein with human $\alpha\beta$ TCR (**Paper IV**). Initial results and the main steps of cryo-EM sample and data processing are shown (Fig. 27-28).

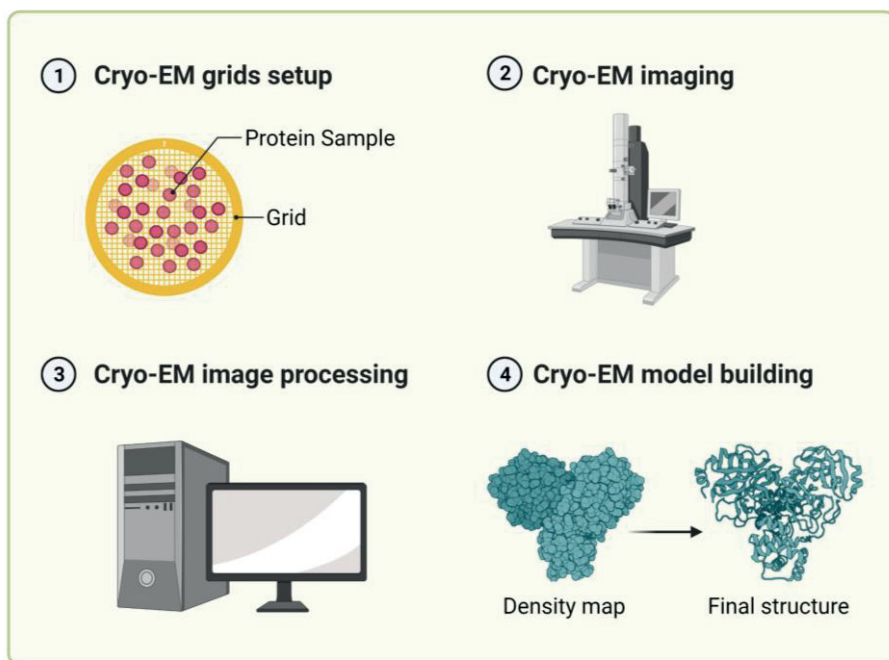


Figure 27: Main steps of single particle cryo-EM sample processing.

The protein sample was suspended onto a grid with a thin layer of graphene and then plunge frozen in liquid ethane using a vitrobot. The screening for optimal condition includes changing the following parameters: grid type, grid coating, protein concentration, buffer composition and blotting time. Optimally, a sample for cryo-EM has a lot of well spread particles in different orientations. The ice layer is supposed to be as thin as possible to achieve high contrast between the molecule and the surrounding ice layer, also to minimize the defocus spread.

The first step is the acquisition of high-quality images. Images were collected by 300 kV cryo-electron microscope (Titan Krios) and then processed in cryoSPARC (108). The main steps are the correction of the data by the contrast transfer function (CTF), picking particles and extraction, alignment, and classification of the particles with similar features (2D classification). The best particles were used for generating an initial structure and followed by its refinement, handling of structural heterogeneity and interpretation of final 3D density map. The refinement progress is monitored particularly with the Fourier shell correlation (FSC) curve (109) (Fig. 28).

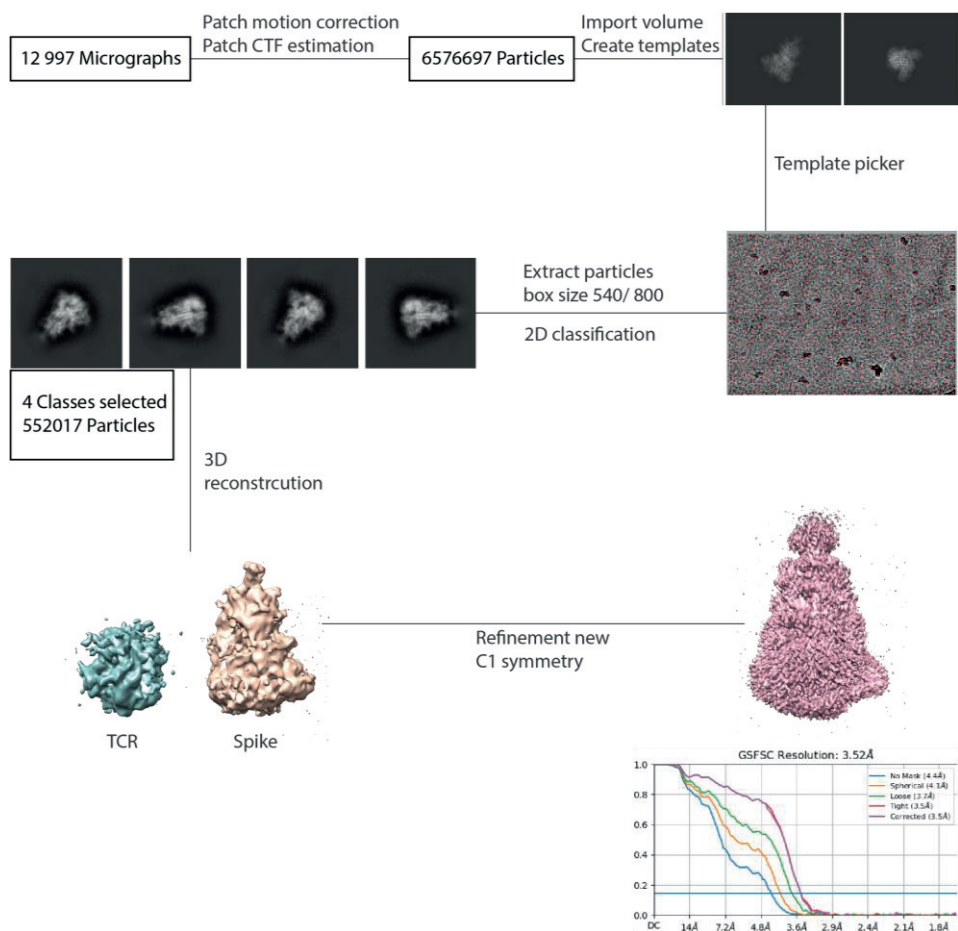


Figure 28: Main steps of cryo-EM data processing (Paper IV).

Single particle cryo-EM in comparison with X-ray crystallography

Even though cryo-EM is rapidly rising there is still a need for the more classical approach of X-ray crystallography. X-ray crystallography has the two main advantages that firstly even very small proteins can be analysed, and secondly very high atomic resolution is reachable. Whereas in cryo-EM, a sample with a molecular mass of at least 50 kDa is needed (110) and only near atomic resolution is reached. The main disadvantages of crystallography compared with cryo-EM are, that more protein sample is needed, and a (well-) diffracting crystal needs to be obtained. Obtaining well-diffracting crystals is harder for more flexible proteins that are non-homogenous and have different conformations. While in cryo-EM, the protein

sample is in solution and does not require crystallization, can have multiple conformations and can be flexible to some extent.

All in all, the two methods can be used complementary. For example, the high-resolution atomic structures obtained by X-ray crystallography can be modelled into cryo-EM density for new complexes.

Concluding remarks and future perspectives

This work has been dedicated to get a deeper understanding of superantigen biology and their interacting partners in human. Still a lot is unresolved, but some important findings were made.

Firstly, an indirect mechanism for $\gamma\delta$ T cells and superantigens was proposed, that relies on monocytes and $\alpha\beta$ T cells. It was observed that cell-cell contact is needed for activity. One of the main functions of $\gamma\delta$ T cells is the priming of $\alpha\beta$ T cells (17). So, one hypothesis would be that $\gamma\delta$ T cells function as antigen presenting cells and present superantigens to $\alpha\beta$ T cells, but this must be proven. Furthermore, human peripheral blood was used in the study, so it can be assumed that most of the $\gamma\delta$ T cells are V γ 9 δ 2, but it was not specifically shown, which variable chains were in the samples and to what extent.

Secondly, a new chimeric $\gamma\delta$ T cell receptor was created, that is stable and easy to purify and was shown to form a complex with the superantigen SEA, which was speculated for more than 20 years. The direct binding of $\gamma\delta$ TCR and SEA needs to be shown with MST or SPR. More biochemical methods like H/D exchange or crosslinking mass spectrometry could be used to further characterize the binding and describe the residues involved. The biological consequences of this binding are not known yet. Furthermore, the $\gamma\delta$ TCR remains an understudied receptor. The $\gamma\delta$ TCR is an unconventional receptor, not only based on its low representation in human but also through its inbetween role being active in innate and adaptive immune response. Moreover, the $\gamma\delta$ TCR recognizes unconventional antigens in an unconventional way that is not MHC restricted. Their role in an immune reaction and the role of their subpopulations is far away from being understood. With this new construct and an easy reproduceable purification protocol, new insights might be won.

Thirdly, the interaction between superantigens (SEA, SEE and SEH) and the cytokine receptor gp130 was further analyzed. It was shown that SEA and LIF bind simultaneously on different binding sites on gp130. Furthermore, it was shown that superantigens interact differently in human than in rodents. Build on our results and literature, we proposed a mechanism for superantigen induced emesis by binding to gp130 on mast cells and a structural model of the gp130-SEA complex was

established. It would be interesting to start a collaboration with researchers working on mast cells or on emesis to prove our hypothesis. Furthermore, it would be of interest to determine an X-ray or a cryo-EM structure of the complex to clarify the details of this interaction and to confirm our findings. Due to the difficulties of obtaining sufficient amounts of gp130 for crystallization, cryo-EM would be the method of choice.

Fourthly, the spike glycoprotein of SARS-CoV-2 was shown to interact with human $\alpha\beta$ TCR. We propose that the binding is specific to TRBV7-9 and that the spike protein binds via its NTD or RBD domain. Our initial cryo-EM data needs further sample optimization to confidently show the TCR-spike complex formation. One way to ensure a complex on the grid would be to use a cross-linked sample for cryo-EM.

This superantigenic character of the spike protein was speculated on, because of its sequence similarity to SEB in a computational study (78). Furthermore, several research groups described an important interaction of the corona virus with T cells and its possible implication in immunity. The classical hallmark of superantigen infection is T cell skewing and was also shown in COVID patients (82,101,102). If this specific TCR is favorable in an infection or increases the risk of a severe disease, needs to be further studied. On one hand, conventional superantigens binding to TCRs leads to a cytokine storm and to an overactivation of the immune system that can be toxic for the host. On the other hand, T cell responses have been associated with reduced disease and might be important for disease control and resolution after primary infection (81). All in all, an atomic structure and more protein-protein interaction studies would be needed to verify our findings. Moreover, it raises interesting questions if other viral proteins might also have superantigenic character. This is still an understudied field with high potential to understand the yet undiscovered mechanism of the immune response to viral infection.

Apart from my papers and manuscripts, during my literature search I crossed path multiple times with Crohn's disease. A connection between my research particularly *Staphylococcal aureus*, superantigens, inflammation of the gastrointestinal (GI) tract, inflammatory bowel disease (IBD), mast cell degranulation and gp130 was made by many research groups, but not really put into context with each other.

IBD is a term for two conditions, namely Crohn's disease and ulcerative colitis that are characterized by chronic inflammation of the gastrointestinal (GI) tract. Crohn's disease can affect any part of the GI tract but is mainly found in the small intestine. Damages appear in patches next to healthy tissue. Common symptoms are abdominal pain, fever, diarrhoea, vomiting, rectal bleeding, weight loss and fatigue. The exact cause of IBD is unknown, but it seems to result from an individual genetic factors, environmental factors, microbiome and a defect in immune response. A

combination of these factors result in the immune system failing to react to bacteria or viruses that cause the inflammation (111).

Already more than 20 years ago it was tried to detect the bacteria *Staphylococcus aureus* in intestinal mucosa to clarify the role in inflammatory bowel disease, particularly Crohn's disease (112). Only in one patient the bacteria were found and the conclusion that staphylococcal superantigens are not involved in Crohn's disease was made. I think one should look for the protein and not the bacteria as it is shown that SAGs are responsible for inflammation.

The connection between gp130 and Crohn's disease has also been discovered (113). It is described that CD patients that carry a high-risk allele, a loss of function mutation in *NOD2*, might benefit from a gp130 blockage. STAT3 has a central role in regulating the expression of *NOD2* risk alleles. Therefore, it was reasoned that the blockage of the upstream receptor gp130 might have a beneficial effect on CD patients (113). Bazedoxifene is a small compound binding to D1 of gp130. Bazedoxifene is used in pancreatic cancer and stops the formation of homodimer of the heterotrimer (IL-6, IL-6R and gp130) (114). It binds close to the D1 binding site of our proposed superantigen-gp130 model (**Paper III**).

Mast cells are found to be involved in IBD and Crohn's disease (115–117). Increased numbers of mast cells were observed in mucosa of the ileum and colon of patients with IBD. Furthermore, an increased expression of TNF- α and IL-16 is seen. Mast cell degranulation is observed and highly elevated histamine and tryptase levels were detected in mucosa of patients with IBD (117). The connection between mast cell degranulation and histamine release and superantigen was also shown and the connection to emesis (96,98) one of the IBD symptoms was made. In **Paper III** we hypothesize that SEA binding to gp130 binding on mast cells results in histamine release and induces emesis.

Furthermore, $\gamma\delta$ T cells were suggested to be a new player in CD pathogenesis (111). Researchers made several observations that $\gamma\delta$ T cells have a key role in defense against infections and wound healing in the gut. Many contradicting observations have been made, so their role in CD remains unclear and $\gamma\delta$ T cells may protect or induce inflammation. One reasoning for these contradictions is that different subtypes of $\gamma\delta$ T cells might have different actions in CD (111).

At this stage one can only speculate if superantigens interaction with gp130 and mast cells and/ or $\gamma\delta$ T cells are involved in the pathogenesis of CD, but I thought it would be worthwhile mentioning it.

Summary

Paper I

Activation of human $\gamma\delta$ T cells and NK cells by Staphylococcal enterotoxin requires both monocytes and conventional T cells

Staphylococcal enterotoxins (SEs) pose a great threat to human health due to their ability to bypass antigen presentation and activate large amounts of conventional T cells resulting in a cytokine storm potentially leading to toxic shock syndrome. Unconventional T- and NK cells are also activated by SE's but the mechanisms remain poorly understood. This study aimed to explore the underlying mechanism behind SE-mediated activation of MAIT-, $\gamma\delta$ T-, and NK cells in vitro. CBMC or PBMC were stimulated with the toxins SEA, SEH, and TSST-1, and cytokine and cytotoxic responses were analysed with ELISA and flow cytometry. All toxins induced a broad range of cytokines, perforin and granzyme B, although SEH was not as potent as SEA and TSST-1. SE-induced IFN- γ expression in MAIT-, $\gamma\delta$ T-, and NK cells was clearly reduced by neutralization of IL-12, while cytotoxic compounds were not affected at all. Kinetic assays showed that unconventional T cell and NK cell-responses are secondary to the response in conventional T cells. Furthermore, co-cultures of isolated cell populations revealed that the ability of SEA to activate $\gamma\delta$ T- and NK cells was fully dependent on the presence of both monocytes and $\alpha\beta$ T cells. Lastly, it was found that SE provoked a reduced and delayed cytokine response in infants, particularly within the unconventional T and NK cell populations. This study provides novel insights regarding the activation of unconventional T- and NK cells by SE, which contribute to understanding of the vulnerability of young children towards Staphylococcus aureus infections.

Paper II

Expression and purification of human $\gamma\delta$ T cell receptor for activity studies

The exact role of $\gamma\delta$ T cells in the immune system is still not resolved. Studies show that $\gamma\delta$ T cells combine features of the conventional adaptive immune system like $\alpha\beta$ T cells, but also rapid innate like responses were observed placing them in the innate immune system. Being able to study these receptors will clarify their distinct function as lymphocytes and shed light into their role in an immune reaction.

The V γ 9 δ 2 T cell receptor (TCR) subset is the most common in human peripheral blood. Here, we report a protocol to produce chimeric $\gamma\delta$ T cell receptor in *Escherichia coli* periplasm using the γ 9 δ 2 as representative. The yield from 1 L of shaker flask culture of each TCR was to approximately 8,5 mg of purified and refolded TCR protein. Using this protocol will enable to refold and purify ca. 5 % of the inclusion bodies. This set up will enable crystallographic, thermodynamic, and other biophysical studies of $\gamma\delta$ TCRs that require vast amounts of homogeneous material to clarify its role in the human immune system. Furthermore, the interaction of $\gamma\delta$ TCRs and the superantigen SEA is investigated.

Paper III

Analyses of the complex formation of staphylococcal enterotoxin A and the human gp130 cytokine receptor

Superantigens (SAGs) are bacterial enterotoxins produced by *Staphylococcus aureus*. Staphylococcal enterotoxin type A (SEA), a staphylococcal superantigen, has been shown to bind to the cytokine signalling receptor glycoprotein 130 (gp130). The structural details, as well as the exact physiological role of this interaction, remain unclear. Here, we describe the structural details of the SEA-gp130 complex by combining crosslinking mass spectrometry and computational modelling. Interestingly, SEA is not able to bind gp130-homologues from rat and mouse. Our data suggest that SEA may interact with human gp130 in a different manner than other known gp130-ligands. Moreover, the fact that SEA does not bind mouse or rat gp130 suggests that SAGs have additional mechanisms of action in humans.

Paper IV

Structural basis for T cell receptor recognition by SARS-CoV-2 glycoprotein

The SARS-CoV-2 outbreak has been declared to be a worldwide pandemic. However, there are many unknowns about the T cell-mediated immune responses to SARS-CoV-2 infection. Interestingly, it has been reported that SARS-CoV-2 causes a skewing of the T cell repertoire in patients during infection. Analogously, bacterial toxins called superantigens are well-known to cause T cell skewing upon activation. Here, we present data supporting that the spike glycoprotein of SARS-CoV-2 can act as a superantigen and bind to the T cell receptor (TCR) in a germline encoded manner and thus cause T cell repertoire skewing. The spike glycoprotein was found to specifically bind directly to T cell receptors expressing the TRBV7-9 sequences. In addition, cross-linking mass spectrometry in

combination with initial single particle cryo-EM data suggest that the TCR interacts with the S1 domain of the spike glycoproteins, likely in between the N-terminal domain and the receptor binding domain. This extraordinary data suggests an explanation to why there are large individual differences upon SARS-CoV-2 infection, as each person has its unique germline encoded T cell profile and thus express different TRBV sequences. Still, the single particle cryo-EM data presented here needs to be further optimized to fully support the hypothesis presented.

References

1. Owen, J. A., Punt, J., Stranford, S. A. and Jones, P. P. *et al.* (2019) *Kuby immunology*. New York: Macmillan education.
2. Janeway, C. A. and Medzhitov, R. (2002) 'Innate immune recognition', *Annual review of immunology*, 20: 197–216.
3. Beutler, B. (2004) 'Innate immunity: an overview', *Molecular immunology*, 40/12: 845–59.
4. Turvey, S. E. and Broide, D. H. (2010) 'Innate immunity', *The Journal of allergy and clinical immunology*, 125/2 Suppl 2: S24–32.
5. Parker, D. C. (1993) 'T cell-dependent B cell activation', *Annual review of immunology*, 11: 331–60.
6. Swain, S. L. (1983) 'T cell subsets and the recognition of MHC class', *Immunological reviews*, 74: 129–42.
7. Meuer, S. C., Schlossman, S. F. and Reinherz, E. L. (1982) 'Clonal analysis of human cytotoxic T lymphocytes: T4+ and T8+ effector T cells recognize products of different major histocompatibility complex regions', *Proceedings of the National Academy of Sciences of the United States of America*, 79/14: 4395–9.
8. Swain, S. L., McKinstry, K. K. and Strutt, T. M. (2012) 'Expanding roles for CD4⁺ T cells in immunity to viruses', *Nature reviews. Immunology*, 12/2: 136–48.
9. Reinherz, E. L. and Schlossman, S. F. (1980) 'The differentiation and function of human T lymphocytes', *Cell*, 19/4: 821–7.
10. van der Merwe, P. A. and Davis, S. J. (2003) 'Molecular interactions mediating T cell antigen recognition', *Annual review of immunology*, 21: 659–84.
11. Smith-Garvin, J. E., Koretzky, G. A. and Jordan, M. S. (2009) 'T cell activation', *Annual review of immunology*, 27: 591–619.
12. Ladel, C. H., Blum, C., Dreher, A. and Reifenberg, K. *et al.* (1995) 'Protective role of gamma/delta T cells and alpha/beta T cells in tuberculosis', *European journal of immunology*, 25/10: 2877–81.
13. Boismenu, R. and Havran, W. L. (1997) 'An innate view of $\gamma\delta$ T cells', *Current Opinion in Immunology*, 9/1: 57–63.

14. Born, W. K., Kemal Aydinoglu, M. and O'Brien, R. L. (2013) 'Diversity of $\gamma\delta$ T-cell antigens', *Cellular & molecular immunology*, 10/1: 13–20.
15. Neefjes, J., Jongstra, M. L. M., Paul, P. and Bakke, O. (2011) 'Towards a systems understanding of MHC class I and MHC class II antigen presentation', *Nature reviews. Immunology*, 11/12: 823–36.
16. He, Y., Wu, K., Hu, Y. and Sheng, L. *et al.* (2014) ' $\gamma\delta$ T cell and other immune cells crosstalk in cellular immunity', *Journal of immunology research*, 2014: 960252.
17. Vantourout, P. and Hayday, A. (2013) 'Six-of-the-best: unique contributions of $\gamma\delta$ T cells to immunology', *Nature reviews. Immunology*, 13/2: 88–100.
18. da Silva, E. Z. M., Jamur, M. C. and Oliver, C. (2014) 'Mast cell function: a new vision of an old cell', *The journal of histochemistry and cytochemistry : official journal of the Histochemistry Society*, 62/10: 698–738.
19. Garcia, K. C., Degano, M., Stanfield, R. L. and Brunmark, A. *et al.* (1996) 'An $\alpha\beta$ T cell receptor structure at 2.5 Å and its orientation in the TCR-MHC complex', *Science (New York, N.Y.)*, 274/5285: 209–19.
20. Churchill, H. R., Andersen, P. S., Parke, E. A. and Mariuzza, R. A. *et al.* (2000) 'Mapping the energy of superantigen Staphylococcus enterotoxin C3 recognition of an $\alpha\beta$ T cell receptor using alanine scanning mutagenesis', *The Journal of experimental medicine*, 191/5: 835–46.
21. Morath, A. and Schamel, W. W. (2020) ' $\alpha\beta$ and $\gamma\delta$ T cell receptors: Similar but different', *Journal of leukocyte biology*.
22. Gao, Y. and Williams, A. P. (2015) 'Role of Innate T Cells in Anti-Bacterial Immunity', *Frontiers in immunology*, 6: 302.
23. Akdis, M., Aab, A., Altunbulakli, C. and Azkur, K. *et al.* (2016) 'Interleukins (from IL-1 to IL-38), interferons, transforming growth factor β , and TNF- α : Receptors, functions, and roles in diseases', *The Journal of allergy and clinical immunology*, 138/4: 984–1010.
24. Boulanger, M. J., Bankovich, A. J., Kortemme, T. and Baker, D. *et al.* (2003) 'Convergent Mechanisms for Recognition of Divergent Cytokines by the Shared Signaling Receptor gp130', *Molecular Cell*, 12/3: 577–89.
25. Taga, T., Hibi, M., Hirata, Y. and Yamasaki, K. *et al.* (1989) 'Interleukin-6 triggers the association of its receptor with a possible signal transducer, gp130', *Cell*, 58/3: 573–81.
26. Boulanger, M. J. and Garcia, K.C. (2004). 'Shared Cytokine Signaling Receptors: Structural Insights from the Gp130 System'. In: *Cell Surface Receptors*., pp. 107–46: Elsevier.
27. Taga, T. and Kishimoto, T. (1997) 'Gp130 and the interleukin-6 family of cytokines', *Annual review of immunology*, 15: 797–819.

28. Bravo, J., Staunton, D., Heath, J. K. and Jones, E. Y. (1998) 'Crystal structure of a cytokine-binding region of gp130', *The EMBO journal*, 17/6: 1665–74.
29. Xu, Y., Garrett, T.P.J. and Zhang, J. G. (2010) *Crystal structure of the full ectodomain of human gp130: New insights into the molecular assembly of receptor complexes*.
30. Boulanger, M. J., Chow, D.-c., Brevnova, E. E. and Garcia, K. C. (2003) 'Hexameric structure and assembly of the interleukin-6/IL-6 alpha-receptor/gp130 complex', *Science (New York, N.Y.)*, 300/5628: 2101–4.
31. Kishimoto, T., Tanaka, T., Yoshida, K. and Akira, S. *et al.* (1995) 'Cytokine signal transduction through a homo- or heterodimer of gp130', *Annals of the New York Academy of Sciences*, 766: 224–34.
32. Heinrich, P. C., Behrmann, I., Müller-Newen, G. and Schaper, F. *et al.* (1998) 'Interleukin-6-type cytokine signalling through the gp130/Jak/STAT pathway', *The Biochemical journal*, 334 (Pt 2): 297–314.
33. Kotb, M. (1995) 'Bacterial pyrogenic exotoxins as superantigens', *Clinical microbiology reviews*, 8/3: 411–26.
34. McCormick, J. K., Yarwood, J. M. and Schlievert, P. M. (2001) 'Toxic shock syndrome and bacterial superantigens: an update', *Annual review of microbiology*, 55: 77–104.
35. Fleischer, B. and Schrezenmeier, H. (1988) 'T cell stimulation by staphylococcal enterotoxins. Clonally variable response and requirement for major histocompatibility complex class II molecules on accessory or target cells', *The Journal of experimental medicine*, 167/5: 1697–707.
36. Choi, Y. W., Kotzin, B., Herron, L. and Callahan, J. *et al.* (1989) 'Interaction of Staphylococcus aureus toxin "superantigens" with human T cells', *Proceedings of the National Academy of Sciences of the United States of America*, 86/22: 8941–5.
37. STEVENS, F. A. (1927) 'THE OCCURRENCE OF STAPHYLOCOCCUS AUREUS INFECTION WITH A SCARLATINIFORM RASH', *JAMA: The Journal of the American Medical Association*, 88/25: 1957.
38. Lowy, F. D. (1998) 'Staphylococcus aureus infections', *The New England journal of medicine*, 339/8: 520–32.
39. Fraser, J. D. and Proft, T. (2008) 'The bacterial superantigen and superantigen-like proteins', *Immunological reviews*, 225: 226–43.
40. Langford, M. P., Stanton, G. J. and Johnson, H. M. (1978) 'Biological effects of staphylococcal enterotoxin A on human peripheral lymphocytes', *Infection and immunity*, 22/1: 62–8.
41. Todd, J., Fishaut, M., Kapral, F. and Welch, T. (1978) 'TOXIC-SHOCK SYNDROME ASSOCIATED WITH PHAGE-GROUP-I STAPHYLOCOCCI', *Lancet (London, England)*, 312/8100: 1116–8.
42. TRANTER, D. (1990) 'Foodborne staphylococcal illness', *Lancet (London, England)*, 336/8722: 1044–6.

43. Le Loir, Y., Baron, F. and Gautier, M. (2003) 'Staphylococcus aureus and food poisoning', *Genetics and molecular research : GMR*, 2/1: 63–76.
44. BERGDOLL, M. S., SURGALLA, M. J. and DACK, G. M. (1959) 'Staphylococcal enterotoxin. Identification of a specific precipitating antibody with enterotoxin-neutralizing property', *Journal of immunology (Baltimore, Md. : 1950)*, 83: 334–8.
45. CASMAN, E. P. and BENNETT, R. W. (1965) 'DETECTION OF STAPHYLOCOCCAL ENTEROTOXIN IN FOOD', *Applied microbiology*, 13: 181–9.
46. Spaulding, A. R., Salgado-Pabón, W., Kohler, P. L. and Horswill, A. R. *et al.* (2013) 'Staphylococcal and streptococcal superantigen exotoxins', *Clinical microbiology reviews*, 26/3: 422–47.
47. Marrack, P. and Kappler, J. (1990) 'The staphylococcal enterotoxins and their relatives', *Science (New York, N. Y.)*, 248/4959: 1066.
48. Swaminathan, S., Furey, W., Pletcher, J. and Sax, M. (1992) 'Crystal structure of staphylococcal enterotoxin B, a superantigen', *Nature*, 359/6398: 801–6.
49. Schad, E. M., Zaitseva, I., Zaitsev, V. N. and Dohlsten, M. *et al.* (1995) 'Crystal structure of the superantigen staphylococcal enterotoxin type A', *The EMBO journal*, 14/14: 3292–301.
50. Rödström, K. E. J., Regenthal, P., Bahl, C. and Ford, A. *et al.* (2016) 'Two common structural motifs for TCR recognition by staphylococcal enterotoxins', *Scientific reports*, 6: 25796.
51. Håkansson, M., Petersson, K., Nilsson, H. and Forsberg, G. *et al.* (2000) 'The crystal structure of staphylococcal enterotoxin H: implications for binding properties to MHC class II and TcR molecules', *Journal of molecular biology*, 302/3: 527–37.
52. Sundström, M., Hallén, D., Svensson, A. and Schad, E. *et al.* (1996) 'The Co-crystal structure of staphylococcal enterotoxin type A with Zn²⁺ at 2.7 Å resolution. Implications for major histocompatibility complex class II binding', *The Journal of biological chemistry*, 271/50: 32212–6.
53. Fraser, J. D. (1989) 'High-affinity binding of staphylococcal enterotoxins A and B to HLA-DR', *Nature*, 339/6221: 221–3.
54. Hudson, K. R., Tiedemann, R. E., Urban, R. G. and Lowe, S. C. *et al.* (1995) 'Staphylococcal enterotoxin A has two cooperative binding sites on major histocompatibility complex class II', *The Journal of experimental medicine*, 182/3: 711–20.
55. Abrahmsén, L., Dohlsten, M., Segrén, S. and Björk, P. *et al.* (1995) 'Characterization of two distinct MHC class II binding sites in the superantigen staphylococcal enterotoxin A', *The EMBO journal*, 14/13: 2978–86.
56. Petersson, K., Thunnissen, M., Forsberg, G. and Walse, B. (2002) 'Crystal Structure of a SEA Variant in Complex with MHC Class II Reveals the Ability of SEA to Crosslink MHC Molecules', *Structure*, 10/12: 1619–26.

57. Li, Y., Li, H., Dimasi, N. and McCormick, J. K. *et al.* (2001) 'Crystal Structure of a Superantigen Bound to the High-Affinity, Zinc-Dependent Site on MHC Class II', *Immunity*, 14/1: 93–104.
58. Petersson, K., Håkansson, M., Nilsson, H. and Forsberg, G. *et al.* (2001) 'Crystal structure of a superantigen bound to MHC class II displays zinc and peptide dependence', *The EMBO journal*, 20/13: 3306–12.
59. Petersson, K., Pettersson, H., Skartved, N. J. and Walse, B. *et al.* (2003) 'Staphylococcal enterotoxin H induces V alpha-specific expansion of T cells', *Journal of immunology (Baltimore, Md. : 1950)*, 170/8: 4148–54.
60. White, J., Herman, A., Pullen, A. M. and Kubo, R. *et al.* (1989) 'The V beta-specific superantigen staphylococcal enterotoxin B: stimulation of mature T cells and clonal deletion in neonatal mice', *Cell*, 56/1: 27–35.
61. Wang, L., Zhao, Y., Li, Z. and Guo, Y. *et al.* (2007) 'Crystal structure of a complete ternary complex of TCR, superantigen and peptide-MHC', *Nature structural & molecular biology*, 14/2: 169–71.
62. Rödström, K. E. J., Elbing, K. and Lindkvist-Petersson, K. (2014) 'Structure of the superantigen staphylococcal enterotoxin B in complex with TCR and peptide-MHC demonstrates absence of TCR-peptide contacts', *Journal of immunology (Baltimore, Md. : 1950)*, 193/4: 1998–2004.
63. Saha, B., Harlan, D. M., Lee, K. P. and June, C. H. *et al.* (1996) 'Protection against lethal toxic shock by targeted disruption of the CD28 gene', *The Journal of experimental medicine*, 183/6: 2675–80.
64. Mittrücker, H. W., Shahinian, A., Bouchard, D. and Kündig, T. M. *et al.* (1996) 'Induction of unresponsiveness and impaired T cell expansion by staphylococcal enterotoxin B in CD28-deficient mice', *The Journal of experimental medicine*, 183/6: 2481–8.
65. Arad, G., Levy, R., Nasie, I. and Hillman, D. *et al.* (2011) 'Binding of superantigen toxins into the CD28 homodimer interface is essential for induction of cytokine genes that mediate lethal shock', *PLoS biology*, 9/9: e1001149.
66. Schlievert, P. M., Cahill, M. P., Hostager, B. S. and Brosnahan, A. J. *et al.* (2019) 'Staphylococcal Superantigens Stimulate Epithelial Cells through CD40 To Produce Chemokines', *mBio*, 10/2.
67. Li, Z., Zeppa, J. J., Hancock, M. A. and McCormick, J. K. *et al.* (2018) 'Staphylococcal Superantigens Use LAMA2 as a Coreceptor To Activate T Cells', *Journal of immunology (Baltimore, Md. : 1950)*, 200/4: 1471–9.
68. Banke, E., Rödström, K., Ekelund, M. and Dalla-Riva, J. *et al.* (2014) 'Superantigen activates the gp130 receptor on adipocytes resulting in altered adipocyte metabolism', *Metabolism: clinical and experimental*, 63/6: 831–40.
69. Choi, Y. W., Herman, A., DiGiusto, D. and Wade, T. *et al.* (1990) 'Residues of the variable region of the T-cell-receptor beta-chain that interact with *S. aureus* toxin superantigens', *Nature*, 346/6283: 471–3.

70. Fields, B. A., Malchiodi, E. L., Li, H. and Ysern, X. *et al.* (1996) 'Crystal structure of a T-cell receptor beta-chain complexed with a superantigen', *Nature*, 384/6605: 188–92.
71. Kappler, J., Kotzin, B., Herron, L. and Gelfand, E. W. *et al.* (1989) 'V beta-specific stimulation of human T cells by staphylococcal toxins', *Science (New York, N.Y.)*, 244/4906: 811–3.
72. Stern, L. J. (1994) *CRYSTAL STRUCTURE OF THE HUMAN CLASS II MHC PROTEIN HLA-DR1 COMPLEXED WITH AN INFLUENZA VIRUS PEPTIDE*.
73. Fraser, J. D., Urban, R. G., Strominger, J. L. and Robinson, H. (1992) 'Zinc regulates the function of two superantigens', *Proceedings of the National Academy of Sciences of the United States of America*, 89/12: 5507–11.
74. Mehindate, K., Thibodeau, J., Dohlsten, M. and Kalland, T. *et al.* (1995) 'Cross-linking of major histocompatibility complex class II molecules by staphylococcal enterotoxin A superantigen is a requirement for inflammatory cytokine gene expression', *The Journal of experimental medicine*, 182/5: 1573–7.
75. Tiedemann, R. E. and Fraser, J. D. (1996) 'Cross-linking of MHC class II molecules by staphylococcal enterotoxin A is essential for antigen-presenting cell and T cell activation', *Journal of immunology (Baltimore, Md. : 1950)*, 157/9: 3958–66.
76. Pumphrey, N., Vuidepot, A., Jakobsen, B. and Forsberg, G. *et al.* (2007) 'Cutting edge: Evidence of direct TCR alpha-chain interaction with superantigen', *Journal of immunology (Baltimore, Md. : 1950)*, 179/5: 2700–4.
77. Saline, M., Rödström, K. E. J., Fischer, G. and Orekhov, V. Y. *et al.* (2010) 'The structure of superantigen complexed with TCR and MHC reveals novel insights into superantigenic T cell activation', *Nature communications*, 1: 119.
78. Cheng, M. H., Zhang, S., Porritt, R. A. and Noval Rivas, M. *et al.* (2020) 'Superantigenic character of an insert unique to SARS-CoV-2 spike supported by skewed TCR repertoire in patients with hyperinflammation', *Proceedings of the National Academy of Sciences of the United States of America*, 117/41: 25254–62.
79. Li, T., Qiu, Z., Zhang, L. and Han, Y. *et al.* (2004) 'Significant changes of peripheral T lymphocyte subsets in patients with severe acute respiratory syndrome', *The Journal of infectious diseases*, 189/4: 648–51.
80. Dan, J. M., Mateus, J., Kato, Y. and Hastie, K. M. *et al.* (2021) 'Immunological memory to SARS-CoV-2 assessed for up to 8 months after infection', *Science (New York, N.Y.)*, 371/6529.
81. Rydzynski Moderbacher, C., Ramirez, S. I., Dan, J. M. and Grifoni, A. *et al.* (2020) 'Antigen-Specific Adaptive Immunity to SARS-CoV-2 in Acute COVID-19 and Associations with Age and Disease Severity', *Cell*, 183/4: 996-1012.e19.
82. Grifoni, A., Weiskopf, D., Ramirez, S. I. and Mateus, J. *et al.* (2020) 'Targets of T Cell Responses to SARS-CoV-2 Coronavirus in Humans with COVID-19 Disease and Unexposed Individuals', *Cell*, 181/7: 1489-1501.e15.

83. Hoffmann, M., Kleine-Weber, H., Schroeder, S. and Krüger, N. *et al.* (2020) 'SARS-CoV-2 Cell Entry Depends on ACE2 and TMPRSS2 and Is Blocked by a Clinically Proven Protease Inhibitor', *Cell*, 181/2: 271-280.e8.
84. Huang, Y., Yang, C., Xu, X.-F. and Xu, W. *et al.* (2020) 'Structural and functional properties of SARS-CoV-2 spike protein: potential antiviral drug development for COVID-19', *Acta pharmacologica Sinica*, 41/9: 1141-9.
85. Harris, T. O., Grossman, D., Kappler, J. W. and Marrack, P. *et al.* (1993) 'Lack of complete correlation between emetic and T-cell-stimulatory activities of staphylococcal enterotoxins', *Infection and immunity*, 61/8: 3175-83.
86. Bertotto, A., Spinozzi, F., Gerli, R. and Bassotti, G. *et al.* (1995) 'Peripheral blood gamma delta T cells in human listeriosis', *Acta paediatrica (Oslo, Norway : 1992)*, 84/12: 1434-5.
87. Rust, C. J., Verreck, F., Vietor, H. and Koning, F. (1990) 'Specific recognition of staphylococcal enterotoxin A by human T cells bearing receptors with the V gamma 9 region', *Nature*, 346/6284: 572-4.
88. Morita, C. T., Li, H., Lamphear, J. G. and Rich, R. R. *et al.* (2001) 'Superantigen Recognition by $\gamma\delta$ T Cells', *Immunity*, 14/3: 331-44.
89. Rust, C. J. and Koning, F. (1993) 'Gamma delta T cell reactivity towards bacterial superantigens', *Seminars in immunology*, 5/1: 41-6.
90. Bigby, M., Markowitz, J. S., Bleicher, P. A. and Grusby, M. J. *et al.* (1993) 'Most gamma delta T cells develop normally in the absence of MHC class II molecules', *Journal of immunology (Baltimore, Md. : 1950)*, 151/9: 4465-75.
91. Groh, V., Steinle, A., Bauer, S. and Spies, T. (1998) 'Recognition of stress-induced MHC molecules by intestinal epithelial gammadelta T cells', *Science (New York, N.Y.)*, 279/5357: 1737-40.
92. Kierkels, G. J. J., Scheper, W., Meringa, A. D. and Johanna, I. *et al.* (2019) 'Identification of a tumor-specific allo-HLA-restricted $\gamma\delta$ TCR', *Blood advances*, 3/19: 2870-82.
93. Matis, L. A., Fry, A. M., Cron, R. Q. and Cotterman, M. M. *et al.* (1989) 'Structure and specificity of a class II MHC alloreactive gamma delta T cell receptor heterodimer', *Science (New York, N.Y.)*, 245/4919: 746-9.
94. Boulter, J. M., Glick, M., Todorov, P. T. and Baston, E. *et al.* (2003) 'Stable, soluble T-cell receptor molecules for crystallization and therapeutics', *Protein engineering*, 16/9: 707-11.
95. Noli Truant, S., Marzi, M. C. de, Sarratea, M. B. and Antonoglou, M. B. *et al.* (2019) 'egc Superantigens Impair Monocytes/Macrophages Inducing Cell Death and Inefficient Activation', *Frontiers in immunology*, 10: 3008.
96. Hu, D. L., Omoe, K., Shimura, H. and Ono, K. *et al.* (1999) 'Emesis in the shrew mouse (*Suncus murinus*) induced by peroral and intraperitoneal administration of staphylococcal enterotoxin A', *Journal of food protection*, 62/11: 1350-3.

97. Hu, D.-L., Omoe, K., Shimoda, Y. and Nakane, A. *et al.* (2003) 'Induction of emetic response to staphylococcal enterotoxins in the house musk shrew (*Suncus murinus*)', *Infection and immunity*, 71/1: 567–70.
98. Ono, H. K., Hirose, S., Narita, K. and Sugiyama, M. *et al.* (2019) 'Histamine release from intestinal mast cells induced by staphylococcal enterotoxin A (SEA) evokes vomiting reflex in common marmoset', *PLoS pathogens*, 15/5: e1007803.
99. Hovde, C. J., Marr, J. C., Hoffmann, M. L. and Hackett, S. P. *et al.* (1994) 'Investigation of the role of the disulphide bond in the activity and structure of staphylococcal enterotoxin C1', *Molecular microbiology*, 13/5: 897–909.
100. Hu, D.-L., Omoe, K., Sashinami, H. and Shinagawa, K. *et al.* (2009) 'Immunization with a nontoxic mutant of staphylococcal enterotoxin A, SEAD227A, protects against enterotoxin-induced emesis in house musk shrews', *The Journal of infectious diseases*, 199/3: 302–10.
101. Zhang, F., Gan, R., Zhen, Z. and Hu, X. *et al.* (2020) 'Adaptive immune responses to SARS-CoV-2 infection in severe versus mild individuals', *Signal transduction and targeted therapy*, 5/1: 156.
102. Shomuradova, A. S., Vagida, M. S., Sheetikov, S. A. and Zornikova, K. V. *et al.* (2020) 'SARS-CoV-2 Epitopes Are Recognized by a Public and Diverse Repertoire of Human T Cell Receptors', *Immunity*, 53/6: 1245-1257.e5.
103. Mascellino, M. T., Di Timoteo, F., Angelis, M. de and Oliva, A. (2021) 'Overview of the Main Anti-SARS-CoV-2 Vaccines: Mechanism of Action, Efficacy and Safety', *Infection and drug resistance*, 14: 3459–76.
104. Chow, D., He, X., Snow, A. L. and Rose-John, S. *et al.* (2001) *CRYSTAL STRUCTURE OF A CYTOKINE/RECEPTOR COMPLEX*.
105. Scarff, C. A., Fuller, M. J. G., Thompson, R. F. and Iadanza, M. G. (2018) 'Variations on Negative Stain Electron Microscopy Methods: Tools for Tackling Challenging Systems', *Journal of visualized experiments : JoVE*, 132.
106. Ohi, M., Li, Y., Cheng, Y. and Walz, T. (2004) 'Negative Staining and Image Classification - Powerful Tools in Modern Electron Microscopy', *Biological procedures online*, 6: 23–34.
107. Hebert, H. (2019) 'CryoEM: a crystals to single particles round-trip', *Current opinion in structural biology*, 58: 59–67.
108. Punjani, A., Rubinstein, J. L., Fleet, D. J. and Brubaker, M. A. (2017) 'cryoSPARC: algorithms for rapid unsupervised cryo-EM structure determination', *Nature methods*, 14/3: 290–6.
109. Cheng, Y., Grigorieff, N., Penczek, P. A. and Walz, T. (2015) 'A primer to single-particle cryo-electron microscopy', *Cell*, 161/3: 438–49.
110. Liu, Y., Huynh, D. T. and Yeates, T. O. (2019) 'A 3.8 Å resolution cryo-EM structure of a small protein bound to an imaging scaffold', *Nature communications*, 10/1: 1864.

111. Catalan-Serra, I., Sandvik, A. K., Bruland, T. and Andreu-Ballester, J. C. (2017) 'Gammadelta T Cells in Crohn's Disease: A New Player in the Disease Pathogenesis?', *Journal of Crohn's & colitis*, 11/9: 1135–45.
112. M. Chiba, S. H. M. K. M. T. (2001) 'Staphylococcus aureus in Inflammatory Bowel Disease', *Scandinavian Journal of Gastroenterology*, 36/6: 615–20.
113. Nayar, S., Morrison, J. K., Giri, M. and Gettler, K. *et al.* (2021) 'A myeloid-stromal niche and gp130 rescue in NOD2-driven Crohn's disease', *Nature*, 593/7858: 275–81.
114. Burkhardt, C., Bühler, L., Tihy, M. and Morel, P. *et al.* (2019) 'Bazedoxifene as a novel strategy for treatment of pancreatic and gastric adenocarcinoma', *Oncotarget*, 10/34: 3198–202.
115. Lloyd, G., Green, F. H., Fox, H. and Mani, V. *et al.* (1975) 'Mast cells and immunoglobulin E in inflammatory bowel disease', *Gut*, 16/11: 861–5.
116. Wouters, M. M., Vicario, M. and Santos, J. (2016) 'The role of mast cells in functional GI disorders', *Gut*, 65/1: 155–68.
117. He, S.-H. (2004) 'Key role of mast cells and their major secretory products in inflammatory bowel disease', *World Journal of Gastroenterology*, 10/3: 309–18.

Figure references

Cover picture: Created with BioRender.com and Adobe Illustrator

Figure 1/2/3/4/5/6/13/15/25/26/27: Created with BioRender.com

Figure 8: Staphylococcus aureus. Photography. Britannica ImageQuest, Encyclopædia Britannica, 25 May 2016.
quest.eb.com/search/139_1910890/1/139_1910890/cite. Accessed 3 Feb 2022.

Figure 7/9/10/11/12/18/20/21/23/24: Created with PyMOL2

Figure 14/15/17/19/22: Created with GraphPad Prism 9

Figure 20/24: Created with Xvis

Figure 23: Created with Photoshop

Figure 28: Created with CryoSPARC and UCSF Chimera

All figure compositions with multiple figures: Created in Adobe Illustrator.

Acknowledgements

I would like to thank my main supervisor **Karin Lindkvist** for the great and life-changing opportunity to do my PhD studies in Lund University. She encouraged and pushed me through 5 years of learning and growth. I also picked up some soft skills like how to write “nicer” e-mails.

My co-supervisor and friend **Raminta** supported me in lab and in life.

Pontus and **Pål** gave constructive criticism in meetings.

Hannah, my officemate, partner in crime and radårpar you made it feel like home in our tiny office. You always lightened up even my darkest days with your accepting and kind nature. My time in Lund would not have been the same without you! Young **Peng** is never short of wisdom and was always checking if my day was fun, interesting, and exciting. **Ping** is one of the most honest people I met and never let me forget that there is a gym upstairs that I could go to. **Niloofar** always had some kind words to say and was up for a cup of nice tea. **Sofia** is a real trend-setter and always knew what to eat or where to buy or what course to go to. **Serena** was my first friend in Lund. I really enjoyed our weekend exploration trips in Skåne. It was nice to have **Jesper**, **Charly**, **Kamil**, **Sandra**, **Emma**, and **Markel** for a while here.

My neighbours in BMC, the Italians: **Rita**, **Tommaso** and **Anna** were always my loving emotional support and care system. They cooked for me more times than I can count, thought me how to be a bit politer and introduced me to some italian words and habits. I really enjoyed our dinners. Special thanks to Anna and **Lotta** for helping me to finish my manuscripts in time. I admire how efficient you both are. **Oktawia**, the booker, I had some fun lunch conversations with you.

Our other neighbours, the clinical people, were initially hard to get to (not that I really tried, but luckily other people did).

Ton and **Giuseppe** brought some southern flair and charm to the floor and thanks for drilling in my apartment through these super thick walls. Life without curtains on ground floor would just not be the same.

Thanks for the nice after-works **Larissa** and **Karim**. **Jakob** and **Mattias** were always very fun and interesting to talk to.

All the other ones, especially **Somadri**, **Saskia**, **Maria R.**, **Maria M.N.**, **Qirui**, **Katrin**, **Niklas**, **Claire**, **Naveen**, **Ram** and **Efe** it was nice to have you around.

Thanks, for all the fika clinical people. I'm especially very grateful that BMC did not close the gym and sauna during the pandemic. It was the only social activity there was for a long time, and I could meet nice people like **Martin**, the **two Christians** and **Mattias**, that were really nice to hang out with.

My Erasmus friends **Yones** and **Luka**, I'm happy to have you boys in my life. Always have so much fun on our trips!

Thanks **Mandy**, **Louise**, **Sebastian**, **Andreas**, **Alma**, and **Aaron** for the great parties and get togethers.

Meine **Eltern** haben mich immer so gut wie möglich unterstützt, auch wenn es Differenzen gab, wurde immer alles ermöglicht. Ich kann mich glücklich schätzen so warmherzige Eltern zu haben.

Meine Schwester **Selin** ist die wichtigste Person in meinem Leben und hat mich immer herausgefordert so gut wie möglich zu sein und alles zu geben und mich unterstützt, wenn es mal nicht so gut lief, auch wenn sie nicht die sensibelste Person ist. Mein Bruder **Kaan** hat mich schon immer zum Lachen gebracht. Danke, an mein mini-me **Dilara**. Ihr seid mir lieb und teuer. :D <3

Ich habe das Glück viele verschiedene und auf ihre eigne Weise tolle Cousins & Cousinen zu haben. Danke **Melisa**, **Ilayda**, **Yonca**, **Aydan**, **Volkan**, **Hülya**, **Çağla**, **Özde**, **Cenk**...usw. Danke auch an **Nuray teyze** und meine **Hala** für alles.

Meine Freundin **Nadiescha** hat mich schon immer mit ihrer Lebensfreude und Liebenswürdigkeit angesteckt. Cool, dass wir es noch nach Budapest geschafft haben, bevor du schwanger wurdest. **Tobi** und **Sonja** danke für eure andauernde Freundschaft und für die warmen Worte die ihr immer für mich übrig habt.

Meine Unizeit in Bochum hätte gar nicht besser sein können. Ich hatte unglaublich viel Spaß. Danke **Lena**, **Marvin**, **Gadu**, **Ramona**, **Felix**, **Nick**, **Christian**, **Debbo**, **Kaibo** und **Luk**.

Ohne **Sven** wäre ich definitiv nicht so weit gekommen. Du hast mir alles gegeben was dafür nötig war und mein Leben bereichert. Danke!



Paper I



Activation of human $\gamma\delta$ T cells and NK cells by Staphylococcal enterotoxins requires both monocytes and conventional T cells

Manuel Mata Forsberg¹ | Claudia Arasa¹ | Willemien van Zwol¹ | Sibel Uzunçayir² | Anna Schönbichler¹ | Paulina Regenthal² | Jenny Schelin³ | Karin Lindkvist-Petersson² | Sophia Björkander¹ | Eva Sverremark-Ekström¹

¹ Department of Molecular Biosciences, The Wenner-Gren Institute, Stockholm University, Stockholm, Sweden

² Department of Experimental Medical Science, Lund University, Lund, Sweden

³ Division of Applied Microbiology, Department of Chemistry, Lund University, Lund, Sweden

Correspondence

Manuel Mata Forsberg, Department of Molecular Biosciences, The Wenner-Gren Institute, Svante Arrhenius väg 20C, SE 106 91, Stockholm, Sweden.

Email: manuel.forsberg@su.se

Professor Eva Sverremark-Ekström, Department of Molecular Biosciences, The Wenner-Gren Institute, Svante Arrhenius väg 20C, SE 106 91, Stockholm, Sweden

Email: eva.sverremark@su.se

Abstract

Staphylococcal enterotoxins (SE) pose a great threat to human health due to their ability to bypass antigen presentation and activate large amounts of conventional T cells resulting in a cytokine storm potentially leading to toxic shock syndrome. Unconventional T- and NK cells are also activated by SE but the mechanisms remain poorly understood. In this study, the authors aimed to explore the underlying mechanism behind SE-mediated activation of MAIT-, $\gamma\delta$ T-, and NK cells *in vitro*. CBMC or PBMC were stimulated with the toxins SEA, SEH, and TSST-1, and cytokine and cytotoxic responses were analyzed with ELISA and flow cytometry. All toxins induced a broad range of cytokines, perforin and granzyme B, although SEH was not as potent as SEA and TSST-1. SE-induced IFN- γ expression in MAIT-, $\gamma\delta$ T-, and NK cells was clearly reduced by neutralization of IL-12, while cytotoxic compounds were not affected at all. Kinetic assays showed that unconventional T cell and NK cell-responses are secondary to the response in conventional T cells. Furthermore, co-cultures of isolated cell populations revealed that the ability of SEA to activate $\gamma\delta$ T- and NK cells was fully dependent on the presence of both monocytes and $\alpha\beta$ T cells. Lastly, it was found that SE provoked a reduced and delayed cytokine response in infants, particularly within the unconventional T and NK cell populations. This study provides novel insights regarding the activation of unconventional T- and NK cells by SE, which contribute to understanding the vulnerability of young children towards *Staphylococcus aureus* infections.

KEYWORDS

MAIT cell, SEA, SEH, TSST-1, unconventional T cells

1 | INTRODUCTION

ABBREVIATIONS: CBMC, cord blood mononuclear cells; CD, cluster of differentiation; MAIT, mucosal associated invariant T; SE, Staphylococcal enterotoxin; SEA, Staphylococcal enterotoxin A; SEH, Staphylococcal enterotoxin H; TCR, T cell receptor; Th, T helper; TRAV, T cell receptor alpha variable; TRBV, T cell receptor beta variable; TRDV, T cell receptor delta variable; TSST-1, Toxic shock syndrome toxin-1

This is an open access article under the terms of the [Creative Commons Attribution](https://creativecommons.org/licenses/by/4.0/) License, which permits use, distribution and reproduction in any medium, provided the original work is properly cited.

©2021 The Authors. *Journal of Leukocyte Biology* published by Wiley Periodicals LLC on behalf of Society for Leukocyte Biology

Staphylococcus aureus (*S. aureus*) is considered a commensal bacterium and a frequent colonizer of the human nasopharynx,

skin, and gut. However, *S. aureus* is also a major cause of nosocomial infections, food poisoning, and sepsis due to production of a wide range of staphylococcal enterotoxins (SE).¹ In addition to causing food poisoning and toxic shock syndrome,^{2,3} certain SE could potentially be weaponized and used in biological warfare.⁴

The virulence of *S. aureus* is mainly determined by its enterotoxins and 26 SE and SE-like proteins have been described and classified.⁵ SE are known to induce polyclonal activation of conventional T cells. This is independent of Ag presentation and potentiated by cross-linking the T cell receptor (TCR) and the MHC class II receptor resulting in proliferation, cytotoxicity and secretion of the cytokines IL-2, IFN- γ , and TNF.⁵ Two frequently studied SE, SEA and toxic shock syndrome toxin-1 (TSST-1), mediate conventional T cell activation through several TCR variable β -chains (TRBV), while the less studied SEH specifically binds the alpha chain (TRAV27).⁶ Notably, although unconventional T cells and NK cells are also readily activated by *S. aureus* and its SE,^{7–9} the mechanisms involved in their activation by SE still remain poorly understood. Unconventional T cells are non-MHC restricted and include, among others, mucosal associated invariant T (MAIT) cells and $\gamma\delta$ T cells. These cell types are described as innate-like lymphocytes that recognize a limited set of microbe-derived antigens and quickly secrete cytokines and act cytotoxic upon immune challenge.^{10,11} MAIT cells are restricted by the MHC class I-like receptor (MR1) and characterized by expression of a semi-variable $\alpha\beta$ TCR with a fixed α -chain (TRAV2-1) and high IL-18R and CD161 expression.¹² $\gamma\delta$ T cells express a γ - and δ -chain TCR of which the majority respond to small, phosphorylated bacterial metabolites or lipid based self-ligands via the receptor butyrophilin 3A1 (BTN3A1) or CD1d, respectively.^{13–16} NK cells are innate lymphocytes lacking a TCR, but capable of clearing infected and transformed cells through cytolytic activities and cytokine production.^{17,18}

Although SEA has been reported to directly activate $\gamma\delta$ T cells,¹⁹ the binding restrictions of most SE suggest a theoretical inability to directly activate $\gamma\delta$ T cells and NK cells, while SEA and TSST-1, but not SEH, could potentially directly activate MAIT cells. On the other hand, these cells are also activated by the presence of inflammatory cytokines in the local environment where APC-derived cytokines are of particular importance. For example, NK cell effector responses are up-regulated by IL-12, IL-15, and IL-18²⁰ and IL-12 and IL-18 can induce effector responses in MAIT cells through a TCR-independent mechanism.^{8,21} However, the involvement of innate cytokines in SE-mediated activation of unconventional T cells and NK cells require further investigations.

In the present study, we aimed to investigate underlying mechanisms of SE-mediated activation of MAIT cells, $\gamma\delta$ T cells and NK cells *in vitro*. Further, as *S. aureus* is one of the leading causes of neonatal sepsis²² and the immune system of neonates and infants have altered characteristics compared to adults,^{23,24} we also wanted to compare neonatal and adult immune cell responses toward SE.

2 | MATERIALS AND METHODS

2.1 | Ethics statement and isolation of cord/peripheral blood mononuclear cells

For the majority of the experiments (Figures 1–4; all Supplementary figures), peripheral blood mononuclear cells (PBMC) from adult volunteers were used, which was approved by the regional Ethics committee at the Karolinska Institute, Stockholm, Sweden. All adult study subjects gave their informed written consent.

In Figure 4, cord blood mononuclear cells (CBMC) were collected from healthy neonates at term deliveries, which was approved by the regional Ethics committee at the Karolinska Institute, Stockholm, Sweden. All mothers gave their informed written consent.

In Figure 5, CBMC/PBMC from healthy children at birth, 2, and 7 years of age, and adults, participating in 2 different cohorts described elsewhere^{25,26} were included. These studies were approved by the Human Ethics Committee at Huddinge University Hospital, Stockholm. According to the regulations present at the time of sample collection, all parents provided informed consent.

Venous or cord blood was collected in heparinized vacutainer tubes (BD Pharmingen, San Diego, CA) and diluted 1:1 with RPMI-1640 supplemented with 20 mM HEPES (HyClone Laboratories, Inc, South Logan, UT). PBMC/CBMC were isolated using Ficoll-Hypaque (GE Healthcare Bio-Sciences AB, Uppsala, Sweden) gradient separation. Next, cells were washed and resuspended in freezing medium containing 40% RPMI-1640, 50% FBS, and 10% dimethyl sulphoxide (both from Sigma Aldrich, St Louis, MO). The cells were frozen gradually at -80°C in freezing containers (Mr. Frosty, Nalgene Cryo 1 $^{\circ}\text{C}$; Nalge Co, Rochester, NY) and stored in liquid nitrogen.

2.2 | Production of SEA, SEAD227A, and SEH

The superantigens (SEA, SEH, and SEA-D227A) were produced as earlier described with minor changes.²⁷ In brief, untagged superantigens were expressed in *E. coli* K12 strain UL635. Cells were cultured in 2xYT media supplemented with 90 mM potassium phosphate. At an OD of 0.6, 3% v/v of 30% D-glucose was added and culturing was continued for 18 h. The cultures were collected, and the pellet was flash frozen. The pellets were homogenized in MES pH 5.5 for SEA and SEAD227A and for SEH in NaAc pH 4.0 buffer supplemented with 0.03 mg/mL lysozyme, 2 protease inhibitors cocktail tablets (Roche Diagnostics, Rotkreuz, Switzerland), 1 mM DTT and 1 mM EDTA to collect the protein from the periplasm. The suspension was centrifuged at 180,000 $\times g$ for 45 min and the supernatant was diluted 3x in homogenization buffer and was subjected to cation exchange chromatography (Res S 6 mL, GE Healthcare, Chicago, IL) on ÄKTA avant (GE Healthcare). For SEA and SEA-D227A, MES pH 5.5 and for SEH NaAc pH 4.0 buffer were used and the protein was eluted in a gradient from 0 to 1 M NaCl. The superantigens were further purified by size exclusion chromatography

(Superdex 75 10/300, GE Healthcare) in HBS buffer pH 7.4. Lastly, the superantigens were confirmed to be free of LPS contamination by measuring IL-6 secretion from PBMC upon 24 hours of stimulation. No IL-6 was detected above background levels at concentrations up to 200 ng/mL (Supplementary Fig. S1).

2.3 | *In vitro* stimulation of CBMC/PBMC

CBMC/PBMC were thawed, washed twice, and viability was assessed by trypan blue staining. Cells were resuspended in cell culture medium (RPMI-1640 supplemented with 20 mM HEPES, 2 mM L-glutamine, 100 U/mL penicillin, 100 µg/mL streptomycin (all from HyClone Laboratories Inc.), and 10% FBS (Sigma Aldrich)) to a final concentration of 1×10^6 cells/mL. Cells were seeded into cell culture plates and stimulated with 20 ng/mL of SEA, SEH, or TSST-1 (Toxin Technology, Inc, Sarasota, FL) and incubated at 37°C with 5% CO₂ atmosphere. Cell culture supernatants were collected and stored at -20°C for subsequent ELISA analyses, and cells were analyzed by flow cytometry.

For cellular assays comparing wild-type and mutant SEA-D227A, PBMC were stimulated with wild-type SEA or mutant SEA-D227A at concentrations ranging from 0.002 to 20 ng/mL for 48 h. Cells were analyzed by flow cytometry.

For kinetic experiments, PBMC were stimulated with 20 ng/mL of SEA and incubated for 4, 8, 12, 16, and 24 h.

2.4 | Cell isolation and co-cultures

Monocytes, total CD3⁺ T cells, γδ T cells and NK cells were isolated from PBMC by negative selection using EasySep™ Human monocyte enrichment kit and CD3⁺ T cell-, γδ T cell-, and NK cell isolation kits, respectively (all from STEMCELL Technologies Inc, Vancouver, Canada) according to manufacturer's instructions. In brief, PBMC were washed and resuspended in PBS supplemented with 2% FBS and 1 mM EDTA (Invitrogen, Waltham, MA) at 50×10^6 cells/mL. PBMC were then incubated with an antibody cocktail, followed by incubation with magnetic particles. The cells of interest were recovered by magnetic separation using an EasySep magnet and re-suspended in cell culture medium. For co-culture experiments, 5×10^4 monocytes/well were primed with SE for 4 h in a V-shaped 96-well plate and subsequently washed carefully by centrifugation. Isolated CD3⁺ T cells (2×10^5 cells/well), γδ T cells (5×10^4 cells/well) or NK cells (5×10^4 cells/well) were added to the SE-primed monocytes in different combinations and incubated for an additional 20 h. Cells were analyzed by flow cytometry.

2.5 | Transwell experiments

Monocytes, total CD3⁺ T cells, γδ T cells, and NK cells were isolated using STEMCELL Technology kits as described above. A total of 1×10^5 γδ T cells or 1×10^5 NK cells were added to the inserts and 1×10^5 monocytes and 4×10^5 total CD3⁺ T cells were added to the bottom

wells of a Costar® 6.5 mm Transwell® 0.4 µm pore polyester plate. SEA was added to the bottom well at a concentration of 20 ng/mL for 24 h at 37°C, 5% CO₂. Cells were then collected and analyzed using flow cytometry. For comparison to membrane separated NK cells; monocytes, total CD3⁺ T cells and NK cells from the same donors were co-cultured in a 48-well plate and stimulated with SEA for 24 h. IFN-γ expression within γδ T cells present among the total CD3⁺ T cells in the bottom well of the transwell plate was used for comparison to membrane separated γδ T cells.

2.6 | Blocking experiments

PBMCs were stimulated in the presence of 2 µg/mL anti-human IL-12 (clone: 24910, R&D Systems Inc, Minneapolis, MN) or 2 µg/mL matched IgG1 isotype control (clone: MOPC-21, BD Biosciences, Franklin Lakes, NJ). In brief, blocking or control antibodies were added to the cells 30 min prior and 24 hours after stimulation with SEA and TSST-1. Cells were analyzed by flow cytometry after a total of 48 h-stimulation.

2.7 | Degranulation assay

Anti-human CD107a V450 antibody (clone H4A3; BD Biosciences) was added to the cells at 0.5 µg/mL immediately prior to stimulation with SEA and TSST-1. Cells were incubated for 48 h and analyzed by flow cytometry.

2.8 | Flow cytometry

For all flow cytometry analyses, except for degranulation experiments, Brefeldin A (GolgiPlug™ BD Biosciences) was added during the last 4 h of stimulation to inhibit protein secretion. After incubation, cells were transferred to 96 well V-shaped staining plates and washed twice in PBS. Cells were stained with LIVE/DEAD Fixable Dead Cell Stain Kit-Aqua (Life Technologies, Carlsbad, CA) or with BD Horizon™ Fixable Viability Stain 780 (BD Biosciences) for 15 min at room temperature. Cell surface Fc receptors were blocked with 10% human serum in FACS-wash buffer (PBS, 2 mM EDTA and 0.1% BSA (Roche Diagnostics) and subsequently stained with the following Abs; CD3-BV510/APC-H7 (clone: UCHT1/SK7), CD28-BV421 (clone: CD28.2), CD56-APC (clone: B159), CD130-BV421 (clone: AM64) (all from BD Biosciences), CD27-PE (clone: M-T271), CD57-PE-Cy7 (clone: HNK-1), CD161-FITC/PE-Cy7/BV421 (clone: HP-3G10), Vα7.2-PE/APC (clone: 3C10), Vδ2-APC (clone: B6) (all from BioLegend, San Diego, CA), Pan γδ TCR-FITC (clone: IMMUS10), Vδ1-PE-Cy7 (clone: R9.12) (both from Beckman Coulter Inc, Brea, CA), and NKG2C-PE (clone: REA205, Miltenyi Biotec, Bergisch Gladbach, Germany). After surface staining, cells were washed and fixed/permeabilized using the Fixation- and Intracellular Staining Permeabilization Wash buffer (BioLegend) according to manufacturer's instructions. Intracellular blocking was done with 10% human serum followed by staining for intracellular

TABLE 1 Primer sequences for RT-qPCR

Target gene	Forward primer	Reverse primer
IL-12	CCATTGAGGTCATGGTGGA	ACGCAGATGTCAGGGAGAA
IL-15	TGTAGGAGGCATCGTGGATG	GTATTGAAGAAGAGCTGCC
IL-18	GCTGAACCACTAGAAGACAATTGC	CCAGGTTTCATCATCTTCAGCTA
TBP ^a	CACGAACCAACGGCACTGATT	TTTCTTGCTGCCAGTCTGGAC

^aTBP: TATA box binding protein.

IFN- γ -PerCP-Cy5.5 (clone: B27), IL-2-BV421 (clone: 5344.111) (both from BD Biosciences) or TNF-BV421 (clone: Mab11, BioLegend). Stained cells were washed, resuspended in FACS-wash buffer, and acquired using a FACSVerse instrument and FACS-Suite software (both BD Biosciences). Specific cell populations were gated using forward and side scatter properties followed by fluorescently labelled antibodies. Fluorescence-minus-one and isotype controls were used for gating when appropriate. For complete gating strategy, the reader is referred to Supplementary Fig. S2A and B. Analyses were done with FlowJo software v10.2 (TreeStar, Ashland, OR).

2.9 | ELISA

The levels of IL-2, IL-6, IL-10, IL-17A, IL-21, IFN- γ , TNF, granzyme B, and perforin were quantified in cell culture supernatants using sandwich ELISA according to manufacturer's instructions (all from MabTech AB, Nacka, Sweden). The optical density was measured using a microplate reader (Molecular Devices Corp, Sunnyvale, CA) at 405 nm wavelength and results were analyzed using SoftmaxPro 5.2 rev C (Molecular Devices Corp).

2.10 | Reverse-transcriptase qPCR

PBMC were stimulated for 4 or 8 h after which total cellular RNA was harvested using a RNeasy mini kit (Qiagen, Hilden, Germany) according to manufacturer's instructions. From 200 ng of extracted RNA, cDNA transcripts were obtained using SuperScript VILO cDNA Synthesis kit (Thermo Fisher Scientific, Waltham, MA). RT-qPCR was performed on a LightCycler[®] 480 II Real-Time PCR instrument (Roche Diagnostics) using gene-specific primers and KAPA SYBR FAST qPCR Master Mix (KAPA Biosystems Inc, Wilmington, MA). Target gene expression was normalized against expression of a housekeeping gene: TATA box binding protein (TBP). Primers were purchased from Eurofins Genomics and primer sequences are shown in Table 1.

2.11 | Statistics

Nonparametrical statistical tests were performed on all data sets. Friedman or Kruskal-Wallis tests followed by Dunn's multiple comparisons were done and Wilcoxon matched-pairs signed rank test was done on comparisons of 2 parameters within the same individual. Analysis and presentation were done using GraphPad Prism

(GraphPad Software, La Jolla, CA). All bar and dot plots show medians with interquartile range (IQR) and boxes show the median as the central line with boxes covering the 25th to 75th percentile and whiskers indicating min-max values. Data was considered significant if $P < 0.05$ and the following significance levels were used: * $P < 0.05$; ** $P < 0.01$; *** $P < 0.001$; **** $P < 0.0001$.

2.12 | Online supplemental material

Figure S1 shows IL-6 secretion upon stimulation with in-house produced SE. Figure S2 shows a complete gating strategy used for flow cytometric analyses. Figure S3 shows the proportion of CD130 expressing cells within unconventional T- and NK cells at baseline and after stimulation. Figure S4 shows a representative FACS plot for the activation kinetics of T- and NK cells. Figure S5 shows a representative FACS plot for the degranulation staining after SEA stimulation.

3 | RESULTS

3.1 | SE-mediated activation of $\gamma\delta$ T- and NK cells is dependent on physical contact with monocytes and conventional T cells

Although structurally and functionally similar, SEA, SEH, and TSST-1 all differ in their binding orientation and specificities toward the MHC class II and TCR.²⁸ If and how this affects the subsequent immunological response is largely unknown. Following PBMC-stimulation with these three toxins, all cell types investigated – conventional T cells, $\gamma\delta$ T cells, MAIT cells, and NK cells – were induced to express IFN- γ , although SEH was comparably less potent (Fig. 1A). Conventional T cells were clearly activated at lower toxin concentrations compared to the other cell types investigated. In addition, following stimulation with a SEA-D227A mutant toxin, which is unable to bind MHC class II, the IFN- γ production was significantly reduced in all investigated cell types at comparable concentrations (Fig. 1B).

$\gamma\delta$ T- and NK cells lack the canonical receptors for superantigen-TCR interaction. Still, SEA also interacts with, and promote signaling through, the IL-6 co-receptor CD130 on adipocytes.²⁹ However, we could not detect expression of CD130 on NK cells or $\gamma\delta$ T cells (Supplementary Fig. S3). In order to further investigate whether SE-mediated activation of $\gamma\delta$ T- and NK cells occur through non-canonical receptors, we developed a co-culture system where isolated $\gamma\delta$ T- or NK cells

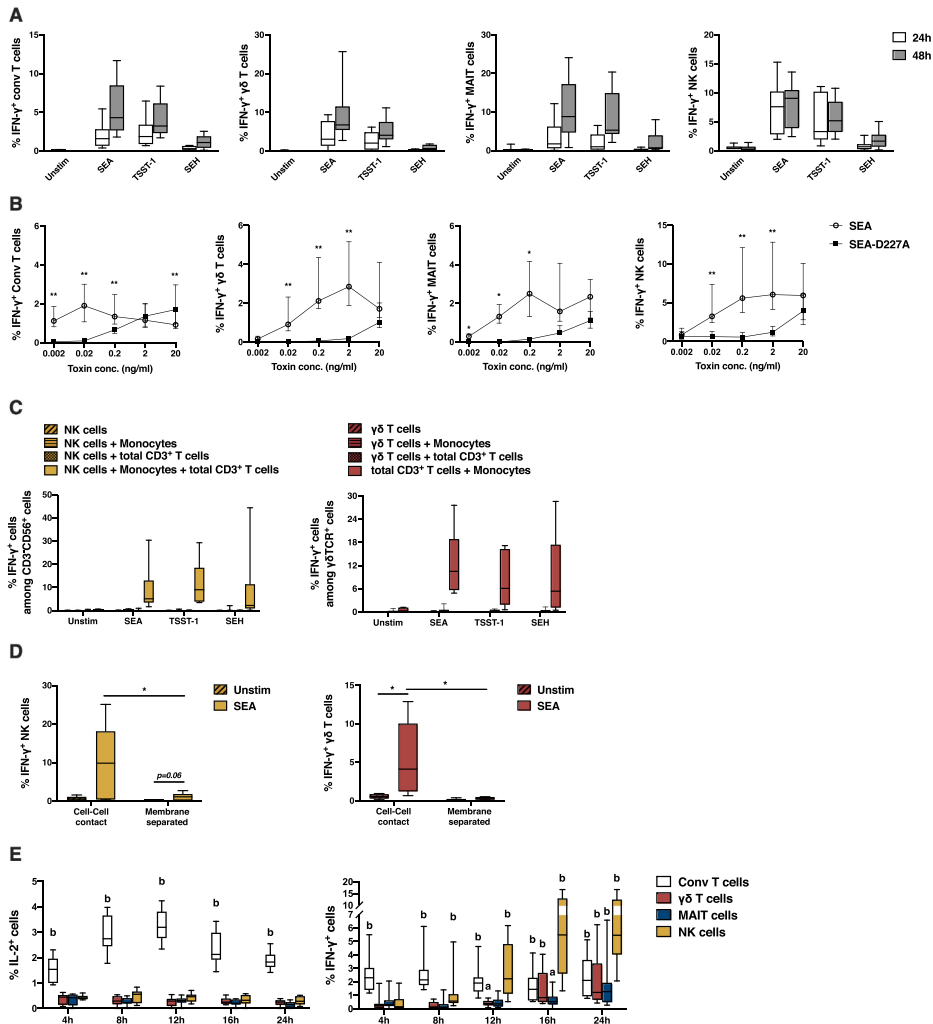


FIGURE 1 Indirect activation of $\gamma\delta$ T- and NK cells by staphylococcal enterotoxins. Stimulated PBMC were stained for intracellular cytokine expression and analyzed using flow cytometry. (A) Proportion of IFN- γ ⁺ conventional (Conv) T-, $\gamma\delta$ T-, MAIT-, and NK cells after 24 and 48 h of stimulation with SEA, TSST-1 or SEH, (n = 10). (B) Proportion of IFN- γ ⁺ cells upon stimulation with wild-type or mutant SEA-D227A, (n = 6-8). The level of significance between wildtype and mutant SEA-D227A for each concentration is shown. (C) IFN- γ expression within NK cells, (n = 6-7) and $\gamma\delta$ T cells, (n = 3-6), upon 20 h of stimulation of purified cells or of co-cultures with isolated monocytes, total CD3⁺ T cells or monocytes + total CD3⁺ T cells combined. (D) IFN- γ expression within NK cells, (n = 6) and $\gamma\delta$ T cells, (n = 6), upon 24 h of stimulation in membrane separated transwell plates. (E) Proportion of IL-2⁺ and IFN- γ ⁺ Conv. T-, $\gamma\delta$ T-, MAIT-, and NK cells after 4, 8, 12, 16 and 24 h of stimulation with SEA, (n = 6-8). a (*) and b (**) represent levels of significance between stimulated and unstimulated samples for each cell type and timepoint. Dot-plots show median with interquartile range, box plots show median as the central line with boxes covering the 25th to the 75th percentile and whiskers represents min-to-max

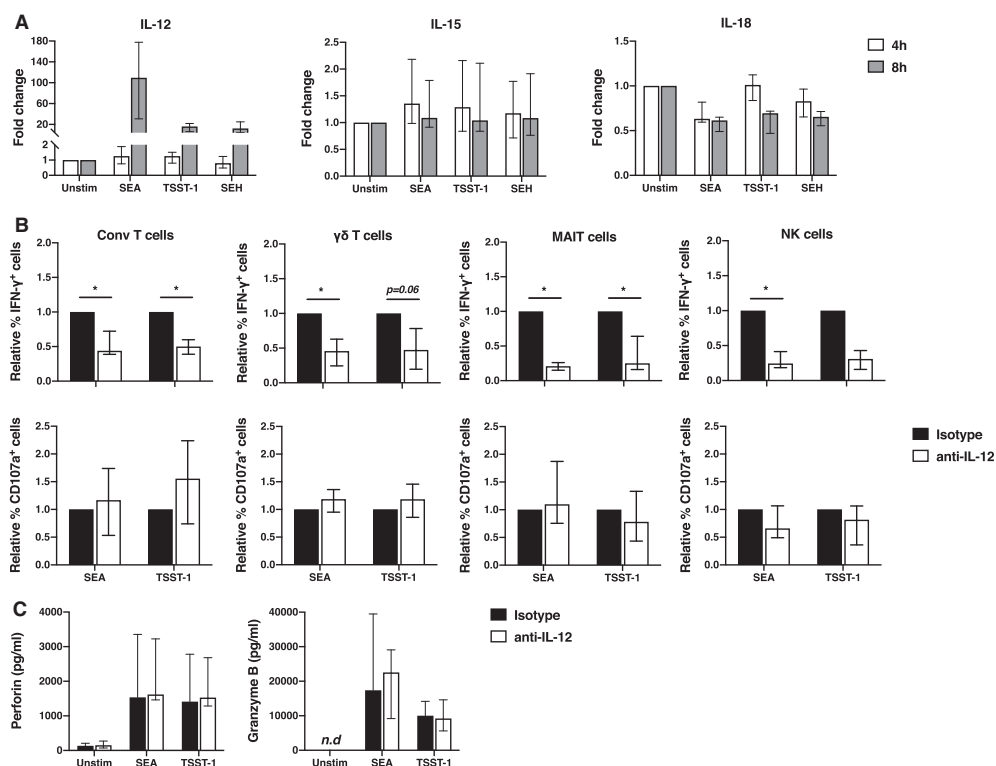


FIGURE 2 Involvement of innate-derived cytokines in SE-mediated activation of T- and NK cells. (A) SE-stimulated PBMC were analyzed for transcriptional activation of IL-12, IL-15 and IL-18 by reverse-transcriptase qPCR after 4- and 8 h of stimulation, ($n = 4$). (B) PBMC were stimulated in the presence of an anti-IL-12 neutralizing Ab or isotype control, ($n = 4-7$), where the proportion of IFN- γ^+ (top row) or CD107a $^+$ cells (bottom row) among each cell type was normalized to the isotype control, which was set to 1. (C) Secretion of Perforin and Granzyme B after anti-IL-12 neutralization was measured with ELISA, ($n = 4-6$). Bar plots show median with interquartile range

were added to SE-primed autologous monocytes followed by analyses of intracellular cytokine responses using flow cytometry. Interestingly, none of the SE were able to induce IFN- γ in pure $\gamma\delta$ T- or NK cell cultures, nor were SE-primed monocytes able to induce IFN- γ expression in autologous $\gamma\delta$ T- or NK cells (Fig. 1C). However, addition of total CD3 $^+$ T cells to either co-culture systems did result in activation of both $\gamma\delta$ T- and NK cells (Fig. 1C), suggesting that SE-induced activation of these cells requires the presence of both $\alpha\beta$ T cells and monocytes. In order to determine whether cell-to-cell contact was required for activation, $\gamma\delta$ T- and NK cells were seeded into inserts of 0.4 μ m pore membrane transwell plates with SEA-stimulated monocytes and total CD3 $^+$ T cells in the bottom well. In the absence of physical contact, $\gamma\delta$ T- and NK cell derived IFN- γ was lost (Fig. 1D), suggesting an important role for surface-expressed co-stimulatory receptors. In addition, conventional T cells expressed IL-2 and IFN- γ already after 4 hours of stimulation whereas NK-, $\gamma\delta$ T-, and MAIT cell-activation required longer durations of stimulation (Fig. 1E; Supplementary Fig. S4). Collectively,

this indicates that SE-mediated activation of $\gamma\delta$ T- and NK cells occur through an indirect mechanism dependent on the presence of monocytes and conventional T cells.

3.2 | SE-induced IFN- γ expression in T- and NK cells is IL-12 dependent

To study the involvement of APC-derived cytokines in SE-mediated activation, we isolated RNA from stimulated PBMC and analyzed the expression of IL-12, IL-15, and IL-18 using RT-qPCR. We observed an up-regulation of IL-12 transcription by all SE while IL-15 and IL-18 levels remained unchanged at both timepoints investigated (Fig. 2A). Next, PBMC were stimulated with SEA or TSST-1 in the presence of an anti-IL-12 neutralizing Ab or isotype control and IFN- γ expression and cytotoxic granule release were analyzed using flow cytometry. For both SE, neutralizing IL-12 reduced the frequency of IFN- γ expressing

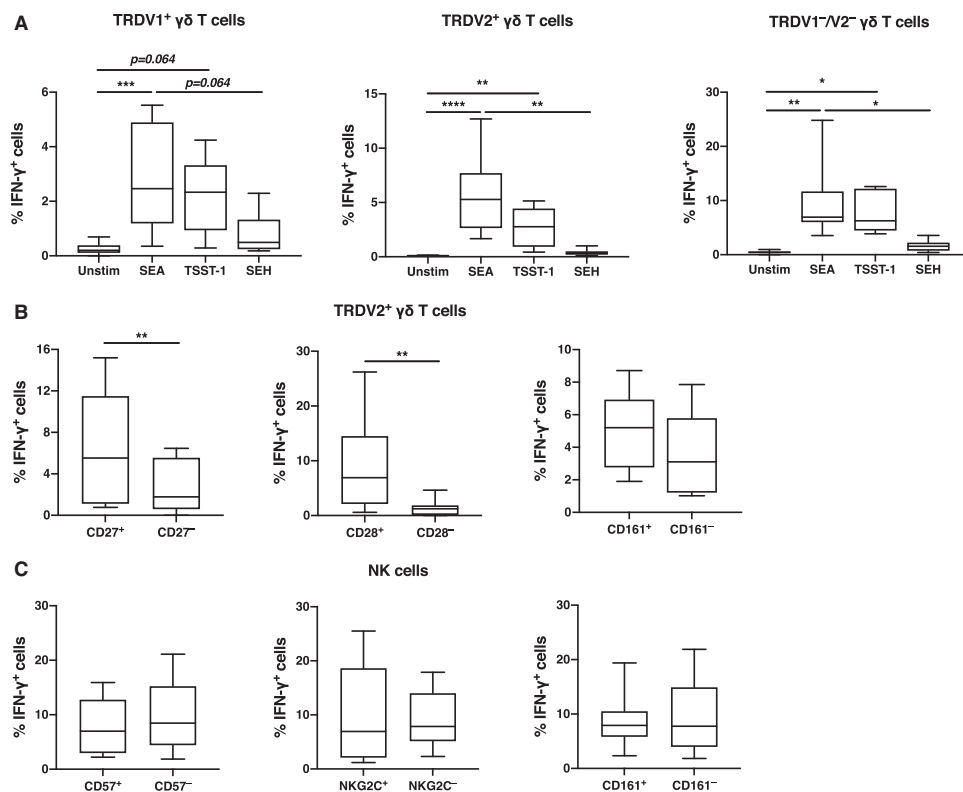


FIGURE 3 Phenotypic characterization of IFN- γ responses in $\gamma\delta$ T- and NK cells. PBMC were stimulated for 48 hours and the association between surface markers and IFN- γ production was evaluated in different NK cell- and $\gamma\delta$ T cell sub-populations using flow cytometry. (A) IFN- γ induction by SEA, TSST-1 and SEH among TRDV1⁺, TRDV2⁺, or TRDV1⁺/V2⁻ $\gamma\delta$ T cells, (n = 7-11). (B) Proportion of IFN- γ ⁺ cells among CD27⁺-, CD28⁺-, or CD161⁺-TRDV2⁺ $\gamma\delta$ T cells in response to SEA stimulation, (n = 6-8). (C) Proportion of IFN- γ ⁺ cells among CD57⁺-, NKG2C⁺-, or CD161⁺-NK cells in response to SEA stimulation, (n = 8-12). Box plots show median as the central line with boxes covering the 25th to the 75th percentile and whiskers represents min-to-max

cells in all cell types investigated (Fig. 2B, top row), however the frequency of CD107a⁺ cells remained unaffected (Fig. 2B, bottom row and supporting information Fig. S5). Furthermore, quantification of secreted perforin and granzyme B in PBMC culture supernatants revealed no differences after neutralization of IL-12 (Fig. 2C). Collectively, our results indicate that SE-induced IFN- γ -responses but not cytotoxic granule release, are dependent on IL-12 production.

3.3 δ -Chain usage and phenotypic markers associate with SE-induced IFN- γ expression in $\gamma\delta$ T cells

$\gamma\delta$ T cells are commonly subdivided according to V δ -chain usage, which also correlates with tissue distribution and function where TRDV2⁺ cells are more frequently found in circulation and TRDV1/3⁺ at

mucosal sites.^{11,30} We first investigated IFN- γ expression in TRDV1⁺, TRDV2⁺, and TRDV1⁺-TRDV2⁻ $\gamma\delta$ T cells upon SE stimulation of PBMC using flow cytometry (Supporting information Fig. S2B). All three $\gamma\delta$ T cell subsets expressed IFN- γ upon stimulation and we observed that SEA and TSST-1 induced a stronger response compared to SEH within each subset (Fig. 3A).

In the circulation, the TRDV2⁺ subpopulation is the most prevalent among $\gamma\delta$ T cells. We therefore investigated whether SE-induced responses in TRDV2⁺ T cells associated with a particular phenotype. We specifically investigated the memory-associated markers CD27, CD28, and CD161, commonly associated with pro-inflammatory responses in memory T cells.³¹ Both CD27- and CD28 expression correlated with increased IFN- γ expression upon SEA stimulation (Fig. 3B). Also, we have previously shown that SEA induces up-regulation of CD161 followed by increased

production of pro-inflammatory cytokine expression in CD4⁺FOXP3⁺ T cells.³² However, we observed no significant association between IFN- γ and CD161 expression within the TRDV2⁺ T cell population (Fig. 3B).

CD57 and NKG2C mark NK cells of a more differentiated state where NKG2C⁺ NK cells associate with increased IFN- γ production during human cytomegalovirus infection.^{33,34} However, we observed no correlation between IFN- γ expression and surface expression of the markers CD57 or NKG2C among NK cells in SEA-stimulated PBMC cultures (Fig. 3C). The relationship between CD161 expression and NK cell activity has been debated. In our current setting, there was no association between IFN- γ and CD161 expression among NK cells (Fig. 3C).

3.3 | The response to SE is delayed and weaker in newborns compared to adults

In order to investigate the response to SE at different stages of immune maturation, we analyzed a set of cytokines (IL-2, IL-10, IL-17A, IL-21, IFN- γ , and TNF) and cytotoxic compounds (granzyme B and perforin) released by CBMC and adult PBMC upon stimulation using ELISA. Twenty-four hours after stimulation, only IL-2 was detected in CBMC supernatants, whereas all the other factors were detected in adult PBMC supernatants (Fig. 4A). After 48 h, CBMC secreted detectable levels of IL-2, IFN- γ , TNF, granzyme B, and perforin, but still in lower amounts compared to adult PBMC (Fig. 4B). IL-10, IL-17A, and IL-21 were not detected or barely detected in cord blood after 48 h of stimulation, although readily secreted by adult PBMC (Figs. 4A, B). Overall, and in accordance with our other findings, SEA induced the highest levels of secreted cytokines and cytotoxic compounds, and SEH the lowest levels, in both CBMC and PBMC, with the exceptions of IL-10 and IL-17A (Figs. 4A, B).

3.4 | SE do not induce IFN- γ in unconventional T cells and NK cells during the neonatal and infant period

We next investigated the activation of different T-cell populations and NK cells at several time points during early childhood by stimulating CBMC or PBMC from 2- and 7-year-old children and adults with SEA or TSST-1 for 48 h.

First, we assessed the frequency of each cell type in absence of stimulation (Fig. 5A). The highest frequency of MAIT cells was found in adults but was barely detectable in cord blood, which is in accordance with previous studies.^{35,36} $\gamma\delta$ T cells were detected in all age groups, and at the highest frequency in 2-year-olds, while NK cells were found in highest frequency in cord blood (Fig. 5A). In terms of the response to SE, conventional T cells from all age groups produced IFN- γ upon stimulation with SEA and TSST-1, with the highest expression noted in adult cells (Fig. 5B). MAIT- $\gamma\delta$ T- and NK cells in cord blood or from 2-year-old children failed to produce IFN- γ in response to the toxins. However,

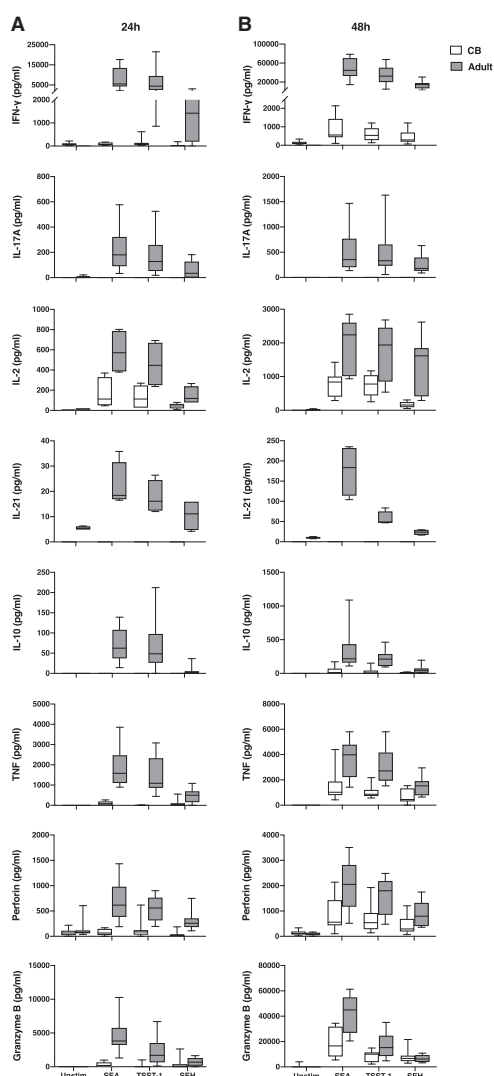


FIGURE 4 Cytokine secretion profile from CBMC and adult PBMC after stimulation with SE. CBMC (white boxes), (n = 4–8) or adult PBMC (grey boxes), (n = 4–10), were stimulated with SEA, TSST-1, or SEH for 24 h (A) or 48 h (B) and the secreted levels of multiple cytokines and cytotoxic compounds were assessed using ELISA. Box plots show median as the central line, with boxes covering the 25th to the 75th percentile and whiskers represent min-to-max

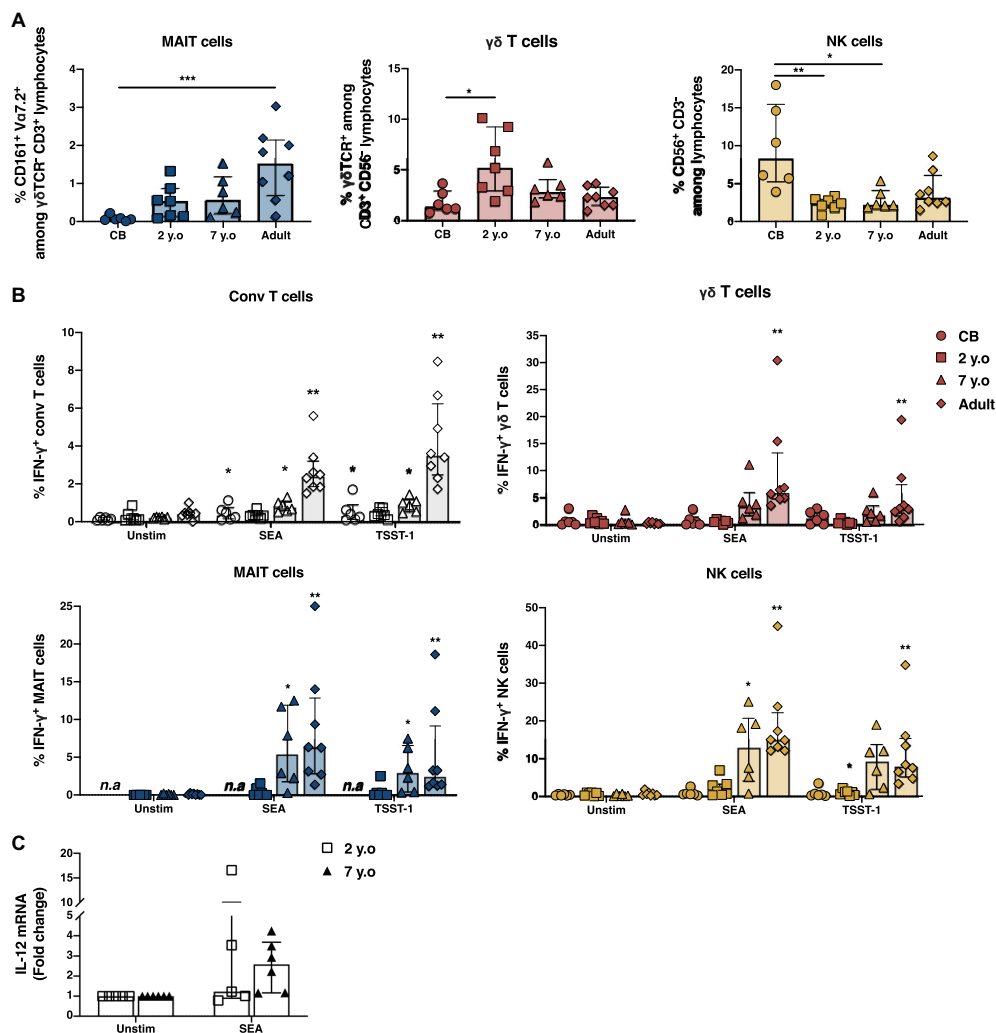


FIGURE 5 The IFN- γ production in response to SE is diminished early in life. CBMC and PBMC from 2-year-olds, 7-year-olds and adults were stimulated with SEA or TSST-1 for 48 h. (A) Frequencies of MAIT-, $\gamma\delta$ T- and NK cells found among lymphocytes from cord blood (CB), ($n = 6$), 2-year-olds, ($n = 7$), 7-year-olds, ($n = 7$), and adults, ($n = 8$), in unstimulated samples. (B) The proportion of IFN- γ ⁺ cells within conventional (Conv) T-, MAIT-, $\gamma\delta$ T- and NK cells in CB, ($n = 6$), 2-year-olds, ($n = 7$), 7-year-olds, ($n = 7$) and adults, ($n = 8$), upon stimulation. (C) SEA-induced IL-12 transcription after 8 hours of stimulation in PBMC from 2- and 7-year-olds ($n = 5-6$). The level of significance between stimulated and unstimulated samples within each age group is shown. Bar plots show median with interquartile range and symbols represent individual values

in the samples from 7-year-olds, MAIT-, $\gamma\delta$ T-, and NK cells significantly responded to both toxins.

Since we observed a significant role of IL-12 production for efficient IFN- γ responses in adult cells, we stimulated PBMC of 2- and 7-year-olds with SEA for 8 h and analyzed IL-12 induction by RT-qPCR.

Interestingly, SEA-induced IL-12 transcription was clearly hampered in both 2- and 7-year-olds, (Fig. 5C) compared to adults (Fig. 2A). Altogether, we have shown that unconventional T- and NK cells from cord blood and 2-year-old children failed to produce IFN- γ in response to SE, and that SEA-induced IL-12 transcription was lower in early life.

4 | DISCUSSION

Several reports have shown that unconventional T cells and NK cells can be activated by bacterial toxins, although the mechanisms and physiological consequences are only just beginning to be revealed.^{7,8,37,38} We have previously shown that SEA induces IFN- γ production in MAIT-, $\gamma\delta$ T-, and NK cells in a partly IL-12 dependent manner.⁷ Here, we have used the toxins TSST-1 and SEH, as well as SEA, to further investigate the mechanisms involved in the activation of unconventional T cells and NK cells by SE. We report that MAIT-, $\gamma\delta$ T-, and NK cells all produced the proinflammatory cytokine IFN- γ toward SEA, TSST-1, and SEH, and that SE-induced activation of $\gamma\delta$ T- and NK cells required physical cell contact with $\alpha\beta$ T cells and monocytes. Furthermore, IL-12 neutralization inhibited SE-induced IFN- γ expression while cytotoxic granule release remained unaffected. Finally, we found that the production of cytokines as well as cytolytic compounds in response to SE-stimulation was absent or diminished in the first years of life.

It is well established that superantigens activate conventional T cells by crosslinking TCR TRBV-chains (SEA, TSST-1) or TRAV27 (SEH) with the MHC class II receptor.⁵ The MAIT cell TCR is comprised of the TRAV1-2 chain paired with a limited number of TRBV-chains, thus some MAIT cells could carry a potential binding site for SEA and TSST-1. In theory, $\gamma\delta$ T- and NK cells are less likely to be directly activated by SE since they do not express an appropriate $\alpha\beta$ TCR. However, we here observe that these cell types express IFN- γ upon SE-stimulation of PBMC. SEH was clearly less potent in activating unconventional T cells and NK cells as compared to SEA and TSST-1 when used at similar concentrations. It is reasonable to assume that the number of TCR V-chains the SE can engage would correlate with the proportion of responding T cells and the amount of cytokine secretion. Of the three SE used in this study, SEA can bind the greatest number of V β -chains, and is also the only included toxin containing two separate binding sites for the MHC class II receptor.⁵ This results in the ability to cross-link multiple MHC class II molecules on the monocyte.³⁹ We also report that higher concentrations of the mutant SEA-D227A are required in order to induce the same level of activation as wild-type SEA. The fact that SEA-D227A binds to MHC class II with a much-reduced affinity, highlights the importance of this interaction to activate also unconventional T cells and NK cells. Indeed, SEA tended to induce the highest frequency of IFN- γ ⁺ cells and the highest levels of secreted IFN- γ compared with the other toxins used.

Despite the fact that $\gamma\delta$ T- and NK cells are unlikely to be direct targets for SE, reports suggest alternative modes of activation that do not rely on crosslinking between the $\alpha\beta$ TCR and MHC class II. SEA has been shown to activate T cells in a TCR-independent manner by binding to the laminin receptor-subunit LAMA2.⁴⁰ Furthermore, SEA binds to the IL-6 co-receptor CD130 and activates STAT3 signaling in human adipocytes²⁹ and a binding site for SEA on the $\gamma\delta$ TCR has been reported.¹⁹ However, the proportion of unconventional T cells and NK cells expressing CD130 was negligible both at baseline and upon stimulation. *S. aureus* infected monocyte-derived dendritic cells specifically activate TRDV2⁺ $\gamma\delta$ T cells in co-culture models,

which is dependent on both IL-12 production and surface expressed receptors including the $\gamma\delta$ TCR.⁴¹ However, by performing co-culture experiments with isolated cell populations, we here demonstrate that activation of $\gamma\delta$ T- and NK cells by SEA was dependent on both monocytes and total CD3⁺ T cells in a contact-dependent manner, but also that IL-12 was necessary for the activation of these cells. We also observed a marked IFN- γ response in TRDV1⁺ and TRDV1/2⁻ subpopulations in addition to TRDV2⁺ $\gamma\delta$ T cells, further highlighting key mechanistic differences between live bacterial infections and SE-induced activation of $\gamma\delta$ T cells. We also investigated the kinetics of cell activation upon SE-stimulation and show that conventional T cells are the first to respond, further indicating that the activation of MAIT-, $\gamma\delta$ T-, and NK cells is secondary to the response elicited by conventional T cells. Taken together, these results suggest an indirect mechanism of activation and an indispensable role for $\alpha\beta$ TCR expressing T cells in the activation of unconventional T- and NK cells. A similar outcome was observed in an *in vivo* study in mice, showing that SEA-mediated activation of $\gamma\delta$ T- and NK cells was dependent on $\alpha\beta$ T cells.⁴²

APC-derived cytokines such as IL-12, IL-15, and IL-18 are known to regulate survival, cytotoxic activity, and IFN- γ responses of T and NK cells.^{43–45} Furthermore, MAIT cells can be indirectly activated in a TCR-independent manner by IL-12 and IL-18.^{21,46} Here, we demonstrate that SE induced a notable upregulation of IL-12 but not of IL-15 or IL-18. Upon IL-12-neutralization, we observed a significant decrease in SE-induced IFN- γ expression in all cell types studied. This was expected since IL-12 is the main driver of Th1 differentiation. In opposite, cell-specific degranulation (CD107a surface expression) and the secreted levels of cytotoxic compounds (granzyme B and perforin) from PBMC-cultures were not significantly affected by IL-12-neutralization. Type 1 IFN are known to be important, especially for cytotoxic activity in NK cells,⁴⁷ and *S. aureus* have been shown to induce IFN α in both mice and humans.^{48,49} Thus, it would be relevant to further investigate the induction of type 1 IFN upon stimulation with SE and its potential involvement in SE-induced cytotoxicity. In summary, we have shown that monocyte-production of IL-12 is crucial to activate conventional T cells, which in turn are required to activate MAIT-, $\gamma\delta$ T- and NK cells to produce IFN- γ .

Further characterization of $\gamma\delta$ T cells and NK cells after activation by SE demonstrated that responding $\gamma\delta$ T cells showed a memory-like phenotype whereas no such associations were found in NK cells by the approach used in this study. SE-induced IFN- γ in $\gamma\delta$ T cells correlated with CD28 expression. Indeed, several SE, including SEA, SEB, and TSST-1, have been shown to bind to CD28, a surface molecule required for induction of SE-mediated lethal cytokine storm in mice.^{50,51} Although the CD28 binding site is relatively conserved among different SE,⁵² it is possible that differences in CD28 binding also contribute to the observed weaker cytokine responses induced by SEH compared with SEA and TSST-1. CD161 is a C-type lectin-like receptor expressed on NK cells as well as on several T cell subsets. CD161 expression associates with a high propensity for cytokine production in T cells,^{32,35,53} while its functional role in NK cell activity is less clear. Studies report CD161-mediated inhibition of NK cell cytotoxicity^{54,55} as well as increased NK cell responsiveness.⁵⁶

Here, we observed no difference in IFN- γ expression between CD161-negative and -positive NK cells or TRDV2⁺ $\gamma\delta$ T cells. CD161 expression correlates with increased expression of the IL-18R α on both conventional and $\gamma\delta$ T cells. Moreover, stimulation of these cells with IL-12 + IL-18 results in production of IFN- γ mainly within the CD161⁺ $\gamma\delta$ T cells.³⁵ SE failed to induce IL-18 transcription, and IL-18 neutralization had no effect on IFN- γ expression (data not shown), which could explain the observed lack of correlation between CD161 and IFN- γ expression among NK and $\gamma\delta$ T cells in our study.

Throughout this study, we have demonstrated that SE activate adult unconventional T cells and NK cells, and that these seem to contribute to the bulk of IFN- γ production. To determine if these responses were influenced by age and level of immune maturation, we investigated the cytokine profile and cellular responses upon stimulation with SE at several time-points during early childhood. NK cells have been reported to be more abundant in cord blood than in adults,⁵⁷ which is in agreement with our results. In addition to being more abundant, cord blood NK cells seem to mount a strong IFN- γ response when stimulated with IL-12 and IL-18.⁵⁸ Also $\gamma\delta$ T cells have been shown to be potent in early life and possess a mature phenotype and a level of response similar to adults already at 2 years of age.⁵⁹ Still, neither MAIT-, $\gamma\delta$ T- nor NK cells responded with IFN- γ production to any of the SE in the samples from cord blood or 2-year-olds. Moreover, production of a broad range of cytokines and cytotoxic compounds was markedly reduced and delayed from stimulated cord blood compared with adult cells, implying that towards certain stimuli, such as SE, cytokine responses from cord blood and young children are indeed impaired. Conventional T cells of all age groups produced IFN- γ in response to SEA and TSST-1, however the proportion of IFN- γ -producing cells notably increased with age, possibly related to different proportion of memory cells in children and adults. In addition, decreased APC capacity to secrete IL-12 in cord blood,⁶⁰ and the Th2 bias early in life^{61,62} might be contributing factors to the lower responsiveness observed in neonates and young children. Previous studies suggest that the lower levels of IL-12 mRNA are not due to decreased transcription but to a lower stability of the transcript.⁶⁰ Here, we assessed IL-12 transcription in 2- and 7-year-olds, which was clearly reduced in response to SEA compared to adults. Altogether, this suggests that the relative unresponsiveness of unconventional T cells and NK cells during infancy could be a consequence of reduced conventional T cell activation due to a decreased APC response.

In this study, we conclude that several SE, with different TCR V-chain specificities, are able to induce IFN- γ expression in MAIT cells, $\gamma\delta$ T cells and NK cells and suggest that their activation is secondary to and requires the presence of $\alpha\beta$ TCR-expressing T cells, APC and IL-12. Importantly, we confirm that neonatal T- and NK cells have a reduced capacity to mount a response towards SE *in vitro* compared with adults. *S. aureus* is a major contributor to hospital and community acquired infections frequently causing severe conditions such as toxic shock and sepsis. Unconventional T cells have a clear role in these life-threatening conditions and elucidating the mechanism behind their involvement is important.^{37,63,64}

Our study expands the understanding of the mechanisms involved in SE-induced activation of unconventional T cells and NK cells and suggests a possible contributor to the vulnerability to infections observed during the neonatal and infant period.

ACKNOWLEDGMENT

This work was financially supported by The Swedish Research Council 2016-01715_3, The Heart- and Lung foundation, The Olle Engkvist Byggmästare Foundation, Freemasons of Sweden, The Golden Jubilee Memorial, The Hesselman Foundation, The Swedish Asthma, and Allergy Association's Research Foundation and Stockholm University.

DISCLOSURE

The authors declare no conflict of interest.

AUTHORSHIP

M.M.F., K.L.P., S.B., and E.S.E. were responsible for the conceptualization. M.M.F., C.A., W.v.Z., S.U., A.S., P.R., J.S., K.L.P., and S.B. took part in the investigation and M.M.F., C.A., S.B., and E.S.E. were responsible for data curation, writing of the original draft, editing, and revision.

Manuel Mata Forsberg and Claudia Arasa share first authorship.

Sophia Björkander and Eva Sverremark-Ekström share senior authorship.

REFERENCES

- Otto M. Staphylococcus aureus toxins. *Curr Opin Microbiol*. 2014;17:32-37.
- McCormick JK, Yarwood JM, Schlievert PM. Toxic Shock Syndrome and Bacterial Superantigens: an Update. *Annu Rev Microbiol*. 2001;55:77-104.
- Lappin E, Ferguson AJ. Gram-positive toxic shock syndromes. *Lancet Infect Dis*. 2009;9:281-290.
- Borchardt SM, Ritger KA, Dworin MS. Categorization, prioritization, and surveillance of potential bioterrorism agents. *Infect Dis Clin North Am*. 2006;20:213-225.
- Tuffs S, Haeryfar S, McCormick J. Manipulation of innate and adaptive immunity by staphylococcal superantigens. *Pathogens*. 2018;7:53.
- Petersson K, Pettersson H, Skartved NJ, et al. Staphylococcal enterotoxin H induces V α -specific expansion of T cells. *J Immunol*. 2003;170:4148-4154.
- Johansson MA, Björkander S, Mata Forsberg M, et al. Probiotic lactobacilli modulate staphylococcus aureus-induced activation of conventional and unconventional T cells and NK cells. *Front Immunol*. 2016;7:273.
- Shaler CR, Choi J, Rudak PT, et al. MAIT cells launch a rapid, robust and distinct hyperinflammatory response to bacterial superantigens and quickly acquire an anergic phenotype that impedes their cognate antimicrobial function: defining a novel mechanism of superantigen-induced immunopathology. *PLOS Biol*. 2017;15:e2001930.
- Ami K, Ohkawa T, Koike Y, et al. Activation of human T cells with NK cell markers by staphylococcal enterotoxin A via IL-12 but not via IL-18. *Clin Exp Immunol*. 2002;128:453-459.
- Godfrey DI, Uldrich AP, McCluskey J, et al. The burgeoning family of unconventional T cells. *Nat Immunol*. 2015;16:1114-1123.
- Gao Y, Williams AP. Role of innate T cells in anti-bacterial immunity. *Front Immunol*. 2015;6:302.

12. Napier RJ, Adams EJ, Gold MC, et al. The Role of Mucosal Associated Invariant T Cells in Antimicrobial Immunity. *Front Immunol.* 2015;6:344.
13. Vavassori S, Kumar A, Wan GS, et al. Butyrophilin 3A1 binds phosphorylated antigens and stimulates human $\gamma\delta$ T cells. *Nat Immunol.* 2013;14:908-916.
14. Sandstrom A, Peigné C-M, Léger A, et al. The intracellular B30.2 domain of butyrophilin 3A1 binds phosphoantigens to mediate activation of human V γ 9V δ 2 T cells. *Immunity.* 2014;40:490-500.
15. Luoma AM, Castro CD, Mayassi T, et al. Crystal structure of V δ 1 T cell receptor in complex with CD1d-sulfatide shows MHC-like recognition of a self-lipid by human $\gamma\delta$ T cells. *Immunity.* 2013;39:1032-1042.
16. Uldrich AP, Le Nours J, Pellicci DG, et al. CD1d-lipid antigen recognition by the $\gamma\delta$ TCR. *Nat Immunol.* 2013;14:1137-1145.
17. Tu MM, Mahmoud AB, Makriganis AP. Licensed and unlicensed NK cells: differential roles in cancer and viral control. *Front Immunol.* 2016;7:166.
18. Melsen JE, Lugthart G, Lankester AC, et al. Human circulating and tissue-resident CD56bright natural killer cell populations. *Front Immunol.* 2016;7:262.
19. Morita CT, Li H, Lamphear JG, et al. Superantigen recognition by $\gamma\delta$ T cells. *Immunity.* 2001;14:331-344.
20. Chijioke O, Münz C. Dendritic cell derived cytokines in human natural killer cell differentiation and activation. *Front Immunol.* 2013;4:365.
21. Ussher JE, Bilton M, Attwod E, et al. CD161 ++ CD8 + T cells, including the MAIT cell subset, are specifically activated by IL-12+IL-18 in a TCR-independent manner. *Eur J Immunol.* 2014;44:195-203.
22. Power Coombs MR, Kronforst K, Levy O. Neonatal host defense against staphylococcal infections. *Clin Dev Immunol.* 2013;2013:1-9.
23. Rudd BD. Neonatal T cells: a reinterpretation. *Annu Rev Immunol.* 2020;38:229-247.
24. Gibbons D, Fleming P, Virasami A, et al. Interleukin-8 (CXCL8) production is a signatory T cell effector function of human newborn infants. *Nat Med.* 2014;20:1206-1210.
25. Saghafian-Hedengren S, Sverremark-Ekström E, Linde A, et al. Early-life EBV infection protects against persistent IgE sensitization. *J Allergy Clin Immunol.* 2010;125:433-438.
26. Björkander S, Johansson MA, Hell L, et al. FOXP3 + CD4 T-cell maturity and responses to microbial stimulation alter with age and associate with early-life gut colonization. *J Allergy Clin Immunol.* 2016;138:905-908.
27. Saline M, Rödström KEJ, Fischer G, et al. The structure of superantigen complexed with TCR and MHC reveals novel insights into superantigenic T cell activation. *Nat Commun.* 2010;1:119.
28. Petersson K, Forsberg G, Walse B. Interplay between superantigens and immunoreceptors. *Scand J Immunol.* 2004;59:345-355.
29. Banke E, Rödström K, Ekellund M, et al. Superantigen activates the gp130 receptor on adipocytes resulting in altered adipocyte metabolism. *Metabolism.* 2014;63:831-840.
30. Bonneville M, O'Brien RL, Born WK. $\gamma\delta$ T cell effector functions: a blend of innate programming and acquired plasticity. *Nat Rev Immunol.* 2010;10:467-478.
31. Takahashi T, Dejbakhsh-Jones S, Strober S. Expression of CD161 (NKR-P1A) defines subsets of human CD4 and CD8 T cells with different functional activities. *J Immunol.* 2006;176:211-216.
32. Björkander S, Hell L, Johansson MA, et al. Staphylococcus aureus-derived factors induce IL-10, IFN- γ and IL-17A-expressing FOXP3+CD161+ T-helper cells in a partly monocyte-dependent manner. *Sci Rep.* 2016;6:22083.
33. Foley B, Cooley S, Verneris MR, et al. Human cytomegalovirus (CMV)-induced memory-like NKG2C + NK cells are transplantable and expand in vivo in response to recipient CMV antigen. *J Immunol.* 2012;189:5082-5088.
34. Kared H, Martelli S, Tan SW, et al. Adaptive NKG2C+CD57+ natural killer cell and Tim-3 expression during viral infections. *Front Immunol.* 2018;9:686.
35. Fergusson JR, Smith KE, Fleming VM, et al. CD161 defines a transcriptional and functional phenotype across distinct human T cell lineages. *Cell Rep.* 2014;9:1075-1088.
36. Chen P, Deng W, Li D, et al. Circulating mucosal-associated invariant T cells in a large cohort of healthy chinese individuals from newborn to elderly. *Front Immunol.* 2019;10:260.
37. Emgård J, Bergsten H, McCormick JK, et al. MAIT cells are major contributors to the cytokine response in group A streptococcal toxic shock syndrome. *Proc Natl Acad Sci.* 2019;116:25923-25931.
38. Kalyan S, Chow AW. Human peripheral $\gamma\delta$ T cells potentiate the early proinflammatory cytokine response to staphylococcal toxic shock syndrome toxin-1. *J Infect Dis.* 2004;189:1892-1896.
39. Hudson KR, Tiedemann RE, Urban RG, et al. Staphylococcal enterotoxin A has two cooperative binding sites on major histocompatibility complex class II. *J Exp Med.* 1995;182:711-720.
40. Li Z, Zeppa JJ, Hancock MA, et al. Staphylococcal superantigens Use LAMA2 as a coreceptor to activate T cells. *J Immunol.* 2018;200:1471-1479.
41. Cooper AJR, Lalor SJ, McLoughlin RM. Activation of human V δ 2 + $\gamma\delta$ T cells by staphylococcus aureus promotes enhanced anti-staphylococcal adaptive immunity. *J Immunol.* 2020;205:1039-1049.
42. Kumar S, Colpitts SL, Ménoret A, et al. Rapid $\alpha\beta$ T-cell responses orchestrate innate immunity in response to Staphylococcal enterotoxin A. *Mucosal Immunol.* 2013;6:1006-1015.
43. Watford WT, Moriguchi M, Morinobu A, et al. The biology of IL-12: coordinating innate and adaptive immune responses. *Cytokine Growth Factor Rev.* 2003;14:361-368.
44. Leong JW, Chase JM, Romeo R, et al. Preactivation with IL-12, IL-15, and IL-18 induces CD25 and a functional high-affinity IL-2 receptor on human cytokine-induced memory-like natural killer cells. *Biol Blood Marrow Transplant.* 2014;20:463-473.
45. Dinarello CA, Novick D, Kim S, et al. Interleukin-18 and IL-18 binding protein. *Front Immunol.* 2013;4:289.
46. Lamichane R, Schneider M, de la Harpe SM, et al. TCR- or cytokine-activated CD8+ mucosal-associated invariant T cells are rapid polyfunctional effectors that can coordinate immune responses. *Cell Rep.* 2019;28:3061-3076.e5.
47. Oh JH, Kim MJ, Choi SJ, et al. Sustained type I interferon reinforces NK cell-mediated cancer immunosurveillance during chronic virus infection. *Cancer Immunol Res.* 2019;7:584-599.
48. Martin FJ, Gomez MI, Wetzel DM, et al. Staphylococcus aureus activates type I IFN signaling in mice and humans through the Xr repeated sequences of protein A. *J Clin Invest.* 2009;119:1931-1939.
49. Parker D, Prince A. Staphylococcus aureus induces type I IFN signaling in dendritic cells via TLR9. *J Immunol.* 2012;189:4040-6.
50. Popugailo A, Rotfogel Z, Supper E, et al. Staphylococcal and streptococcal superantigens trigger B7/CD28 costimulatory receptor engagement to hyperinduce inflammatory cytokines. *Front Immunol.* 2019;10:942.
51. Arad G, Levy R, Nasie I, et al. Binding of superantigen toxins into the CD28 homodimer interface is essential for induction of cytokine genes that mediate lethal shock. *PLoS Biol.* 2011;9:e1001149.
52. Zeng C, Liu Z, Han Z. Structure of staphylococcal enterotoxin N: implications for binding properties to its cellular proteins. *Int J Mol Sci.* 2019;20:5921.
53. Pesenacker AM, Bending D, Ursu S, et al. CD161 defines the subset of FoxP3+ T cells capable of producing proinflammatory cytokines. *Blood.* 2013;121:2647-2658.
54. Marrufo AM, Mathew SO, Chaudhary P, et al. Blocking LLT1 (CLEC2D, OCIL)-NKR1A (CD161) interaction enhances natural killer cell-mediated lysis of triple-negative breast cancer cells. *Am J Cancer Res.* 2018;8:1050-1063.

55. Rosen DB, Cao W, Avery DT, et al. Functional consequences of interactions between human NKR-P1A and its ligand LLT1 expressed on activated dendritic cells and B cells. *J Immunol.* 2008;180:6508-6517.
56. Kurioka A, Cosgrove C, Simoni Y, et al. CD161 defines a functionally distinct subset of pro-inflammatory natural killer cells. *Front Immunol.* 2018;9:486.
57. Dalle J-H, Menezes J, Wagner É, et al. Characterization of cord blood natural killer cells: implications for transplantation and neonatal infections. *Pediatr Res.* 2005;57:649-655.
58. Le Garff-Tavernier M, Béziat V, Decocq J, et al. Human NK cells display major phenotypic and functional changes over the life span. *Aging Cell.* 2010;9:527-535.
59. Heiden M, Björkander S, Rahman Qazi K, et al. Characterization of the $\gamma\delta$ T-cell compartment during infancy reveals clear differences between the early neonatal period and 2 years of age. *Immunol Cell Biol.* 2020;98:79-87.
60. Lee S, Suen Y, Chang L, et al. Decreased interleukin-12 (IL-12) from activated cord versus adult peripheral blood mononuclear cells and upregulation of interferon- γ , natural killer, and lymphokine-activated killer activity by IL- 12 in cord blood mononuclear cells. *Blood.* 1996;88:945-954.
61. Hebel K, Weinert S, Kuropka B, et al. CD4 + T cells from human neonates and infants are poised spontaneously to run a nonclassical IL-4 program. *J Immunol.* 2014;192:5160-5170.
62. Debock I, Flamand V. Unbalanced neonatal CD4+ T-cell immunity. *Front Immunol.* 2014;5:393.
63. Davey MS, Morgan MP, Liuzzi AR, et al. Microbe-specific unconventional t cells induce human neutrophil differentiation into antigen cross-presenting cells. *J Immunol.* 2014;193:3704-3716.
64. Andreu-Ballester JC, Tormo-Calandín C, Garcia-Ballesteros C, et al. Association of $\gamma\delta$ T cells with disease severity and mortality in septic patients. *Clin Vaccine Immunol.* 2013;20:738-746.

SUPPORTING INFORMATION

Additional supporting information may be found online in the Supporting Information section at the end of the article.

How to cite this article: Mata Forsberg M, Arasa C, van Zwol W, et al. Activation of human $\gamma\delta$ T cells and NK cells by Staphylococcal enterotoxins requires both monocytes and conventional T cells. *J Leukoc Biol.* 2021;1–14.
<https://doi.org/10.1002/JLB.3A1020-630RR>

Paper II



Expression and Purification of human $\gamma\delta$ T Cell Receptor for Activity Studies

Sibel Uzunçayır¹, Ganna Petruk², Karin Lindkvist-Petersson^{1*}

1. Department of Experimental Medical Science, Lund University, BMC C13, 22184 Lund, Sweden
2. Department of Clinical Sciences, Lund University, BMC B14, 22814 Lund, Sweden

^{*}To whom correspondence may be addressed: Dr. Karin Lindkvist, Department of Experimental Medical Science, Lund University, BMC C13, 221 84 Lund, Sweden, +46 46 2228041, E-mail: karin.lindkvist@med.lu.se

Abstract

The exact role of $\gamma\delta$ T cells in the immune system is still not resolved. Studies show that $\gamma\delta$ T cells combine features of the conventional adaptive immune system like $\alpha\beta$ T cells, but also rapid innate like responses placing them in the innate immune system. Being able to study the receptors of these cells will clarify their distinct function as lymphocytes and shed light into their role in an immune reaction.

The $\gamma 9\delta 2$ T cell receptor (TCR) subset is the most common in human peripheral blood. Here we report a protocol to produce a chimeric variant $\gamma 9\delta 2$ TCR in *Escherichia coli* periplasm. The TCR is produced as inclusion bodies and refolded resulting in approximately 8.5 mg/ L culture of pure and homogenous TCR. This set up is facilitating the possibility for further structural and functional studies that require large amounts of homogenous $\gamma\delta$ TCR.

Key words: unconventional T cell receptor, $\gamma\delta$ TCR, refolding, recombinant expression, protein purification

Introduction

T cells are divided into $\alpha\beta$ and $\gamma\delta$ T cells based on the expression of their respective T cell receptor (TCR). The $\gamma\delta$ T cells were identified as late as 1984 as a separate T lymphocyte lineage (Chien et al. 1984; Hayday 1985; Brenner et al. 1986), and due to their low representation (0.5-16% in human peripheral blood) $\gamma\delta$ T cells remain the least studied ones. $\gamma\delta$ T cells are known to interact with epithelial cells, monocytes, dendritic cells, neutrophils, B cells and $\alpha\beta$ T cells (He et al. 2014). $\gamma\delta$ T cells activation results in cytokine production (IFN- γ , TNF- α , IL-17), chemokine production, lysis of infected cells, inflammation, wound healing, antigen presentation, cytotoxicity, dendritic cell maturation, epithelial growth, B cell help and antibody production (Vantourout and Hayday 2013; He et al. 2014).

In contrast to $\alpha\beta$ T cells, $\gamma\delta$ T cells can be activated in an MHC independent manner (Bigby et al. 1993). Still, several $\gamma\delta$ TCR were reported to bind to MHC or MHC like molecules (Groh et al. 1998; Matis et al. 1989; Kierkels et al. 2019; Uldrich et al. 2013). $\gamma\delta$ T cells can be further divided into three subgroups (V δ 1, V δ 2 and V δ 3 T cells) according to their δ chain expression. These are then paired with a distinct γ chain (γ 2, γ 3, γ 4, γ 5, γ 8 or γ 9), that then display strikingly different functions (Wesch et al. 1998). These unconventional T cells have oligoclonal subpopulations in tissue specific locations sharing the same distinct TCR chains (Gao and Williams 2015). The TCR of human peripheral blood $\gamma\delta$ T cells for instance largely consist of the variable chains γ 9 and δ 2 (V γ 9 δ 2).

The ligands of human $\gamma\delta$ TCRs remain largely unknown. The chains δ 1 and δ 3 are located in mucosal tissue and are activated by viral and stress-induced antigens presented via CD1. Recent studies show the recognition of phosphorylated prenyl metabolites lipids in complex with CD1 molecules are markers of cellular stress (Bonneville et al. 2010). Phospho-antigen 4-hydroxy-3methyl-but-2-enyl pyrophosphate (HMBPP) is generated during isoprenoid

synthesis and is known to bind the $\delta 2$ chain of circulating $V\gamma 9\delta 2$ T cells. All these molecules are upregulated in various cancer types paving the way of $\gamma\delta$ T cells and $\gamma\delta$ TCR to potential in cancer immune therapy (Legut et al. 2015).

Moreover, reports have shown that the $\gamma\delta$ TCR might interact with bacterial toxins, such as staphylococcal enterotoxin A (SEA) and that SEA could activate those cells (Morita et al. 2001; Rust et al. 1990). However, the mechanism, if and how MHC class II or other receptors participate upon activation, is not known yet. Still, Rust and co-worker showed that activated T cells can express MHC-II and that these cells can present SEA to other T cells and thus may be involved in on-site immune response (Rust and Koning 1993; Rust et al. 1993). Furthermore, Morita et al. claimed that $\gamma\delta$ T cell expressing $V\gamma 9^+$ TCR proliferate upon SEA recognition. However, the binding pattern of SEA differed from the prenyl pyrophosphate and alkylamine antigens binding site, as residue Asn25_{SEA} was crucial for the interaction between SEA and TRGV9. The authors suggest that $\alpha 2$ helix of SEA (including residues aa residues 20-27), is of importance for binding to $\gamma\delta$ TCR (Morita et al. 2001; Morita et al. 2000). Furthermore, an indirect mechanism for the activation of $\gamma\delta$ TCR by SEA, that would utilize monocytes and $\alpha\beta$ TCR in a direct cell to cell manner, has been proposed (Mata Forsberg et al. 2021). A SE mediated human T cell -T cell interaction has already been suggested before, where it was shown that TCR $\alpha\beta^+$ T effector cells presented SEA to either TCR $\alpha\beta^+$ T cells TCR $\gamma\delta^+$ T cells (Koning and Rust 1992).

So far, only four human $\gamma\delta$ TCR's are deposited in the protein data bank, whereas it is one hundred for human $\alpha\beta$ TCR's, highlighting the importance for more structural studies of $\gamma\delta$ TCR.

Here, we report a periplasmic bacterial system for the rapid expression of soluble $\gamma\delta$ TCR, adapted from the $\alpha\beta$ TCR protocol (Boulter et al. 2003). The $\gamma 9\delta 2$ TCR was successfully

expressed with final yields of 8,5 mg/ L culture at >90 % purity and correct folding was demonstrated by Circular Dichroism (CD). This expression system facilitates the production and use of $\gamma\delta$ TCR to enable studies of their interactions and potential in biomedical applications. Furthermore, we show direct binding of V γ 9 δ 2 TCR to the superantigen SEA by using BN-PAGE, validating the activity of the produced $\gamma\delta$ TCR.

Results and Discussion

Construct design of a chimera of $\gamma\delta$ TCR and $\alpha\beta$ TCR

The production of T cell receptors, especially the $\gamma\delta$ TCR, have been hampered by difficulties in finding a high-level expression system and subsequent purification protocol. Here we have developed a protocol to express and purify a refolded and stable chimeric $\gamma\delta$ TCR construct.

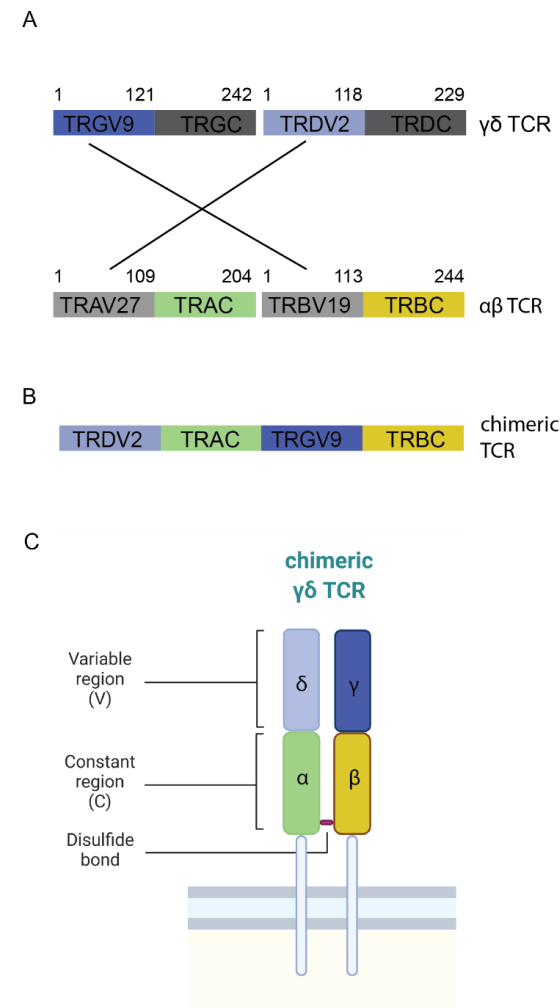


Figure 1: Fusion of TCR chains to create chimeric $\gamma\delta$ TCR

TCR chain subdivision of amino acids in TCRs. (A) $\gamma\delta$ TCR (TRGV9/TRDV2) with blue (γ) and light blue (δ) highlighted variable domains and $\alpha\beta$ TCR (TRAV 27/ TRBV 19) with green (α) and yellow (β) highlighted constant domains. (B-C) Fused chimeric $\gamma\delta$ TCR chain subdivision of amino acids, TRDV2/TRAC (light blue/green) and TRGV9/TRBC (blue/yellow) are shown. Introduced S-S bridge between the constant domains shown in purple.

This $\gamma\delta$ TCR construct is designed by using the constant domains of the $\alpha\beta$ TCR and fusing them with the variable chains from $\gamma\delta$ TCR (TRGV9/ TRDV2) (Fig. 1A-B). TRGV9 was paired with the beta constant domain and the TRDV2 to the alpha constant domain generating two chimeric constructs, TRDV2/TRAC and TRGV9/TRBC. To increase the stability of the folded TCR, one cysteine was introduced in each constant chain (TRAC/TRBC) to facilitate the formation of an S-S bridge in the final receptor (Fig. 1 C).

Protein production of large amounts of homogenous $\gamma\delta$ TCR

The chimeric TCR chains (TRDV2/TRAC and TRGV9/TRBC) were separately expressed in *E.coli* as inclusion bodies, washed, refolded and then further purified with ion exchange chromatography and size-exclusion chromatography (SEC). The schematic workflow of the full process is shown in figure 2 and the amount of protein material obtained in each purification step is shown in Table 1 (Fig. 2, Table 1).

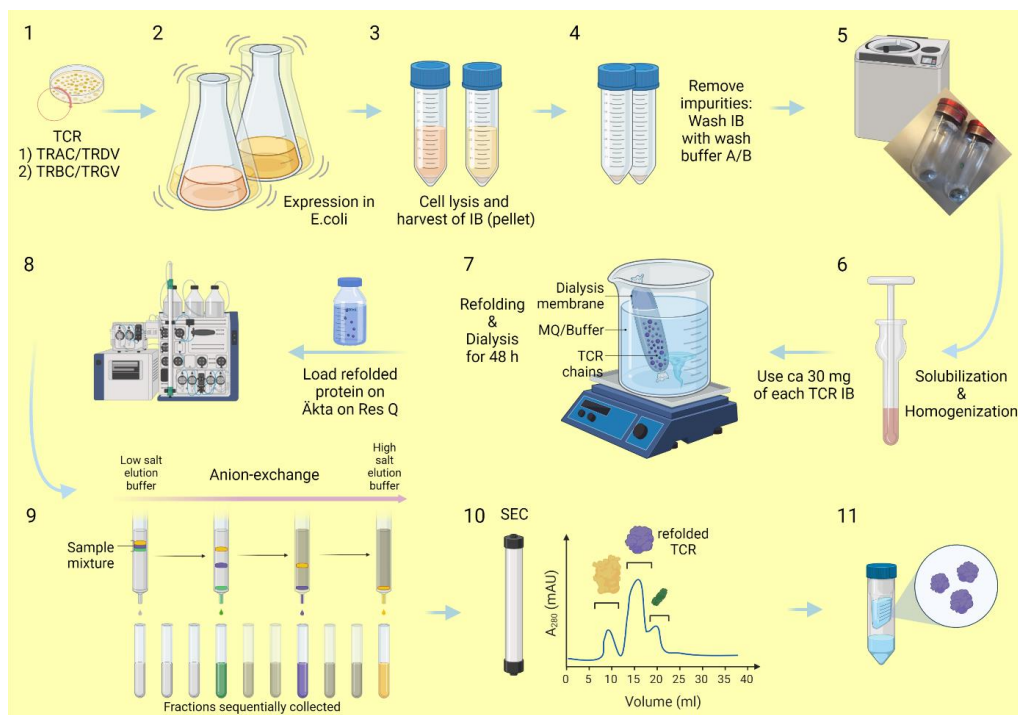


Figure 2: Schematic workflow of production of chimeric $\gamma\delta$ TCR

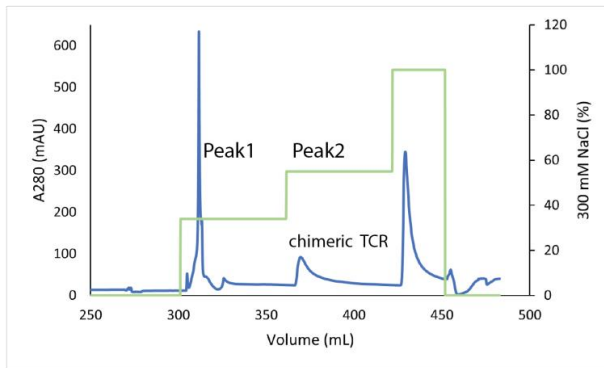
1) Transformation of chimeric $\delta\alpha$ - and $\gamma\delta$ -TCR inserts into *E.coli*. 2) Expression of separate chains in shaking culture 3) Cell lysis and harvest of inclusion bodies (IB in pellet) 4) Several washing and centrifugation steps 5) Isolated inclusion bodies 6) Solubilization and homogenization 7) Refolding of separate chains to chimeric TCR 8) Purification using ÄKTA system 9) Anion-exchange chromatography 10) Size exclusion chromatography 11) Concentration of purified refolded TCR.

Table 1: Protein material in different production stages

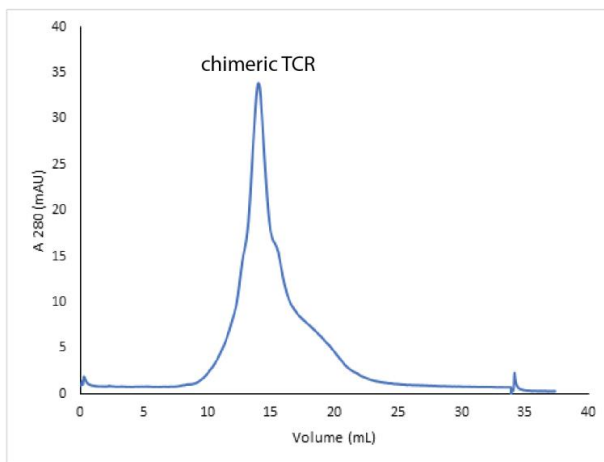
Stage	Amount
Inclusion bodies from 1L cell culture	Construct: $\gamma\alpha$: 403 mg; $\delta\beta$: 227 mg
Refolded protein (from 28 mg of each TCR) after anion-exchange	1,8 mg
Purified refolded protein (after SEC)	~ 1 mg
Extrapolation of 1 L culture of each TCR chain to final refolded protein	1 L culture -> 8,5 mg

After 48 h of refolding by dialysis, the protein solution was loaded on ion exchange column and the eluted peak containing TCR was subsequently loaded onto a size-exclusion column and all the eluted samples were analysed by Coomassie-stained SDS-PAGE (Fig. 3A-C). A stepwise elution was applied for the anion-exchange chromatography resulting in three peaks (Fig. 3A). Impurities are eluted in the first step (peak 1) while the second peak mainly contains refolded chimeric TCR, while aggregated TCR is eluted in the third peak (Fig. 3C). The fractions in peak 2 were concentrated and applied twice on a SEC column and a monodisperse peak was obtained (Fig. 3B). Coomassie-stained SDS-PAGE was used to analyze the purity of the samples (Fig. 3C). To confirm that the bands analysed by the SDS-PAGE corresponds to $\gamma\delta$ TCR, the samples were run with and without the reducing agent DTT. Clearly, upon addition of the reducing agent, the bands sperate into two differently sized band, while without a single band is seen, confirming that the sample contains refolded chimeric TCR (TRDV2/TRAC and TRGV9/TRBC) with the stabilizing disulside bond. (Fig. 3C). By using this purification procedure 8.5 mg/L culture refolded and pure $\gamma\delta$ TCR can be obtained that can be used for biological studies.

A



B



C

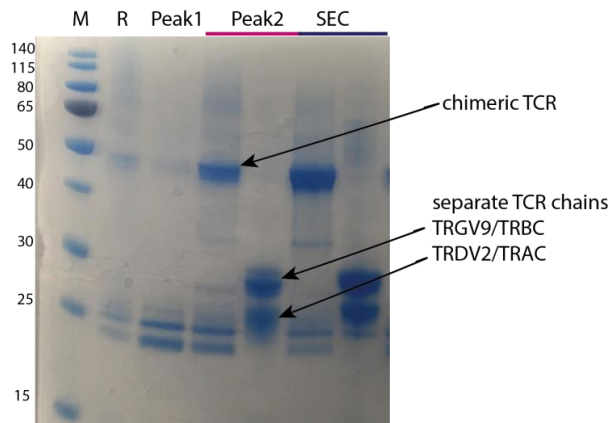


Figure 3: Production of homogenous chimeric $\gamma\delta$ TCR

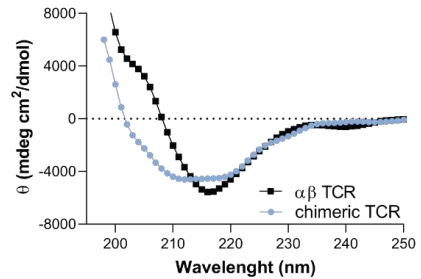
(A) Anion-exchange chromatogram with 3 steps of increasing NaCl concentration (33 %, 60 % and 100 %) with Peak 2 containing the refolded TCR (B) Size exclusion chromatogram with Superdex 200 (C) Coomassie stained gel: After refolding (R), Step 1 of NaCl increase of anion-exchange containing mainly impurities (Peak 1), Step 2 of NaCl increase of anion-exchange containing mainly refolded chimeric TCR (Peak 2), Peak 2 sample with DTT, main peak of size-exclusion chromatography (SEC) and (SEC) sample with DTT.

Chimeric $\gamma\delta$ TCR is folded with α -helical content

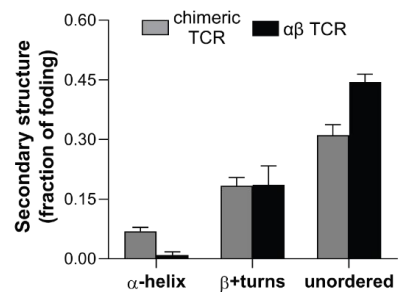
To verify the correct folding of recombinantly produced chimeric $\gamma\delta$ TCR we analyzed the sample with circular dichroism (CD) and compared to $\alpha\beta$ TCR (Fig. 4A-B). The $\alpha\beta$ TCR showed a CD spectrum very much resembling what has previously been published with most of the protein folding into a β -sheet structure (Fig. 4B-C). The chimeric $\gamma\delta$ TCR, on the other hand, showed somewhat different features with minima at 208 nm and 222 nm, which is the characteristics of α -helical protein. This was confirmed by the the online CD analysis site DICHROWEB

(<http://dichroweb.cryst.bbk.ac.uk>), where the $\gamma\delta$ TCR had a larger fraction α -helical content than the $\alpha\beta$ TCR (Fig. 4B). This clearly demonstrated that the $\gamma\delta$ TCR produced is a well-folded protein that has interesting structural features that could explain the differences in antigen specificity compared to $\alpha\beta$ TCR, which needs to be studied further.

A



B



C

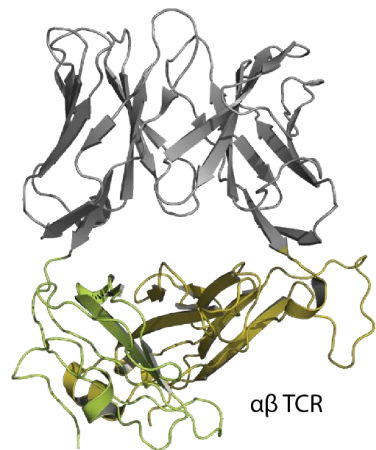


Figure 4: Secondary structure of chimeric $\gamma\delta$ TCR

(A) Circular dichroism (CD) spectra of $\alpha\beta$ TCR (black squares) and $\gamma\delta$ TCR (blue spheres). (B) Secondary structure composition of $\gamma\delta$ TCR and $\alpha\beta$ TCR estimated from the CD spectra. Indicated are α -helix, β -strand and unordered structure, respectively. (C) Cartoon presentation of $\alpha\beta$ TCR (2XN9) created in PyMOL, the constant domains TRAC (green) and TRBC (yellow) and variable domains (grey) are shown.

Well-separated protein particles detected by negative stain

Very few three-dimensional structures of human $\gamma\delta$ TCR are available, thus the goal would be to retrieve a high-resolution three-dimensional structure of the chimeric $\gamma\delta$ TCR. To determine the 3D structure applying X-ray crystallography the protein must form a well-packed crystal. Numerous crystallization trials have been executed without the success of retrieving well-diffracting crystals. An alternative method to retrieve high-resolution structural information but without having to crystallize the protein, is single particle cryo-EM. However, commonly higher molecular weight proteins (>150 kDa) results in better final resolution, still recently also smaller proteins have been successful. A pre-requisite for successful single particle cryo-EM data collection is a well dispersed protein sample. Thus, negative staining was performed to visualize if the protein is well behaving under those conditions. Single particle of the chimeric $\gamma\delta$ TCR with the characteristic opposing double V-form could be seen in negative stain (Fig. 5A-B). A model of the 3D structure of the chimeric $\gamma\delta$ TCR was created in PyMOL, by aligning TRGV9/TRDV2 (PDB ID:1HXM) (Allison et al. 2001) and TRAC/TRBC (PDB ID: 2XN9) (Saline et al. 2010). The surface presentation of the model of chimeric $\gamma\delta$ TCR (Fig. 5C) is overlayed with the negative stain zoom-in picture (Fig. 5B) to highlight the particle features (Fig. 5D), concluding that although the protein is rather small it would be valuable to collect cryo-EM data aiming at retrieving a high-resolution structure.

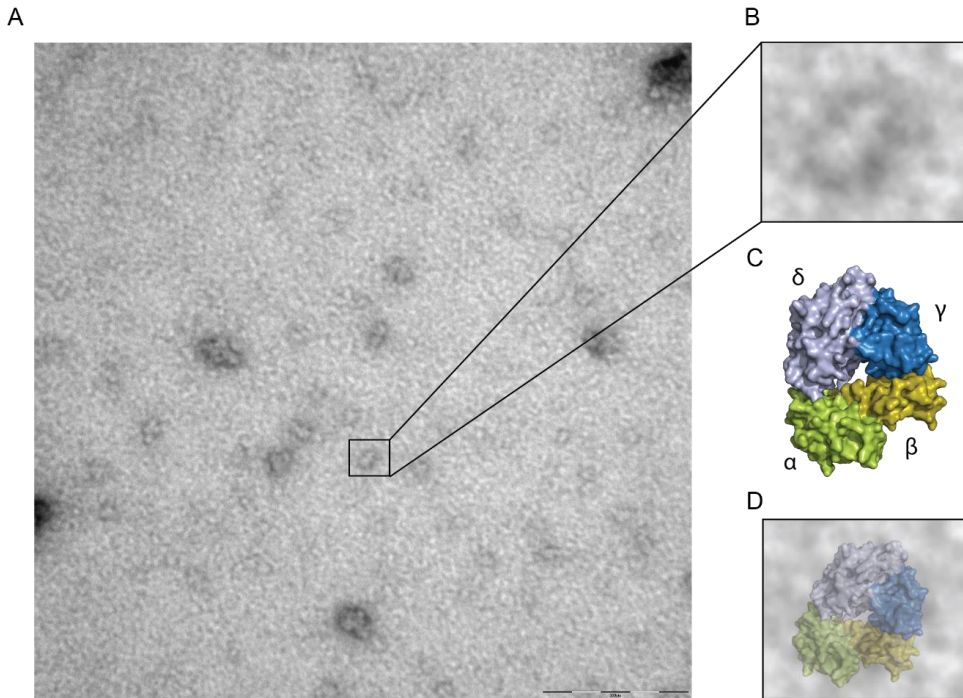


Figure 5: Negative stain of chimeric $\gamma\delta$ TCR

(A) TEM micrograph of chimeric $\gamma\delta$ TCR. (B) Zoom-in picture of single particle. (C) Surface presentation of model of chimeric $\gamma\delta$ TCR created in PyMOL. The constant domains are shown in green (TRAC) and yellow (TRBC) and the variable domains TRGV9 and TRDV2 in light blue and blue, respectively. (D) Overlay of model of chimeric $\gamma\delta$ TCR in surface presentation and single negative stain particle to highlight structural features.

The chimeric $\gamma\delta$ TCR is activate and forms a complex with staphylococcal enterotoxin A

To investigate if the $\gamma\delta$ TCR produced is active, native PAGE electrophoresis was performed to evaluate the binding between Staphylococcal Enterotoxin A (SEA) and the chimeric $\gamma\delta$ TCR (Fig. 6). SEA: $\gamma\delta$ TCR and SEA: $\alpha\beta$ TCR as positive control (Rödström et al. 2016) were mixed in a molar ratio (1:1, 1:2 or 2:3). To confirm that SEA and TCR forms a complex, a specific anti-SEA antibody was used. As can be seen in figure 6, an extra band with a molecular weight approximately 70 kDa is detected, suggesting that SEA can form a complex with both $\gamma\delta$ TCR and $\alpha\beta$ TCR. This is supported by the increasing concentrations of the respective TCRs in the samples we noted that 70 kDa band became stronger (Figure 6, blue arrows). Interestingly the

higher molecular band formation of $\alpha\beta$ TCR and $\gamma\delta$ TCR with SEA look very similar, further emphasizing that SEA directly binds $\gamma\delta$ TCR and is active.

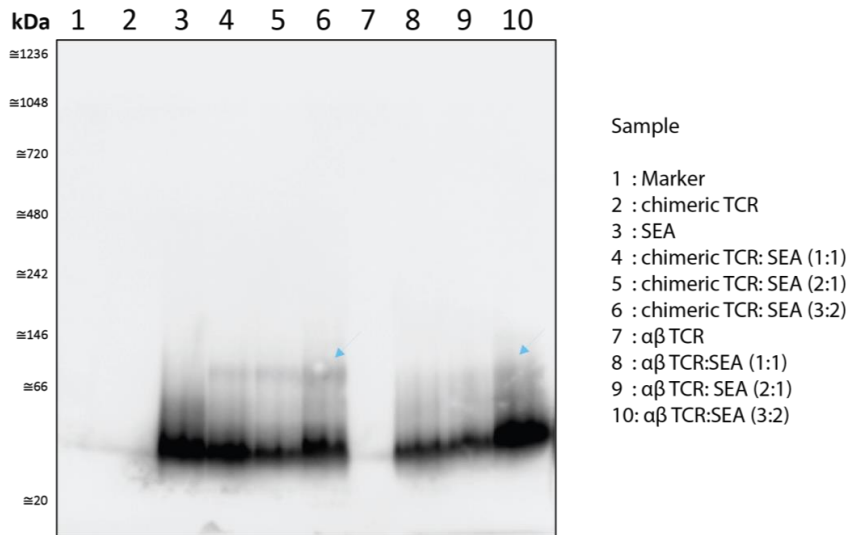


Figure 6: Complex formation of $\gamma\delta$ TCR and SEA shown with native page western blot

Native PAGE western blot (α -SEA) with SEA: chimeric $\gamma\delta$ TCR (left) and SEA: $\alpha\beta$ TCR (right). Proteins were loaded alone in their highest concentration and were also mixed in a molar ratio (1:1, 1:2 or 2:3) and loaded in increasing concentrations.

Conclusion

$\gamma\delta$ T cells are shown to be involved in a variety of diseases in humans and needs to be further studied to deepen the understanding of the role of $\gamma\delta$ T cells in these pathologies. Here, we report a periplasmic bacterial system for the rapid expression of soluble $\gamma\delta$ TCR. A chimeric version of $\gamma 9\delta 2$ TCR was successfully expressed with final yields of 8.5 mg/L culture. Moreover, the $\gamma 9\delta 2$ TCR showed a well-dispersed profile as judged by negative stain and size exclusion chromatography. Interestingly, the chimeric version of $\gamma 9\delta 2$ TCR showed a rather high content of α -helical secondary structure suggesting that it adopts somewhat different fold than $\alpha\beta$ TCR, which could explain the differences in antigen specificity between these two

TCRs. Finally, the activity was confirmed by detecting a complex formation with the superantigen SEA. The availability of large amounts of pure $\gamma\delta$ TCR will facilitate future experiments to understand the role of $\gamma\delta$ T cells in the immune system and shed light in the mechanism of the interaction of superantigens with this unconventional TCR that is discussed for more than 30 years.

Methods

Construct design, strains and plasmid preparation

The chimeric construct was designed by using the constant domains of the $\alpha\beta$ TCR and adding the variable chains from (TRGV9/ TRDV2) (Fig. 1A-B). V γ 9 was fused with the beta constant domain and the V δ 2 to the alpha constant domain. The constant domains are stabilized by an S-S bridge (Fig. 1C). The single chain constructs (Fig. S1) were subcloned into a pUC57 vector (AmpR) harbouring a lac promoter. The construct was cloned in the restriction sites *NdeI* and *HindIII*. The plasmids were ordered from GenScript.

Protein production

The schematic of the overall workflow is shown in Figure 2.

Transformation and expression

The plasmids of the TCR chain constructs (Fig. 1 A-B) were transformed into *E.coli* BL21 (DE) chemically competent cells by heat shocking at 42 °C for 45 s. 1 mL LB (10 g/L tryptone, 5 g/L yeast extract, 5 g/L NaCl) was added to each and incubated at 37 °C for 1 h. They were plated on LB (Ampicillin) plates (10 g/ L tryptone, 5 g/L yeast extract, 5g /L NaCl, 5 g/L agar) and incubated ON at 37 °C. Colonies were picked and a pre-culture of 5 mL LB supplemented

with Ampicillin was grown for 8 h at 37 °C at 180 rpm. The pre-cultures were inoculated in 1 L phosphate buffered SB media (32 g/L tryptone, 20 g/L yeast extract, 5 g/L NaCl adjust pH to 7) and grown at 33 °C at 180 rpm ON. The cultures were spun down at 5000 xg for 20 min at 4 °C and resuspended in fresh media (phosphate buffered SB) and further grown at 33 °C. After 30 min protein expression was induced with 500 µM IPTG and the temperature was lowered to 29 °C. After 4 h expression the cells were harvested by centrifugation, 5000 xg for 20 min at 4 °C. The pellets were flash frozen in liquid nitrogen and stored in -20 °C. Afterwards the pellets were resuspended in 100 mL homogenizing buffer (50 mM Tris-HCl pH 8, 750 mM sucrose, 1 mM EDTA, 10 mM DTT) and stirred for 1 h. 250 mL lysis buffer (20 mM Tris-HCl pH 8, 100 mM NaCl, 1 % (w/v) deoxycholate, 1 % (v/v) Triton X-100, 10 mM DTT, 0,3 mg/mL lysozyme, DNase and MgCl₂ to final concentration of 0.5 mM were added and continued stirring for another couple of hours. The lysates were frozen in -20 °C.

Washing of inclusion bodies

The lysates were thawed and more DNase and MgCl₂ was added, stirred for another hour, and spun down at 10000 xg for 30 min at 4 °C. The supernatant was discarded, and the pellets were resuspended with 100 mL of wash buffer A (50 mM Tris-HCl pH 8, 100 mM NaCl, 1 mM EDTA, 0,5 % (v/v) Triton, 10 mM DTT) and washed at 4 °C ON. The inclusion bodies were harvested at 10000 xg for 20 min at 4 °C and the washed with buffer A and centrifugation was repeated. After the second wash, the inclusion bodies were resuspended in 50 mL wash buffer B (50 mM Tris-HCl pH 8, 1 mM EDTA, 0,5 % (v/v) Triton, 10 mM DTT). The inclusion bodies were washed at 4 °C ON by continuous stirring. The inclusion bodies were spun down at 10000 xg for 20 min at 4 °C. The inclusion bodies were dissolved with the homogenizer in 30 mL solubilization buffer (50 mM Tris-HCl pH 8, 10 mM EDTA, 6 M guanidinium chloride, 100 mM NaCl, 5 mM DTT) and centrifuged again at 20000 xg for 1 h at 4 °C. The supernatant

containing the dissolved inclusion bodies with a protein concentration of 7-13 mg/mL were flash frozen in liquid nitrogen.

Refolding

A 1:1 ratio of each TCR chain (~28 mg) was used for refolding in 200 mL refolding buffer (100 mM Tris-HCl pH 8, 5 M urea, 400 mM L-arginine, 0.83 mg/ L cysteamine hydrochloride, 0.73 mg/ L cysteamine dihydrochloride). The protein solution was transferred into a dialysis membranes (Spectra/Por^(R), USA) MWCO 14,000 Da and dialysed ON night at 4 °C against 5 L MQ water and then again ON night against 5 L 5 mM Tris pH 8 with continued stirring.

Purification

The refolded solution was filtered (0.45 µm filter). The supernatant was loaded via sample pump on a 6 mL Res Q (Cytiva) column. The column was washed with 5 CV buffer (20 mM Tris- HCl pH 8). To remove contaminants and aggregates a stepwise elution with an increasing NaCl concentration of the elution buffer was conducted. With 10 CV 33 %, 10 CV 60 % and 5 CV 100 % of elution buffer (20 mM Tris-HCl pH 8, 300 mM NaCl). Unfolded and contaminating proteins were eluted by the 30 % step, most of the folded TCR was eluted in the 60 % step, and aggregated TCR was eluted in the 100 % step. Folded TCR was concentrated and loaded on Superdex 200 increase (GE Healthcare) (20 mM HEPES pH 7.4, 150 mM NaCl, 5 % glycerol). The main peak was collected, concentrated (Amicon^(R) Ultra, Merck, Millipore Ltd. Cork, Ireland) and re-run on Superdex 200 (GE Healthcare) to obtain a monodisperse peak.

Circular dichroism spectroscopy

Circular dichroism (CD) was used to analyse the secondary structure of $\gamma\delta$ TCR. Protein was resuspended in HBS buffer (10 mM HEPES pH 7.4, 150 mM NaCl) at 1 μ M as final concentration. The $\alpha\beta$ TCR (1 μ M) in the same buffer was used as a control. The measurements were performed on a Jasco J-810 spectropolarimeter (Jasco, Tokyo, Japan) equipped with a Jasco CDF-426S Peltier set to 20 °C. Quartz cuvettes (0.1 cm) (Hellma, GmbH & Co, KG, Müllheim, Germany) was used. The spectra were recorded at 200–260 nm (scan speed: 20 nm min⁻¹) as an average of 3 measurements. Raw spectra were corrected for buffer contribution and converted to the mean residue ellipticity, (mdeg cm² dmol⁻¹). The Secondary structure composition of $\gamma\delta$ TCR and $\alpha\beta$ TCR was estimated from the CD spectra with the online CD analysis site DICHROWEB (<http://dichroweb.cryst.bbk.ac.uk>).

Negative stain

Negative staining was used to visualise $\gamma\delta$ TCR and demonstrate that the protein is well behaved for future cryo-EM studies. 5 μ L of 0.02 mg/mL of $\gamma\delta$ TCR were transferred to a carbon coated/ piolo term 400 mesh copper grid (Maxtaform) and incubated for 20 min. Left over material was removed with blotting paper. 5 μ L uranyl acetate (2 %) was used as a staining solution and was incubated for 2 min. Afterwards 5 μ L MQ was used for washing also incubated for 2 min. Samples were analysed with an electron microscope (TECNAI Biotwin 120 kV, FEI).

Native polyacrylamide gel electrophoresis and western blot

To analyse the binding between SEA (produced according (Uzunçayır et al. 2022) and $\gamma\delta$ TCR, the proteins were mixed in a molar ratio (1:1, 1:2 or 2:3). Binding of SEA with $\alpha\beta$ TCR (molar ratio 1:1, 1:2 or 2:3) was used as positive control (Rödström et al. 2016). Samples were incubated for 15 min at RT, then mixed with loading buffer (Invitrogen, Carlsbad, CA, USA) and loaded on BN-PAGE (NativePAGE Bis-Tris Gels System 4–16%, Invitrogen, Carlsbad, CA, USA). The Marker Native Mark™ Protein Std (Invitrogen, Carlsbad CA) was used. Electrophoresis was performed at 150 V for 100 min according to the manufacturer's instructions. For western blotting, the material was subsequently transferred to a PVDF membrane using a Trans-Blot Turbo system (Bio-Rad, Laboratories, Hercules, CA, USA). SEA was detected using monoclonal rabbit antibodies against SEA (diluted 1:1000, Santa Cruz Biotechnology, Inc., Dallas, Texas, U.S.A.), followed by swine anti-rabbit HRP conjugated antibodies (1:1000, Dako, Glostrup, Denmark). The protein was visualized by incubating the membrane with SuperSignal West Pico Chemiluminescent Substrate (Thermo Scientific, Rockford, IL, USA) for 5 min, followed by detection using a ChemiDoc XRS Imager (Bio-Rad Laboratories, Hercules, CA, USA).

Acknowledgements

We would like to thank Lina Gerfors for helping us with the electron microscope and Jonas Ahlstedt from LBIC for refining our pictures with photoshop.

Publication bibliography

Allison, T. J.; Winter, C. C.; Fournie, J. J.; Bonneville, M.; Garboczi, D. N. (2001): Crystal Structure of a Human Vgamma9/Vdelta2 T Cell Receptor.

Bigby, M.; Markowitz, J. S.; Bleicher, P. A.; Grusby, M. J.; Simha, S.; Siebrecht, M. et al. (1993): Most gamma delta T cells develop normally in the absence of MHC class II molecules. In *Journal of immunology (Baltimore, Md. : 1950)* 151 (9), pp. 4465–4475.

Bonneville, Marc; O'Brien, Rebecca L.; Born, Willi K. (2010): Gammadelta T cell effector functions: a blend of innate programming and acquired plasticity. In *Nature reviews. Immunology* 10 (7), pp. 467–478. DOI: 10.1038/nri2781.

Boulter, Jonathan M.; Glick, Meir; Todorov, Penio T.; Baston, Emma; Sami, Malkit; Rizkallah, Pierre; Jakobsen, Bent K. (2003): Stable, soluble T-cell receptor molecules for crystallization and therapeutics. In *Protein engineering* 16 (9), pp. 707–711. DOI: 10.1093/protein/gzg087.

Brenner, M. B.; McLean, J.; Dialynas, D. P.; Strominger, J. L.; Smith, J. A.; Owen, F. L. et al. (1986): Identification of a putative second T-cell receptor. In *Nature* 322 (6075), pp. 145–149. DOI: 10.1038/322145a0.

Chien, Y.; Becker, D. M.; Lindsten, T.; Okamura, M.; Cohen, D. I.; Davis, M. M. (1984): A third type of murine T-cell receptor gene. In *Nature* 312 (5989), pp. 31–35. DOI: 10.1038/312031a0.

Gao, Yifang; Williams, Anthony P. (2015): Role of Innate T Cells in Anti-Bacterial Immunity. In *Frontiers in immunology* 6, p. 302. DOI: 10.3389/fimmu.2015.00302.

Groh, V.; Steinle, A.; Bauer, S.; Spies, T. (1998): Recognition of stress-induced MHC molecules by intestinal epithelial gammadelta T cells. In *Science (New York, N.Y.)* 279 (5357), pp. 1737–1740. DOI: 10.1126/science.279.5357.1737.

Hayday, A. (1985): Structure, organization, and somatic rearrangement of T cell gamma genes. In *Cell* 40 (2), pp. 259–269. DOI: 10.1016/0092-8674(85)90140-0.

He, Ying; Wu, Kangni; Hu, Yongxian; Sheng, Lixia; Tie, Ruxiu; Wang, Binsheng; Huang, He (2014): $\gamma\delta$ T cell and other immune cells crosstalk in cellular immunity. In *Journal of immunology research* 2014, p. 960252. DOI: 10.1155/2014/960252.

Kierkels, G. J. J.; Scheper, W.; Meringa, A. D.; Johanna, I.; Beringer, D. X.; Janssen, A. et al. (2019): Identification of a tumor-specific allo-HLA-restricted $\gamma\delta$ TCR. In *Blood advances* 3 (19), pp. 2870–2882. DOI: 10.1182/bloodadvances.2019032409.

Koning, F.; Rust, C. (1992): Staphylococcal enterotoxin-mediated human T-T cell interactions. In *Journal of immunology (Baltimore, Md. : 1950)* 149 (1), pp. 317–322.

Legut, Mateusz; Cole, David K.; Sewell, Andrew K. (2015): The promise of $\gamma\delta$ T cells and the $\gamma\delta$ T cell receptor for cancer immunotherapy. In *Cellular & molecular immunology* 12 (6), pp. 656–668. DOI: 10.1038/cmi.2015.28.

Mata Forsberg, Manuel; Arasa, Claudia; van Zwol, Willemien; Uzunçayır, Sibel; Schönrichler, Anna; Regenthal, Paulina et al. (2021): Activation of human $\gamma\delta$ T cells and NK cells by Staphylococcal enterotoxins requires both monocytes and conventional T cells. In *Journal of leukocyte biology*. DOI: 10.1002/JLB.3A1020-630RR.

- Matis, L. A.; Fry, A. M.; Cron, R. Q.; Cotterman, M. M.; Dick, R. F.; Bluestone, J. A. (1989): Structure and specificity of a class II MHC alloreactive gamma delta T cell receptor heterodimer. In *Science (New York, N.Y.)* 245 (4919), pp. 746–749. DOI: 10.1126/science.2528206.
- Morita, C. T.; Mariuzza, R. A.; Brenner, M. B. (2000): Antigen recognition by human gamma delta T cells: pattern recognition by the adaptive immune system. In *Springer seminars in immunopathology* 22 (3), pp. 191–217. DOI: 10.1007/s002810000042.
- Morita, Craig T.; Li, Hongmin; Lamphear, James G.; Rich, Robert R.; Fraser, John D.; Mariuzza, Roy A.; Lee, Hoi K. (2001): Superantigen Recognition by $\gamma\delta$ T Cells. In *Immunity* 14 (3), pp. 331–344. DOI: 10.1016/s1074-7613(01)00113-3.
- Rödröm, Karin E. J.; Regenthal, Paulina; Bahl, Christopher; Ford, Alex; Baker, David; Lindkvist-Petersson, Karin (2016): Two common structural motifs for TCR recognition by staphylococcal enterotoxins. In *Scientific reports* 6, p. 25796. DOI: 10.1038/srep25796.
- Rust, C.; Orsini, D.; Kooy, Y.; Koning, F. (1993): Reactivity of human gamma delta T cells to staphylococcal enterotoxins: a restricted reaction pattern mediated by two distinct recognition pathways. In *Scandinavian journal of immunology* 38 (1), pp. 89–94. DOI: 10.1111/j.1365-3083.1993.tb01698.x.
- Rust, C. J.; Koning, F. (1993): Gamma delta T cell reactivity towards bacterial superantigens. In *Seminars in immunology* 5 (1), pp. 41–46. DOI: 10.1006/smim.1993.1006.
- Rust, C. J.; Verreck, F.; Vietor, H.; Koning, F. (1990): Specific recognition of staphylococcal enterotoxin A by human T cells bearing receptors with the V gamma 9 region. In *Nature* 346 (6284), pp. 572–574. DOI: 10.1038/346572a0.
- Saline, M.; Rodstrom, K.E.J.; Fischer, G.; Orekhov, V. Y.; Karlsson, B. G.; Lindkvist-Petersson, K. (2010): Crystal structure of the ternary complex between human T cell receptor, staphylococcal enterotoxin H and human major histocompatibility complex class II.
- Uldrich, Adam P.; Le Nours, Jérôme; Pellicci, Daniel G.; Gherardin, Nicholas A.; McPherson, Kirsty G.; Lim, Ricky T. et al. (2013): CD1d-lipid antigen recognition by the $\gamma\delta$ TCR. In *Nature immunology* 14 (11), pp. 1137–1145. DOI: 10.1038/ni.2713.
- Uzunçayır, Sibel; Vera-Rodriguez, Arturo; Regenthal, Paulina; Åbacka, Hannah; Emanuelsson, Cecilia; Bahl, Christopher D.; Lindkvist-Petersson, Karin (2022): Analyses of the complex formation of staphylococcal enterotoxin A and the human gp130 cytokine receptor. In *FEBS letters*. DOI: 10.1002/1873-3468.14292.
- Vantourout, Pierre; Hayday, Adrian (2013): Six-of-the-best: unique contributions of $\gamma\delta$ T cells to immunology. In *Nature reviews. Immunology* 13 (2), pp. 88–100. DOI: 10.1038/nri3384.
- Wesch, D.; Hinz, T.; Kabelitz, D. (1998): Analysis of the TCR Vgamma repertoire in healthy donors and HIV-1-infected individuals. In *International immunology* 10 (8), pp. 1067–1075. DOI: 10.1093/intimm/10.8.1067.

Expression and Purification of human $\gamma\delta$ T Cell Receptor for Activity Studies

Sibel Uzunçayır¹, Ganna Petruk², Karin Lindkvist-Petersson^{1*}

1. Department of Experimental Medical Science, Lund University, BMC C13, 22184 Lund, Sweden
2. Department of Clinical Sciences, Lund University, BMC B14, 22814 Lund, Sweden

TRDV2/TRAC

MAIELVPEHQTVPVSIGVPATLRCSMKGEAIGNYYINWYRKTQGNTMTFIYREKDIYGPG

FKDNFQGDIDIAKNLAVLKILAPSERDEGSYYCACDTLGMGGEYTDKLIFGKGTRVTVE

PNIQNPDPAVYQLRDSKSSDKSVCLFTDFDSQTNVSQSKDSDVYITDK

CVLDMRSMDFKSNSAVAWSNKSDFACANAFNNSIIPEDTFFPSPESS

TRGV9/TRBC

MAGHLEQPQISSTKTLSKTARLECVVSGITISATSVYWRERPGEVIOFLVSISYDGTVRK

ESGIPSGKFEVDRIPETSTSTLTIHNVEKQDIATYYCALWEAQQELGKKIKVFGPGTKLII

EDLKNVFPPEVAVFEPSEAEISHTQKATLVCLATGFYPDHVELSWWVNGKEVHSGVCTDPQPLKE

QPALNDSRYSLSSRLRVSATFWQNPRNHFRCQVQFYGLSENDEWTQDRAKPVTOIVSAEAWGRAD


Figure S1: Amino acid sequence of chimeric chains

TRDV2 fused to TRAC are underlined in light blue and green, respectively. TRGV9 fused to TRBC are underlined in dark blue and yellow, respectively. Cysteines that form the disulfide bond are highlighted in purple.

Paper III



Analyses of the complex formation of staphylococcal enterotoxin A and the human gp130 cytokine receptor

Sibel Uzunçayır¹, Arturo Vera-Rodriguez^{2,3}, Paulina Regenthal¹, Hannah Åbacka¹, Cecilia Emanuelsson⁴, Christopher D. Bahl^{2,3} and Karin Lindkvist-Petersson^{1,5} 

¹ Department of Experimental Medical Science, Lund University, Sweden

² Institute for Protein Innovation, Boston, MA, USA

³ Division of Hematology-Oncology, Boston Children's Hospital, Harvard Medical School, Boston, MA, USA

⁴ Department of Chemistry, Division for Biochemistry and Structural Biology, Lund University, Sweden

⁵ LINXS – Lund Institute of Advanced Neutron and X-ray Science, Sweden

Correspondence

K. Lindkvist-Petersson, Department of Experimental Medical Science, Lund University, BMC C13, 221 84 Lund, Sweden
Tel: +46 46 2228041
E-mail: karin.lindkvist@med.lu.se

(Received 28 October 2021, revised 14 December 2021, accepted 10 January 2022)

doi:10.1002/1873-3468.14292

Edited by Dietmar Manstein

Superantigens (SAGs) are bacterial enterotoxins produced by *Staphylococcus aureus*. Staphylococcal enterotoxin type A (SEA), a staphylococcal superantigen, has been shown to bind to the cytokine signalling receptor glycoprotein 130 (gp130). The structural details, as well as the exact physiological role of this interaction, remain unclear. Here, we describe the structural details of the SEA–gp130 complex by combining crosslinking mass spectrometry and computational modelling. Interestingly, SEA is not able to bind gp130-homologues from rat and mouse. Our data suggest that SEA may interact with human gp130 in a different manner than other known gp130-ligands. Moreover, the fact that SEA does not bind mouse or rat gp130 suggests that SAGs have additional mechanisms of action in humans.

Keywords: food poisoning; gp130; SEA; SPR; superantigen

The bacterium *Staphylococcus aureus* produces a wide range of different virulence factors that cause disease, among these are the staphylococcal enterotoxins, abbreviated SE-A,B,C...etc. SEs can be divided into five distinct evolutionary groups (I–V) depending on sequence similarity [1]. The SEs are known to bind to both the major histocompatibility complex (MHC) class II on antigen-presenting cells and to the T cell receptor (TCR) on T cells. Thus, the SEs are able to trigger a polyclonal activation of T cells which results in cellular proliferation and production of proinflammatory cytokines such as tumour necrosis factor (TNF) α and β , and interleukin-2 (IL-2) [2]. Exposure to SEs commonly results in food poisoning, emesis, fever, and it can lead to multi-organ failure and death.

Because of the extreme polyclonal activation of T cells, they have received the designation: superantigen (SAG). All studied SAGs from *S. aureus* have a similar overall three-dimensional fold, containing one N-terminal domain and one C-terminal domain with a shallow cleft in the middle where TCR binds [3]. SEs can either use the N- or the C-terminal domain to bind MHC class II, and some SEs can use both domains to crosslink two MHC class II molecules on the surface of cells [4]. The interaction between MHC class II and the C-terminal domain is of high affinity (nano-molar range) and dependent on the presence of Zn^{2+} [5], while the interaction with the N-terminal domain is of lower affinity (micro-molar range) [6]. Recently, it was demonstrated that both a classical

Abbreviations

CNTF, ciliary neurotrophic factor; FNIII, fibronectin type III; Gp130, glycoprotein 130; IL, interleukin; IL-6R, interleukin-6 receptor; JAK, janus activated kinase; LIF, leukaemia inhibitory factor; MHC, major histocompatibility complex; OSM, oncostatin M; SAg, superantigen; SE, staphylococcal enterotoxin; SPR, surface plasmon resonance; STAT, signal transducer and activator of transcription; TCR, T cell receptor; XL-MS, crosslinking mass spectrometry.

SAG and SE-like SAGs, can bind to another receptor glycoprotein 130 (gp130) [7,8]. Gp130 is the signalling receptor for the IL-6 family of cytokines, including IL-6, LIF, IL-11, CNTF and OSM [9]. Binding to the gp130 receptor by cytokines, such as interleukin-6 (IL-6) and leukaemia inhibitory factor (LIF), is often overlapping [10]. Gp130 activation results in intracellular phosphorylation cascades primarily involving janus activated kinase (JAK) and signal transducer and activator of transcription (STAT) family members [11]. However, each cytokine also has its own unique binding mode, which is achieved through the assembly of extracellular receptor/ligand complexes, and differences can lead to altered signalling outcomes. The three-dimensional structure of human gp130 is known and it can be divided into six extracellular domains: an N-terminal Ig-like domain (D1); a cytokine-binding module (D2–D3); and three fibronectin type III (FNIII) domains (D4–D6) [10,12]. SEA utilizes its C-terminal domain for binding to gp130 in a similar fashion as it binds to MHC class II, as MHC and gp130 bind competitively to SEA [7]. Further supporting this, substituting the central zinc coordinating residue (D227) abolishes gp130 binding [7]. Moreover, it was demonstrated that SEA binds to domain D1–D3 of gp130 with low micromolar affinity (0.9 μM) [7], which is in the same range as SEA binds to its other ligand TCR (2.2 μM) [13].

Here, we show that SEE can bind gp130 with a similar affinity as SEA while SEH has a ten times lower affinity, demonstrating that the ability to bind gp130 is not unique to SEA. Moreover, we describe the atomic details of the SEA-gp130 complex formation by combining lysine-specific crosslinking mass spectrometry (XL-MS) and computational simulations. Strikingly, the structural model shows that SEA utilize both its C-terminal domain and the N-terminal domain to bind gp130, in a similar fashion as SEA crosslinks two MHC molecules [4].

Results

The superantigens SEA and SEE interact with the human gp130 receptor

To first sought to determine if SEs other than SEA can bind human gp130 receptor [7], we expressed and purified SEE and SEH and investigated their ability to bind gp130 using surface plasmon resonance (SPR) analyses. Different concentrations of SEA, SEE and SEH, ranging from 30 nM to 40 μM , were injected over immobilized gp130 receptor and the responses were recorded (Fig. 1). Plotting the responses at steady state

against the concentrations and fitting the data with nonlinear regression showed that SEA and SEE clearly bind to the gp130 receptor with micro molar affinity (Fig. 1A,B). From the kinetic data, we calculated the equilibrium dissociation constant (K_D) for the SEA-gp130 complex to be 0.5 μM and for the SEE-gp130 complex to be 2.7 μM (Fig. 1A,B). The binding of SEH was much weaker compared to SEA and SEE (Fig. 1C). We calculated the K_D of the SEH-gp130 complex to be approximately 35 μM ; this value is an estimation as the binding curves did not reach saturation (Fig. 1C). Within the SAGs of group III, SEA has the highest sequence identity with SEE (82%) and a much lower identity with SEH (31%), based on sequence alignments with CLUSTAL W [14]. Thus, this suggests that although the C-terminal domain of SEA and SEH are similar, crucial differences must be present at residues important for gp130 binding activity.

The SAG-gp130 complex formation is zinc-dependent

SEA binding to gp130 has previously been shown to require the zinc coordinating residue Asp227, which is located at the C-terminal domain of SEA [7]. To investigate if the binding between SEE and gp130 also is Zn²⁺-dependent, SPR experiments were repeated (with an analyte concentration of 20 μM), in the presence of either Zn²⁺ or EDTA (a metal chelating agent). As seen in Fig. 2, both SEA and SEE lost their ability to bind gp130 when EDTA was included in the buffer (Fig. 2A,B), showing that the gp130 binding is Zn²⁺-dependent for both SEA and SEE. Importantly, the Zn²⁺-coordinating aspartate (D227) in SEA is conserved in SEE, and the activity of SEE has also been suggested to be regulated by the presence of Zn²⁺ [15,16]. Thus, it is likely that SEE coordinates with the Zn²⁺ and binds to gp130 in a similar manner as SEA [17]. SEH has also been shown to coordinate Zn²⁺ but there are some differences in the residues in this region, compared to SEA (Fig. 2D,E) [18]. The aspartate is conserved, but SEH only uses two residues to coordinate the Zn²⁺-ion, while SEA and SEE use three residues. Overlaying the structures of SEA (PDB ID: 1SXT) and SEH (PDB ID: 1EWC) [17,18] reveals a 3 Å movement of the Zn²⁺ ion (Fig. 2C); this could contribute to a modulation of the affinity between SEH and gp130.

SEA and SEE are selective for human gp130

SEs are known to activate T cells by binding to the TRAV/TRBV domains of the TCR, and each

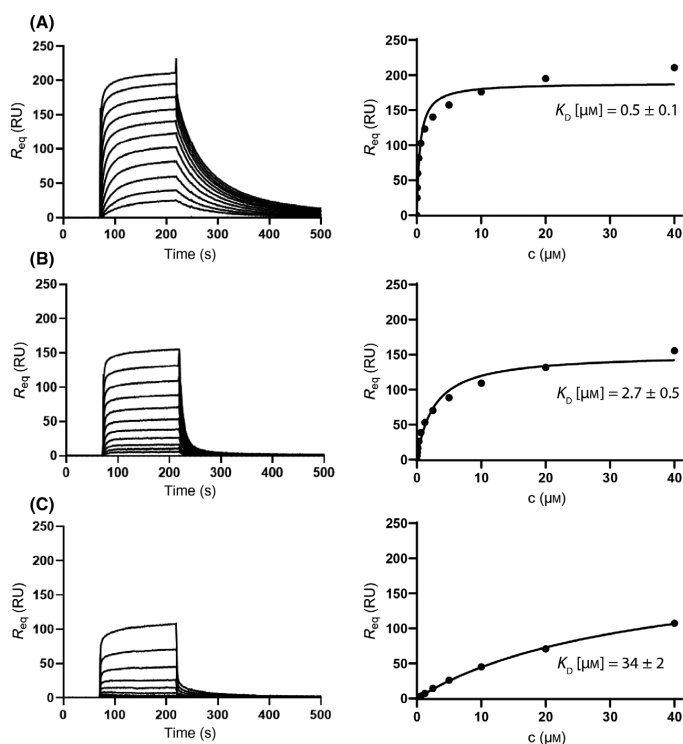


Fig. 1. SEA and SEE bind to the gp130 receptor with low micro molar affinity. SPR sensorgrams showing the binding for superantigens to gp130. A two-fold concentration series of (A) SEA, (B) SEE and (C) SEH were injected over immobilized human gp130-Fc dimer. The concentrations shown are ranging from 30 nM to 40 μ M. The affinity is calculated via nonlinear regression and the standard error is shown.

enterotoxin commonly binds a repertoire of different TRAV/TRBV domains [2]. SEH is an exception as it has been shown to bind only TRAV27 [13,19] and as a consequence it cannot activate T cells in mice, where TRAV27 is not expressed [20]. Along those lines, we set out to investigate whether SEA and SEE could bind to gp130 from mouse and rat. Again, using SPR, gp130 from human, mouse and rat was immobilized, and different concentrations of either SEA or SEE (1–16 μ M) were injected. Interestingly, both SEA (Fig. 3A–C) and SEE (Fig. 3D–F) showed a clear lack of binding to both gp130 from mouse and rat, while binding to human gp130 was able to be recorded. To validate the specific recognition of the analysed gp130 proteins, LIF was used as positive control and showed clear binding to all the gp130 variants (Fig. S1). Sequence alignment between the mouse, rat and human gp130 (domains D1–D3) showed that there are certain regions that are more conserved than others (Fig. 3G). Overall, the sequence identity between gp130 D1–D3 in mouse and rat is high (~86% according to CLUSTAL w), while the human sequence has only approximately 70% sequence identity. Previously, it

was reported that SEA can activate rat adipocytes presumably through gp130 [7]. The results presented here suggest that superantigen biology is likely even more complex than previously believed and possibly other receptors can contribute to the superantigen-induced activation in adipocytes. These results point at molecular differences for the recognition of human and mouse/rat gp130 receptors by SAgS.

XL-MS suggest dual binding modes between SEA and gp130

To further explore the interaction between SEA and gp130, we used XL-MS to detect residues at the binding interface within the SEA-gp130 complex in order to obtain distance constraints for structural modelling of the complex. Equimolar amounts of SEA were mixed with either full-length human gp130 Fc dimer or human gp130_{D1–D3} (only including D1–D3 of gp130); the lysine-specific crosslinker BS3 was added at different molar ratios relative to protein. Cross-linked samples inspected after sample fractionation by denaturing electrophoresis showed multiple higher

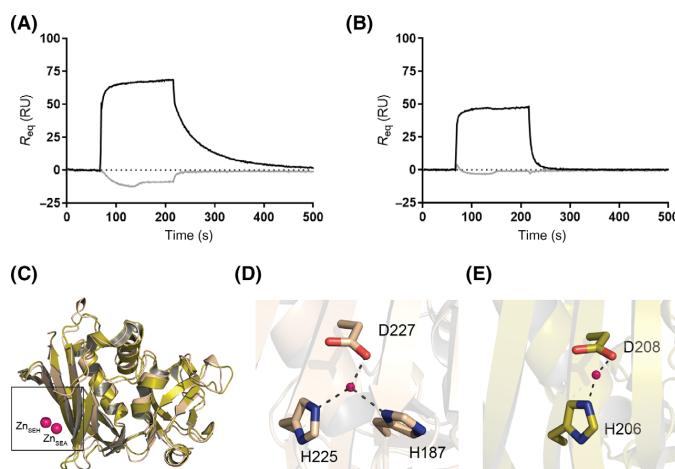


Fig. 2. The interaction between SEA/SEE and gp130 is Zn^{2+} dependent. Surface plasmon resonance sensorgram showing in (A) SEA injected over immobilized gp130-Fc dimer at a concentration of $20 \mu\text{M}$ in the presence of 0.1 mM ZnCl_2 (black) or EDTA (grey) and in (B) SEE injected over immobilized gp130-Fc dimer at a concentration of $20 \mu\text{M}$ in the presence of 0.1 mM ZnCl_2 (black) or EDTA (grey). The responses units (RU) were recorded and plotted against time (s). (C) SEA (PDB ID: [1SXT](#), model in wheat) and SEH (PDB ID: [1EWC](#), model in gold) structures with the coordinated zinc were overlaid, shown in cartoon representation. (D) SEA coordination of zinc (magenta) with residues H187, H225 and D227 shown as sticks. (E) SEH coordination of zinc (magenta) with residues D206 and H208 shown as sticks.

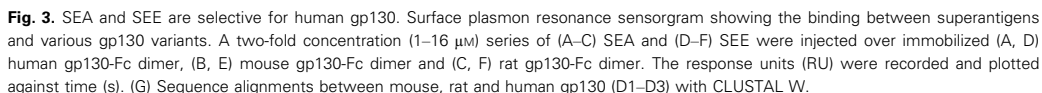
molecular weight bands, including a band in the expected size for the possible SEA-gp130 (D1–D3) complex (62 kDa; Fig. S2). These bands were excised and analysed after proteolytic in-gel digestion, and crosslinked peptides were detected by mass spectrometry. All the samples used for the electrophoretic pre-fractionation were also analysed by proteolytic in solution digestion, in order to maximize the chance to reliably detect and identify crosslinks. Data were collected after both in-gel digestion and in solution digestion, with and without prior alkylation and cleavage with the AspN protease. The sequence coverage was $>50\%$ for SEA and approximately 30% for gp130_{D1–D3}. To exclude false positives, only crosslinked peptides that were validated by MSMS were considered in the subsequent data analysis. The detected crosslinks are presented in Fig. 4 and in the Fig. S3 and Table S1.

Four intermolecular crosslinks between SEA and gp130 were detected, Lys79_{SEA} and Lys29_{gp130}, Lys14_{SEA} and Lys151_{gp130}, Lys79_{SEA} and Lys139_{gp130}, Lys79_{SEA} and Lys151_{gp130} (Fig. 4A, Table S1). We used the software xVis to visualize the crosslink-derived distance restraints of the SEA-gp130 protein complex (Fig. 4A). Although the crosslinked residues on SEA are sequentially distant from each other (Lys14 and Lys79), they are both situated on the Zn-coordinating

side of SEA (Fig. 4B). These findings support the hypotheses that the C-terminal domain interacts directly with gp130 upon complex formation, and this correlates well with previously published data [7]. Moreover, the three lysines from gp130 (Lys29, Lys139, Lys151) that form crosslinks with SEA are all situated in D1 and D2 and are pointing towards each other. This suggests that SEA binds between D1 and D2 on gp130 (Fig. 4C). However, as Lys79 in SEA could be crosslinked with all the detected lysines in gp130, and Lys29 and Lys139/151 are far apart in the three-dimensional structure of gp130, two distinct crosslink models between the C-terminal domain of SEA and the D1/D2 domains of gp130 were generated in order to satisfy all of the crosslinks that we detected (Fig. 4D,E).

Computational docking analyses conclude a three-dimensional model of the complex

Next, we performed computational modelling to evaluate the two binding modes suggested by the XL-MS experiments. To that extent the identified crosslinks were used as distant constraints (from 26 to 30 \AA) during docking simulations between the crystal structures of SEA (bound to Zn^{2+}) (PDB ID: [1SXT](#)) [17,18] and human gp130 (PDB ID: [1IIR](#)) [21] using HADDOCK 2.4



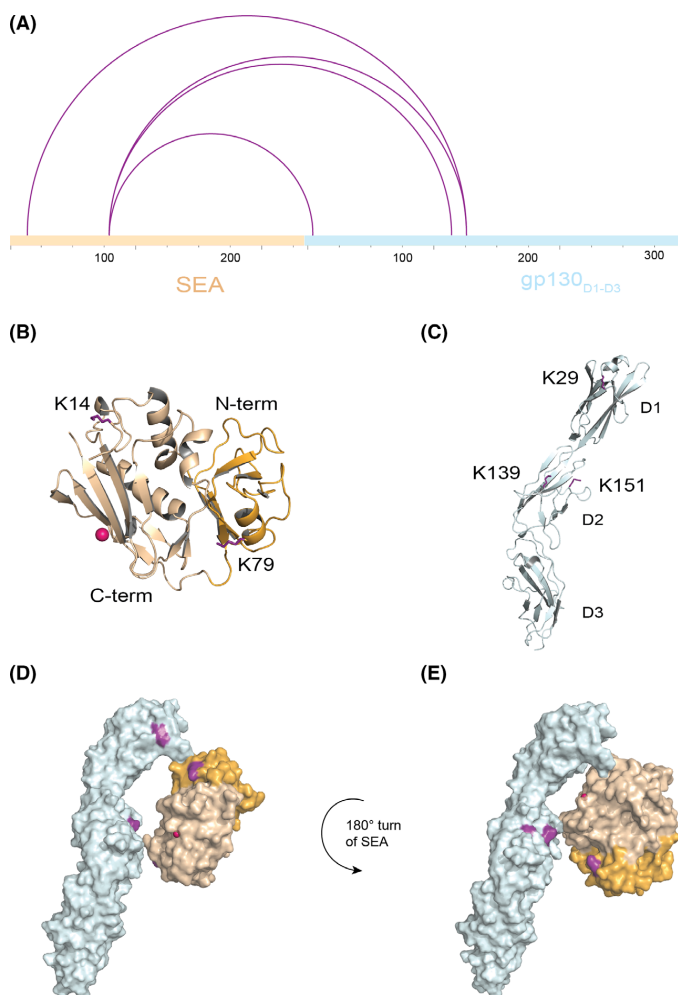


Fig. 4. XL-MS suggests dual binding modes between SEA and gp130. (A) The software xVis was used to visualize the crosslink derived distance restraints (purple lines) of the SEA-gp130 protein complex. A scale for the amino acid sequence number of SEA and gp130 is displayed. (B) Cartoon representation of SEA, N-terminal domain (orange), C-terminal domain (wheat), Zn²⁺ (magenta) and identified crosslinks shown as sticks (purple). (C) Cartoon representation of gp130 D1–D3 (cyan) with identified crosslinks shown as sticks (purple). (D–E) Surface representation of two alternative placements created in PyMOL using XL-MS data, varying by a 180° vertical turn over SEA. The crosslinks with the highest scores are highlighted (purple). SEA is divided into: C-term (wheat) and N-term (orange). (D) Placement A fulfils crosslinks between Lys79_{SEA} – Lys29_{gp130} and Lys14_{SEA} – Lys151_{gp130} which are shown in purple. (E) Placement B fulfils crosslinks between Lys79_{SEA} – Lys139_{gp130} and Lys79_{SEA} – Lys151_{gp130} which are shown in purple.

[22]. Simulations produced 57 different models with relatively low energy scores that satisfied the distance constraints and had a zinc ion at the binding interface. However, only a few models had the zinc ion close to a residue on gp130 that could potentially coordinate it (His, Asp, Glu or Cys). Remarkably, in all those cases, His145 at the D2 domain of gp130 appeared to coordinate Zn²⁺ together with His187, His225 and Asp227 in the C-terminal domain of SEA. We then used Rosetta to refine these initial docked models. We successfully produced two models of the complex between SEA and gp130 that contain a zinc coordination site at the protein–protein interface and satisfy the

crosslinking data (Fig. 5A,B). Both models show that most of the interactions within the complex are located at the D2 domain in gp130. This region is poorly conserved between human and mouse/rat gp130, including His145 that is not conserved (Fig. 3G). Additionally, we observed another interface between D1 of gp130 and the N-terminal domain of SEA (Fig. 5B). Interestingly, this contact site is very similar to how SEA recognizes the α -chain of MHC class II [4], utilizing Phe47, Leu48 and His50. Thus, the presented gp130-SEA models very much structurally resemble how SEA crosslinks two MHC class II molecules on the surface of cells.

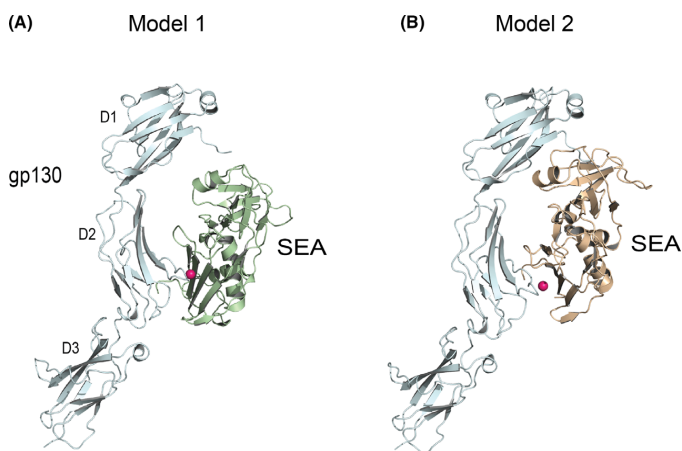


Fig. 5. Computational docking analyses narrows down the possible binding modes between SEA and gp130. DOCKING software (HADDOCK 2.4) produced models that were refined with Rosetta. The two most likely models are shown: (A) Model 1 of SEA (green) binding to gp130 D1–D3 (cyan) in cartoon representation. (B) Model 2 of SEA (wheat) binding to gp130 D1–D3 (cyan) in cartoon representation. The coordinated zinc is shown in magenta.

SEA and LIF occupy different binding sites of gp130

As described above, the computational docking analyses suggested a binding mode where a zinc ion is coordinated between the C-terminal domain of SEA and the His145 situated on the D2 domain of gp130. Importantly, the two generated models had different tilting of SEA but similar docking scores (Fig. 5A,B). Interestingly, when superimposing the two models with the available gp130-LIF complex structure (PDB ID: 1PVH), model 1 and LIF would sterically clash, while model 2 would allow SEA and LIF to bind gp130 simultaneously (Fig. 6A,B). Thus, we used SPR to determine whether LIF and SEA compete for binding to gp130. Human gp130 was immobilized and single injections of SEA and LIF or combined injection with the same concentrations were performed. As the combined level was exactly the sum of the two single injections (Fig. 6C and Table S2), we conclude that SEA and LIF can bind to gp130 simultaneously and thus do not compete for the same binding site. Consequently, model 2 (Fig. 5B) is more likely to represent the binding mode of SEA and gp130. The Zn coordination of the final gp130 and SEA model involves His145 at the D2 domain of gp130 to coordinate Zn^{2+} , together with His187, His225 and Asp227 of the C-terminal domain of SEA (Fig. 7C). The second interface between SEA and D1 (Fig. 7B) displays a hydrogen bond between Ser10_{gp130} and Gln49_{SEA} (Ser10 is not conserved in mouse/rat gp130, Fig. S4) and a π -CH interaction between Tyr8_{gp130} and the backbone of Leu48_{SEA}. In addition, the N terminus of gp130 packs against the flexible disulfide-containing loop of SEA (residues 96–106; Fig. 7A–C).

Computational alanine-scanning mutagenesis

To compare the binding modes between LIF and SEA to gp130, computational alanine scanning mutagenesis was performed using ROBETTA to estimate the $\Delta\Delta G$ value of critical residues for complex formation [23]. ROBETTA has been proven to be an outstanding prediction tool to evaluate protein–protein interactions with approximately 80% correct predictions [24]. Each residue in the interface was substituted individually to an alanine and the predicted effect of the substitution on the binding energy of the complex was calculated as $\Delta\Delta G_{\text{complex}}$ (Table 1). Hot-spot residues are defined as those alanine substitutions on gp130 having a destabilizing effect on the $\Delta\Delta G_{\text{complex}}$ of more than 1 kcal·mol^{−1}. As seen in Table 1, there are three regions in model 2 where hot-spot residues are found, the N-terminal domain (that is in close distance to the disulfide loop of SEA), Tyr8 that make a π -CH interaction with SEA and the putative Zn-coordinating residue His145 (Table 1). Interestingly, none of these residues are defined as hot-spot residues upon complex with LIF, which correlates well with the experimental data showing that LIF and SEA can bind gp130 simultaneously (Fig. 6C).

Discussion

SEA is a leading causative toxin of staphylococcal food poisoning with rapid onset of symptoms such as nausea and violent vomiting. However, the complete molecular mechanism behind the induction of the emetic response in humans remains unclear. Here, we present the finding that the two classical superantigens, SEA and SEE, can bind to the IL-6 family signalling

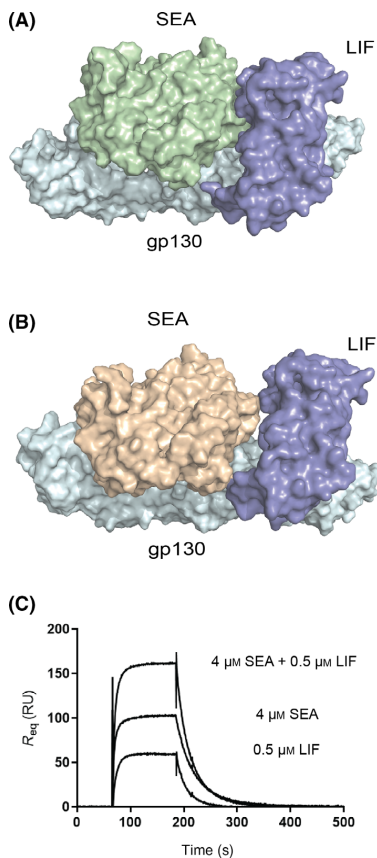


Fig. 6. SEA and LIF can bind to gp130 simultaneously. Surface representation of Model 1: SEA (green) binding to gp130 D1–D3 (cyan) superimposed onto the gp130–LIF structure, LIF shown in purple (PDB ID: 1PVH). (B) Surface representation of Model 2 of SEA (wheat) binding to gp130 D1–D3 (cyan) superimposed onto the gp130–LIF structure and LIF shown in purple (PDB ID: 1PVH). Models were created in PyMOL. (C) Surface plasmon resonance sensorgrams with immobilized human gp130-Fc and as analytes LIF (0.5 μ M), SEA (4 μ M) or LIF+SEA (0.5 μ M + 4 μ M). The response units (RU) were recorded and plotted against time (s).

receptor gp130. Interestingly, we found that SEA and SEE do not bind to mouse or rat gp130, only the human variant. From the structural model of the complex between gp130 and SEA presented here, Ser10 and His145 are both important residues for the formation of the complex. Intriguingly, none of these are conserved in rat and mouse, which could contribute to the lack of interaction (Fig. S4). Strikingly primates are the standard model for emetic assays and analysis of emetic activity and mice have no emetic response

upon ingestion of high doses of SEs. Thus, the selective SAg-gp130 interaction described here may explain the emetic activity of SEA in humans.

Gp130 is a remarkably cross-reactive signalling receptor that is activated by several four-helix cytokines termed the 'IL-6-type cytokines'. In mammals, gp130 is involved in a wide variety of critical processes, illustrated by the fact that gp130-deficient mice are embryonically lethal [25], and humans deficient in gp130 develop the lethal Stüve-Wiedemann-like disease [26]. Moreover, the preclinical mouse model for gastric cancer expresses the hyperactive gp130, (*gp130^{F/F}*) [27], and the gastric tumour burden is reduced in mast cell-deficient hyperactive gp130 tumour mice [28]. This suggests that gp130 expressed on gastric mast cells strongly contribute to tumorigenesis. Mast cells respond to extrinsic signals through a multitude of cell surface receptors which cause them to secrete histamine and proteases, for instance STAT3 is essential for immunologically mediated degranulation of human mast cells and inhibition of STAT3 results in decreased histamine secretion [29]. Along these lines, SEA has been shown to bind gp130 and to induce strong upregulation and phosphorylation of STAT3 in *in vitro* systems [30]. Moreover, SEA was recently shown to bind to submucosal mast cells in the gut and trigger degranulation and histamine release *via* an unknown receptor in callithrix jacchus (marmoset), independent of MHC class II [31]. Marmoset is a primate model that is widely used to assess the emesis-inducing activity of SEs, as SEA evokes a vomiting reflex in these animals [31]. Thus, it is tempting to speculate that the unknown SEA-receptor evoking emetic activity is gp130. The genome of marmoset is available [32], and the sequence identity with human gp130_{D1–D3} is 95%, and His145 (suggested to be the Zn-coordinating residue in the presented structural model) and Ser10 (hydrogen bonding to the N-terminal domain of SEA) are both conserved (Fig. S4). Moreover, it is well known that the residues in SEA that are crucial for T cell activation do not completely overlap with the residues that are important for the emetic activity of SEA; as Phe47 and Leu48 are important for SEA's emetic activity but their mutation does not affect T cell activity. Strikingly, these residues in SEA are positioned in close proximity to D1 of gp130 in the presented gp130-SEA complex model and contribute to the π -CH interaction (Fig. 7B). Furthermore, the highly flexible disulfide-containing loop within the N-terminal domain of SEA, which has previously been implicated to be important to stabilize a crucial conformation important for SAg-induced emetic activity [33], packs towards the N

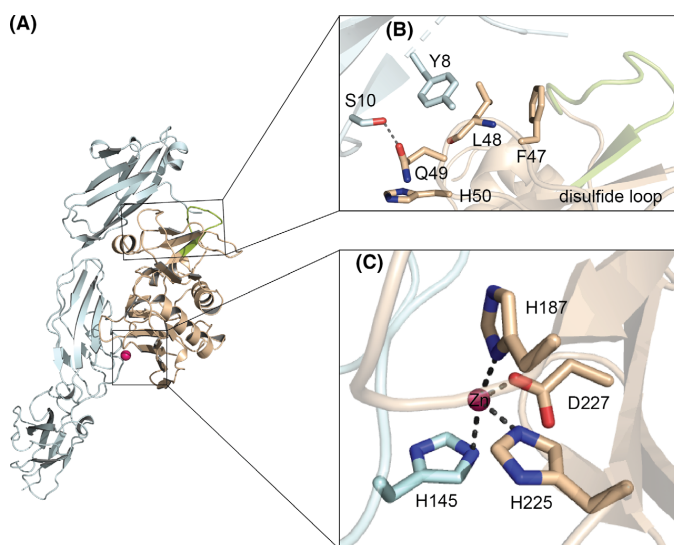


Fig. 7. SEA crosslink D1 and D2 of gp130.

(A) Cartoon representation of Model 2 with SEA (wheat) and gp130_{D1-D3} (cyan) and Zn²⁺ (magenta). (B, C) Zoom-in of gp130 D1 and D2 binding interfaces with SEA; residues at the binding sites are shown as sticks and the SEA disulfide-containing loop in green, and hydrogen bonds are marked as dotted lines.

Table 1. Residues in gp130 affected by *in silico* alanine-scanning mutagenesis.

Residue	$\Delta\Delta G_{\text{complex}}$	Residue	$\Delta\Delta G_{\text{complex}}$	Residue	$\Delta\Delta G_{\text{complex}}$
gp130-SEA (model 1)		gp130-SEA (model 2)		gp130-LIF (PDB ID: 1PVH)	
Leu2	1.01	Leu2	1.30	Glu141	1.32
Leu3	1.28	Tyr8	1.74	Trp142	1.51
His145	1.57	His145	1.94	Thr144	1.45
Asp149	2.20	Phe146	1.07	Phe169	1.85
				Asn171	1.08
				Asp193	1.43

terminus of D1 in gp130 where it could contribute to the stabilization of the complex. Moreover, upon substitution of Asp227 for alanine, SEA cannot bind gp130 and there is no emetic activity [7,34]. Taken together, this suggests that SEA may bind to gp130 on gastric mast cells, utilizing its crosslinking capability to bind both D1 and D2 and thereby contribute to the triggering of vomiting reflexes.

Another peculiarity with the SEs is that there is yet no clear answer to why *Staphylococcus aureus* harbour these toxins. Recently Noli Truant and co-workers discovered that nonclassical SAGs (such as SEG, SEI, SEM, SEO) also can bind gp130 [8]. They speculate that the physiological role of this complex formation could be that SAGs block binding of IL-6 and thereby inhibit the synthesis of IL-30, which would be beneficial for the spread of *S. aureus*. When superimposing the hexameric IL-6/IL-6 α R/gp130 complex with SEA-gp130, the binding sites SEA utilizes for gp130 would sterically block the full complex formation (Fig. S5).

Thus, it is not unlikely that SEA could inhibit the IL-6-type cytokine signalling. Along these lines, Bazedoxifene, which targets gp130, is thought to work by blocking the hexameric formation of IL-6/IL-6 α R/gp130 complex by binding to D1 of gp130 [35]. Specifically, this binding site is in close proximity to where SEA is modelled to bind gp130. Our presented structural model thus suggests that SEA could use a similar mechanism of action to Bazedoxifene, that is it inhibits the full complex formation, rather than only blocking the cytokine binding site, by utilizing a dual binding mode to both D1 and D2 of gp130 (Fig. S5).

In summary, here, we present supporting evidence that SEA binds to human gp130, but it does not bind to mouse or rat gp130. Furthermore, we present a structural model of the SEA-gp130 complex. Since the emetic reflex of SEA is not present in mice, we suggest that the binding to gp130 may contribute to the primate-specific emetic symptoms through a mechanism where SEA binds to gp130 on mast cells.

Experimental procedures

Protein expression and purification

SEA and SEH were expressed and purified as described previously with minor modifications [36]. Briefly, two plasmids (from Active Biotech Research AB, Lund, Sweden) containing a constitutive promoter, kanamycin resistance and the SEA or the SEH gene, were transformed into *Escherichia coli* K12 strain UL635. The bacteria were cultured in 2xYT media (16 g·L⁻¹ tryptone, 10 g·L⁻¹ yeast extract, 5 g·L⁻¹ NaCl) supplemented with 100 mg·L⁻¹ kanamycin, 90 mM potassium phosphate pH 7.0 and 0.5% w/v glucose. Proteins were constitutively expressed at 25 °C for 18 h. The cells were harvested by centrifugation at 6500 g at 4 °C for 15 min and subsequently flash frozen in liquid nitrogen. The samples were thawed in a cold-water bath, resuspended in 20 mM MES pH 5.5 buffer for SEA extraction (20 mM NaAc pH 4.0 for SEA extraction), supplemented with 1 mM EDTA and 0.5 mg·mL⁻¹ lysozyme and incubated on ice for 1 h with agitation. The suspension was lysed by 30 passes in a dounce homogenizer to extract the protein from the periplasm, followed by centrifugation at 20,000 g at 4 °C for 30 min to remove the cell debris. The SEA/SEH supernatant was diluted three times in 20 mM MES pH 5.5 buffer and 20 mM NaAc pH 4.0, respectively. Both protein solutions were filtered through a 0.45 µm filter and loaded onto a 6 mL Resource S column (GE Healthcare) for purification using cation exchange chromatography. SEA/SEH were purified with a linear gradient of 0–1 M NaCl. The proteins were further purified by size-exclusion chromatography (SEC) on a Superdex 75 10/300 GL column (Cytiva, Uppsala, Sweden) using HBS buffer (10 mM HEPES pH 7.4 and 150 mM NaCl) supplemented with either 0.1 mM ZnCl₂ or 0.1 mM EDTA, as running buffer. For SPR experiments, 0.005% v/v Tween-20 was added to the purified SEA and SEH proteins.

Purified SEE was a gift from Active Biotech Research AB (Lund, Sweden), which was expressed and purified according to published protocols [20]. For SPR experiments, SEE was subjected to size exclusion chromatography (Superdex 75 10/300 GL column, GE Healthcare) in HBS buffer supplemented with 0.005% v/v Tween-20.

Human gp130_{D1-D3} with a C-terminal 6xHis-tag was expressed in Sf9 insect cells. Sf9 insect cells were grown in Insect-Xpress (LONZA) media and infected with gp130 virus when reaching 3 mln·mL⁻¹. The 2L cell culture was harvested after 48–60 h of shaking at

27 °C at 110 rpm. The protein was released into the media *via* a signal peptide. The cells were spun down at 6500 g at 4 °C for 15 min. The media was concentrated *via* tangential flow filtration and the buffer was exchanged to 20 mM HEPES, 300 mM NaCl pH 7.4. Next, 20 mM imidazole was added to the protein solution and bound to Ni-NTA beads O/N at 4 °C. The protein was eluted with 300 mM imidazole and further purified with SEC on Superdex 75 10/300 GL column (GE Healthcare) using HBS pH 7.4 buffer (20 mM HEPES pH 7.4 and 150 mM NaCl). The gp130 Fc dimer (human #671-GP, mouse #468-MG and rat #5029-RG) was purchased from R&D Systems, Inc. (Minneapolis, MN, USA), which was used for all SPR experiments.

Surface plasmon resonance

Experiments were performed on a BIAcore 2000 system at 25 °C using HBS as running buffer (10 mM HEPES pH 7.4, 150 mM NaCl, 0.1 mM ZnCl₂, 0.005% v/v Tween-20). Recombinant human gp130-Fc dimer (R&D Systems) was immobilized to 780 RU of a CM5 chip (GE Healthcare) using amine-coupling chemistry. For the binding assay, a two-fold concentration series of SEA, SEE and SEH (concentrations ranged from 30 nM to 40 µM) in HBS were injected over the immobilized gp130-Fc dimer. Binding curves showing the response difference for each concentration were recorded and the background was subtracted using a blank flow channel with only running buffer. The responses at steady state were plotted against the respective SAg concentrations. Equilibrium dissociation constants (K_D) for all three SAg-gp130 complexes were determined by fitting the data in GraphPad Prism using nonlinear regression as published previously [7]. For investigation of Zn²⁺-dependent SEA and SEE binding to gp130-Fc dimer, the CM5 chip with immobilized gp130-Fc dimer (780 RU) was reused and 20 µM of SEA and SEE in HBS buffer (containing 0.1 mM ZnCl₂) was injected, followed by 20 µM SEA and SEE in HBS buffer (containing 0.1 mM EDTA). Binding curves showing the response for each SAg were recorded, and the background was subtracted using the blank flow channel. Spikes, due to buffer effects, were removed.

Human-, mouse- and rat gp130 (R&D Systems) were immobilized to 900 RU as described before, to further investigate the binding in different species. SEA and SEE were injected in a two-fold concentration series ranging from 1 to 16 µM. The K_D was calculated utilizing the Biacore evaluation software by using the curves for 1, 2 and 4 µM of SEA/SEE.

LIF was used as binding partner for gp130 for competition experiment. Gp130 was immobilized to 600 RU and LIF (0.5 μ M), SEA (1–16 μ M) and LIF (0.5 μ M) + SEA (1–16 μ M), were injected.

Chemical crosslinking mass spectrometry

Samples were crosslinked and prepared for mass spectrometric analysis as previously described [37]. Briefly, during crosslinking the protein concentration was 50 μ M and the buffer contained 50 mM HEPES pH 8, 100 mM NaCl, 10 mM DTT, 5 mM MgCl₂. SEA and gp130, or gp130_{D1–D3}, were mixed at 1 : 1 molar ratio and the BS3 (Thermo Scientific, Stockholm, Sweden) crosslinker added in different crosslinker to protein molar ratios, 10 : 1, 25 : 1 and 44 : 1. The lysine-specific crosslinker BS3 was added and after 20 min the samples were quenched by addition of a surplus of primary amine (Tris, final concentration 20 mM). The crosslinked samples were analysed by taking aliquots and performing denaturing gel electrophoresis (SDS/PAGE). Bands were excised and subjected to in-gel digestion, whereas unfractionated samples were subjected to in-solution digestion. Samples were digested with the protease AspN, with and without alkylation of cysteine residues.

Mass spectrometric data acquisition and data analysis were performed as previously described [37]. Briefly, after protease treatment the peptide mixtures were subjected to a clean-up step on 3 mm microcolumns and inspected for quality by MALDI mass spectrometry. Thereafter, peptides were subjected to reversed phase nano-LC source (Proxeon Biosystems, Odense, Denmark) coupled to an LTQ-Orbitrap Velos Pro mass spectrometer equipped with a nano Easy spray ion source (Thermo Fisher Scientific, Stockholm, Sweden). The chromatographic separation was performed on a 2 cm C18 Acclaim PepMap precolumn (75 μ m i.d.) packed with 3 μ m particle size resin and a 15 cm C18 EASY-Spray LC Capillary Separation Column (75 μ m i.d.) packed with 3 μ m particle size resin from Thermo Fisher. The gradient was created by solvent A (1% v/v acetonitrile, 0.1% v/v FA in water) and solvent B (0.1% v/v FA in 100% v/v acetonitrile). The gradient was run for 120 min with a flow rate of 300 nL·min⁻¹. An MS scan (400–1400 m/z) was recorded using an Orbitrap mass analyser set at a resolution of 60,000 at 400 m/z and one MS scan was followed by data-dependent collision-induced dissociation MS/MS scans on the four most intense ions.

After data acquisition, the raw files were processed and converted to peak lists in Mascot Generic Format (mgf-files) by MASCOT DISTILLER (version 2.3). The software MASSAI (<http://www.massai.dk/>) was used for

detection and identification of crosslinks, with the following settings: mc 2, AspN, tolerance 10 ppm MS, 0.1 Da for crosslinked peptides, tolerance 0.2 m/z in MSMS, with the following variable modifications: IAA (for alkylated samples) or internal SS (for nonalkylated samples), hydrolysed BS3 as dead end, methionine sulfoxidation, 4 allowed modifications per peptide, crosslinker BS3 and the setting 'Also Xlink peptides with variable modifications'. Variations in the settings (1–3 mc, 3–5 allowed variable modifications, and including N-deamidation as variable modification) slightly affected the sequence coverage but did not cause any major change in which crosslinks that were identified. No crosslinks were detected in the corresponding control samples with no crosslinker, using identical settings. MSMS spectra were only approved if fragments were detected from both peptides in the crosslinked pair, at least 3 fragments from each. The BS3 crosslinker can span distances up to approximately 30 Å due to lysine side chain dynamics, backbone motions, movement of flexible loops, and N- and C-terminal regions. The approved MSMS spectra are provided in the Fig. S3. The sequences used for data analyses were as follows:

SEA:

SEKSEEINEKDLRKKSELQGTALGNLQIYYY
NEKAKTENKESHDQFLQHTILFKGFFTDHSWYN
DLLVDFDSKDIVDKYKGGKVDLYGAYYGYQCA
GGTPNKATACMYGGVTLHDNNRLTEKKVPINL
WLDGKQNTVPLETVKTNKKNVTVQELDLQAR
RYLQEKYNLYNSDVFQKGVQRGLIVFHTSTEPS
VNYDLFGAQQQYSNTLLRIYRDNKTINSENMHI
DIYLYTS.

gp130_{D1–D3}:

ELLDPCGYISPESPVVQLHSNFTAVCVLKEKCM
DYFHVNANYIVWKTNHFTIPKEQYTIINRTASSV
TFTDIASLNILQTLTNILTFGQLEQNVYGITHISGLP
PEKPKNLSCIVNEGKKMRCEWDGGRETHLETN
FTLKSEWATHKFADCKAKRDTPTSTCTVDYSTVY
FVNIEVWVEAENALGKVTSDHINFDPVYKVPNP
PHNLSVINSEELSSILKLTWTNPISIKSVILKYNIQY
RTKDASTWSQIPPEDASTRSSFTVQDLKPFTEYV
FRIRCMKEDGKGYWSDWSEESAGIT.

Docking simulation between SEA and gp130

The docking of *Staphylococcal* SEA (PDB ID: 1SXT, chain A) and human gp130 (PDB ID: 1ILR, chain A) was performed using the High Ambiguity Driven protein–protein DOCKing software (HADDOCK 2.4). Prior to the docking simulations, a distance-restricted accessibility space calculation was performed to find the most likely

interacting residues within the complex using the DisVis software [38]. These residues were used in conjunction with the data obtained by crosslink mass spectroscopy to guide the docking protocol in HADDOCK 2.4. Specifically, the crosslink data were used as distance restraints and enforced throughout the entire docking process in HADDOCK (unambiguous constraints). An unbiased docking simulation was performed after generating 10,000 decoys to ensure the analysis of a large ensemble of different orientations of the two modelled proteins.

After docking, models were selected for further refinement based on the following criteria: a low energy score (~ 2% of the top energy scored models), the presence of a zinc ion at the interface between the two proteins, and a coordinating residue on gp130 close to the zinc ion. Next, the binding interface of the models was refined using the FastRelax algorithm in Rosetta [39,40] and the binding interface energy was calculated using RosettaScripts; 25 decoys were generated for each docked model. Additionally, distance constraints were also used to enforce coordination of the zinc metal ion [41].

Computational alanine scanning mutagenesis

Computational alanine scanning mutagenesis was performed on three different protein complexes, gp130-SEA (model 1), gp130-SEA (model 2) and gp130-LIF (PDB: 1PVH), using ROSETTA (<http://rosetta.bakerlab.org/alascansubmit.jsp>). The ROSETTA protocol has been previously described by Kortemme & Baker [23]. Briefly, two partners in each structure (SEA/LIF and gp130) were selected and all residues in the interface between the two partners were individually substituted to an alanine and the predicted effect on the binding energy of the protein–protein complexes were computed, to find the hot-spots for complex formation. Hot-spot residues were defined as those for which alanine substitutions have predicted destabilizing effects on $\Delta\Delta G_{\text{complex}}$ of more than or equal to Rosetta energy units (approximating 1 kcal·mol⁻¹).

Acknowledgements

We thank Active Biotech Research AB for the superantigen constructs (SEA and SEH) and for the purified SEE protein. We thank Katja Bernfur for running our mass spectrometry samples.

Author contributions

Designed the experiments: SU, AV, PR, HÅ, CE, CDB, KL-P Conducted the experiments: SU, AV, PR,

HÅ Analysed data: SU, AV, CE, CDB, KL-P Wrote the manuscript: SU, AV, CE, CDB, KL-P with contributions from all authors.

Data accessibility

The data supporting the findings of this study are available within the article and its [Supplementary Materials](#).

References

- Brouillard JN, Gunther S, Varma AK, Gryski I, Herfst CA, Rahman AK, et al. Crystal structure of the streptococcal superantigen SpeI and functional role of a novel loop domain in T cell activation by group V superantigens. *J Mol Biol.* 2007;**367**:925–34.
- Petersson K, Forsberg G, Walse B. Interplay between superantigens and immunoreceptors. *Scand J Immunol.* 2004;**59**:345–55.
- Rodstrom KE, Regenthal P, Bahl C, Ford A, Baker D, Lindkvist-Petersson K. Two common structural motifs for TCR recognition by staphylococcal enterotoxins. *Sci Rep.* 2016;**6**:25796.
- Petersson K, Thunnissen M, Forsberg G, Walse B. Crystal structure of a SEA variant in complex with MHC class II reveals the ability of SEA to crosslink MHC molecules. *Structure.* 2002;**10**:1619–26.
- Petersson K, Hakansson M, Nilsson H, Forsberg G, Svensson LA, Liljas A, et al. Crystal structure of a superantigen bound to MHC class II displays zinc and peptide dependence. *EMBO J.* 2001;**20**:3306–12.
- Rodstrom KE, Elbing K, Lindkvist-Petersson K. Structure of the superantigen staphylococcal enterotoxin B in complex with TCR and peptide-MHC demonstrates absence of TCR-peptide contacts. *J Immunol.* 2014;**193**:1998–2004.
- Banke E, Rodstrom K, Ekelund M, Dalla-Riva J, Lagerstedt JO, Nilsson S, et al. Superantigen activates the gp130 receptor on adipocytes resulting in altered adipocyte metabolism. *Metab, Clin Exp.* 2014;**63**:831–40.
- Noli Truant S, De Marzi MC, Sarrate MB, Antonoglou MB, Meo AP, Iannantuono Lopez LV, et al. egc superantigens impair monocytes/macrophages inducing cell death and inefficient activation. *Front Immunol.* 2019;**10**:3008.
- Bravo J, Heath JK. Receptor recognition by gp130 cytokines. *EMBO J.* 2000;**19**:2399–411.
- Boulanger MJ, Bankovich AJ, Kortemme T, Baker D, Garcia KC. Convergent mechanisms for recognition of divergent cytokines by the shared signaling receptor gp130. *Mol Cell.* 2003;**12**:577–89.
- Heinrich PC, Behrmann I, Muller-Newen G, Schaper F, Graeve L. Interleukin-6-type cytokine signalling

- through the gp130/Jak/STAT pathway. *Biochem J.* 1998;**334**(Pt 2):297–314.
- 12 Boulanger MJ, Chow DC, Brevnova EE, Garcia KC. Hexameric structure and assembly of the interleukin-6/IL-6 alpha-receptor/gp130 complex. *Science.* 2003;**300**:2101–4.
 - 13 Pumphrey N, Vuidepot A, Jakobsen B, Forsberg G, Walse B, Lindkvist-Petersson K. Cutting edge: evidence of direct TCR alpha-chain interaction with superantigen. *J Immunol.* 2007;**179**:2700–4.
 - 14 Thompson JD, Higgins DG, Gibson TJ. CLUSTAL W: improving the sensitivity of progressive multiple sequence alignment through sequence weighting, position-specific gap penalties and weight matrix choice. *Nucleic Acids Res.* 1994;**22**:4673–80.
 - 15 Cavallin A, Arozenius H, Kristensson K, Antonsson P, Otzen DE, Björk P, et al. The spectral and thermodynamic properties of staphylococcal enterotoxin A, E, and variants suggest that structural modifications are important to control their function. *J Biol Chem.* 2000;**275**:1665–72.
 - 16 Driessen C, Hirv K, Kirchner H, Rink L. Zinc regulates cytokine induction by superantigens and lipopolysaccharide. *Immunology.* 1995;**84**:272–7.
 - 17 Sundstrom M, Hallen D, Svensson A, Schad E, Dohlsten M, Abrahmsen L. The Co-crystal structure of staphylococcal enterotoxin type A with Zn²⁺ at 2.7 Å resolution. Implications for major histocompatibility complex class II binding. *J Biol Chem.* 1996;**271**:32212–6.
 - 18 Håkansson M, Petersson K, Nilsson H, Forsberg G, Björk P, Antonsson P, et al. The crystal structure of staphylococcal enterotoxin H: implications for binding properties to MHC class II and TcR molecules. *J Mol Biol.* 2000;**302**:527–37.
 - 19 Petersson K, Pettersson H, Skartved NJ, Walse B, Forsberg G. Staphylococcal enterotoxin H induces V alpha-specific expansion of T cells. *J Immunol.* 2003;**170**:4148–54.
 - 20 Pettersson H, Forsberg G. Staphylococcal enterotoxin H contrasts closely related enterotoxins in species reactivity. *Immunology.* 2002;**106**:71–9.
 - 21 Chow D, He X, Snow AL, Rose-John S, Garcia KC. Structure of an extracellular gp130 cytokine receptor signaling complex. *Science.* 2001;**291**:2150–5.
 - 22 van Zundert GCP, Rodrigues J, Trellet M, Schmitz C, Kastrius PL, Karaca E, et al. The HADDOCK2.2 web server: user-friendly integrative modeling of biomolecular complexes. *J Mol Biol.* 2016;**428**:720–5.
 - 23 Kortemme T, Baker D. A simple physical model for binding energy hot spots in protein-protein complexes. *Proc Natl Acad Sci USA.* 2002;**99**:14116–21.
 - 24 Kortemme T, Kim DE, Baker D. Computational alanine scanning of protein-protein interfaces. *Science's STKE.* 2004;**2004**(219):pl2.
 - 25 Yoshida K, Taga T, Saito M, Suematsu S, Kumanogoh A, Tanaka T, et al. Targeted disruption of gp130, a common signal transducer for the interleukin 6 family of cytokines, leads to myocardial and hematological disorders. *Proc Natl Acad Sci USA.* 1996;**93**:407–11.
 - 26 Chen YH, Grigelsoni G, Newton PT, Gullander J, Elfving M, Hammarsjö A, et al. Absence of GP130 cytokine receptor signaling causes extended Stuve-Wiedemann syndrome. *J Exp Med.* 2020;**217**:e20191306.
 - 27 Tebbutt NC, Giraud AS, Inglese M, Jenkins B, Waring P, Clay FJ, et al. Reciprocal regulation of gastrointestinal homeostasis by SHP2 and STAT-mediated trefoil gene activation in gp130 mutant mice. *Nat Med.* 2002;**8**:1089–97.
 - 28 Eissmann MF, Dijkstra C, Jarnicki A, Phesse T, Brunnberg J, Poh AR, et al. IL-33-mediated mast cell activation promotes gastric cancer through macrophage mobilization. *Nat Commun.* 2019;**10**:2735.
 - 29 Erlich TH, Yagil Z, Kay G, Peretz A, Migalovich-Sheikhet H, Tshori S, et al. Mitochondrial STAT3 plays a major role in IgE-antigen-mediated mast cell exocytosis. *J Allergy Clin Immunol.* 2014;**134**:460–9.
 - 30 Willerslev-Olsen A, Krejsgaard T, Lindahl LM, Litvinov IV, Fredholm S, Petersen DL, et al. Staphylococcal enterotoxin A (SEA) stimulates STAT3 activation and IL-17 expression in cutaneous T-cell lymphoma. *Blood.* 2016;**127**:1287–96.
 - 31 Ono HK, Hirose S, Narita K, Sugiyama M, Asano K, Hu DL, et al. Histamine release from intestinal mast cells induced by staphylococcal enterotoxin A (SEA) evokes vomiting reflex in common marmoset. *PLoS Pathog.* 2019;**15**:e1007803.
 - 32 Sasaki E, Suemizu H, Shimada A, Hanazawa K, Oiwa R, Kamioka M, et al. Generation of transgenic non-human primates with germline transmission. *Nature.* 2009;**459**:523–7.
 - 33 Hovde CJ, Marr JC, Hoffmann ML, Hackett SP, Chi YI, Crum KK, et al. Investigation of the role of the disulphide bond in the activity and structure of staphylococcal enterotoxin C1. *Mol Microbiol.* 1994;**13**:897–909.
 - 34 Hu DL, Omoe K, Sashinami H, Shinagawa K, Nakane A. Immunization with a nontoxic mutant of staphylococcal enterotoxin A, SEAD227A, protects against enterotoxin-induced emesis in house musk shrews. *J Infect Dis.* 2009;**199**:302–10.
 - 35 Wu X, Cao Y, Xiao H, Li C, Lin J. Bazedoxifene as a novel GP130 inhibitor for pancreatic cancer therapy. *Mol Cancer Ther.* 2016;**15**:2609–19.
 - 36 Nilsson H, Björk P, Dohlsten M, Antonsson P. Staphylococcal enterotoxin H displays unique MHC class II-binding properties. *J Immunol.* 1999;**163**:6686–93.
 - 37 Ruttsdotir G, I. Rasmussen M, Hojrup P, Bernfur K, Emanuelsson C, Söderberg CAG. Chaperone-client

- interactions between Hsp21 and client proteins monitored in solution by small angle X-ray scattering and captured by crosslinking mass spectrometry. *Proteins*. 2018;**86**:110–23.
- 38 van Zundert GC, Bonvin AM. DisVis: quantifying and visualizing accessible interaction space of distance-restrained biomolecular complexes. *Bioinformatics*. 2015;**31**:3222–4.
 - 39 Maguire JB, Haddox HK, Strickland D, Halabiya SF, Coventry B, Griffin JR, et al. Perturbing the energy landscape for improved packing during computational protein design. *Proteins*. 2021;**89**:436–49.
 - 40 Tyka MD, Keedy DA, Andre I, Dimaio F, Song Y, Richardson DC, et al. Alternate states of proteins revealed by detailed energy landscape mapping. *J Mol Biol*. 2011;**405**:607–18.
 - 41 Ireland SM, Martin ACR. ZincBind-the database of zinc binding sites. *Database (Oxford)*. 2019;**2019**: baz006.

Supporting information

Additional supporting information may be found online in the Supporting Information section at the end of the article.

Fig. S1. Gp130 mouse, rat, human are active as they bind LIF.

Fig. S2. Complex formation of gp130 and SEA detected using BS3 cross-linker.

Fig. S3. MSMS-validation of detected crosslinks.

Fig. S4. Sequence alignment of gp130 (D1–D2) in human, marmoset, mouse and rat.

Fig. S5. SEA sterically clash with IL6 when superimposed on hexameric (IL-6/IL-6 α R/gp130) structure with SEA-gp130 model.

Table S1. Summarized XL-MS data.

Table S2. RU values for SEA and SEA + LIF.

Paper IV



Structural basis for T cell receptor recognition by SARS-CoV-2 spike glycoprotein

Sibel Uzunçayır¹, Raminta Venskutonytė^{1,2}, Lotta Happonen^{3,4}, Markel Martinez Carranza¹,
James Bowman⁵, Cristopher Bahl⁵, Karin Lindkvist-Petersson^{1,2}

1. Department of Experimental Medical Science, Lund University, BMC C13, 22 184, Lund, Sweden
2. LINXS - Lund Institute of Advanced Neutron and X-ray Science, Scheelevägen 19, SE-223 70, Lund, Sweden.
3. Division of Infection Medicine, Department of Clinical Sciences, BMC, Lund University, 22184, Lund, Sweden
4. Swedish National Infrastructure for Biological Mass Spectrometry (BioMS), Lund University, Lund, Sweden
5. Institute for Protein Innovation, Boston, USA.

Abstract

The SARS-CoV-2 outbreak has been declared to be a worldwide pandemic. However, there are many unknowns about the T cell-mediated immune responses to SARS-CoV-2 infection. Interestingly, it has been reported that SARS-CoV-2 causes a skewing of the T cell repertoire in patients during infection. Analogously, bacterial toxins called superantigens are well-known to cause T cell skewing upon activation. Here we present data supporting that the spike glycoprotein of SARS-CoV-2 can act as a superantigen and bind to the T cell receptor (TCR) in a germ-line encoded manner and thus cause T cell repertoire skewing. The spike glycoprotein was found to specifically bind directly to T cell receptors expressing the TRBV7-9 sequences. In addition, cross-linking mass spectrometry in combination with initial single particle cryo-EM data suggest that the TCR interacts with the S1 domain of the spike glycoproteins, likely in between the N-terminal domain and the receptor binding domain. This extraordinary data suggests an explanation to why there are large individual differences upon SARS-CoV-2 infection, as each person has its unique germline encoded T cell profile and thus express different TRBV sequences. Still, the single particle cryo-EM data presented here needs to be further optimized to fully support the hypothesis presented.

Introduction

Severe acute respiratory syndrome coronavirus 2 (SARS-CoV-2) can cause severe interstitial pneumonia with hyperinflammation referred to as COVID-19². The characteristic feature of SARS-CoV-2 and other coronaviruses is spike glycoproteins covering the surface of the viral capsid. The spike glycoproteins are harboring the receptor binding domain (RBD) which is responsible for targeting the virus for receptors on cells, and subsequent entry to the host cell³. Angiotensin converting enzyme 2 (ACE2) serves as a spike-receptor for SARS-CoV-2 virus⁴. The spike glycoprotein forms homotrimers and undergoes substantial structural rearrangements upon cell entry⁵. Interestingly, next-generation sequencing analysis of the T cell repertoires from patients with COVID-19 indicated that severe COVID-19 was associated with a strong TCRV β (T cell receptor variable chain beta) skewing⁶, strongly resembling the outcome after exposure to bacterial superantigens. Bacterial superantigens are known to bind and activate T cells through the germline encoded parts of the TCRV β domain, resulting in upregulation of those T cells expressing TCRs that can bind to the superantigen, which results in a skewed T cell repertoire in the patient. Based on this, Cheng and co-workers suggested that the spike glycoprotein may act as a superantigen and directly bind to the T cell receptor and activate T cells⁷. More recently, an unpaired TCR repertoire analysis in 34 convalescent COVID-19 patients showed that 16 % of HLA-A2^{S269–277}-specific CD8⁺ T cells used the TRBV7-9 gene segment⁸, and along these lines, in a comparative analysis of the TCR repertoire in COVID-19 patients using single cell sequencing, the TCR combination with the highest frequency was TRAV12-2/TRBV7-9⁹. Taken together, this suggests that if the spike glycoproteins could act as superantigens, it would likely bind TCRs having TRBV7-9.

Here, we structurally and functionally investigated if there is a direct interaction between the spike glycoprotein from SARS-CoV-2 and TCRs expressing TRBV7-9. Using binding studies

utilizing surface plasmon resonance technique, we show that the spike glycoprotein binds to TCRs in a TRBV selective manner. Moreover, to investigate the details of this interaction a combination of single particle cryo-EM and cross-linking mass spectrometry was applied.

Results and discussion

The Spike Glycoprotein binds to the human T Cell Receptor

In a computational study, the spike glycoprotein was suggested to have superantigenic characteristics, based on sequence and structural similarities with the superantigen staphylococcal enterotoxin B (SEB)⁷. SEB is known to active T cells in a TRBV restrictive manner. Thus, the authors speculated that the spike glycoprotein would interact with the TCR, utilizing the TRBV, but no experimental data was presented. The latter study together with the fact that the T cell repertoire in COVID-19 patients show the highest frequency of T cells displaying TRBV7-9, as demonstrated previously provides a strong case to test if spike can interact with the TCR in TRBV7-9 specific manner⁹. In order to experimentally investigate if the spike protein can in fact directly bind to the TCR via TRBV7-9, we applied surface plasmon resonance. Human TCRs and the spike glycoprotein were expressed and purified to homogeneity judged by Coomassie stained SDS-PAGE (Fig S1 and S2). Three different TCRs were investigated displaying TRAV22/TRBV7-9, TRAV26-2/TRBV7-9 and TRAV22/TRBV11-2.

The TCRs were used as analytes (in a concentration range of 0.9-5 μM) and applied over the spike glycoprotein, which was immobilized on the SPR chip at 150 RU (Fig. 1). A clear increase in RU upon increasing concentration was observed for both TCRs displaying TRBV7-9 (Fig. 1A-B). In contrast, TCR displaying TRBV11-2 did not show an increase in RU even at the highest concentration (5 μM) (Fig. 1C). Interestingly, the TCRs displaying TRBV7-9 showed different RU value, although the amount of captured spike glycoprotein was constant, suggesting that the TRAV domain may also contribute to the binding interface (Fig. 1C). As the highest levels were detected for TRAV26-2/TRBV7-9, the data suggests that TRAV26-2 in addition to TRBV7-9 specifically contribute to the binding interface.

This is also supported by that

TRAV26 has previously been shown to be among the highest frequency TRAVs in COVID-19 patients⁹.

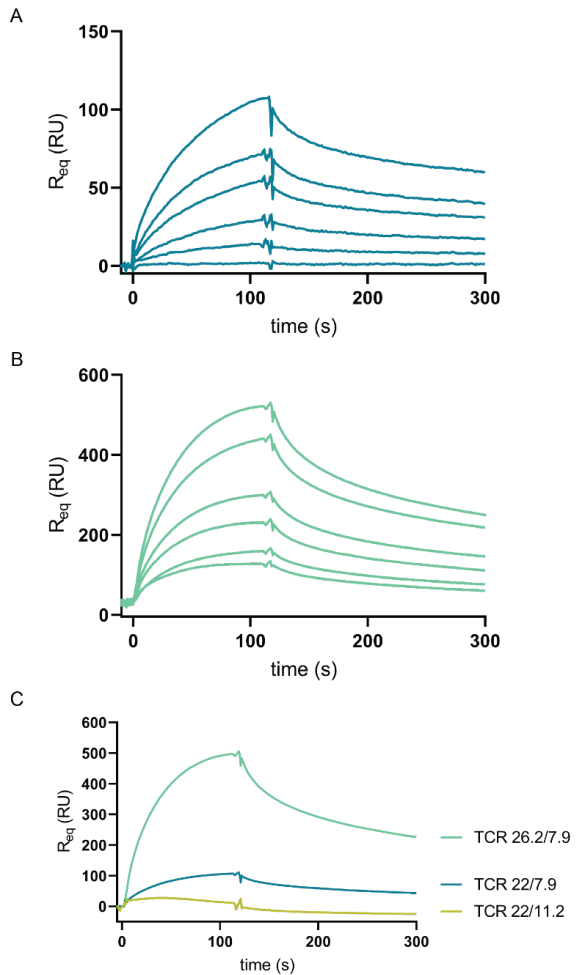


Figure 1: Binding of $\alpha\beta$ TCR and spike glycoprotein shown by surface plasmon resonance highlighting the importance of specific TCR V β chain

Surface plasmon resonance sensogram with (A) TCR 22/7-9 (0.89-5 μM) as analyte run over immobilised spike glycoprotein at 150 RU, (B) TCR 26-2/7-9 (0.89-5 μM) as analyte run over immobilised spike glycoprotein at 150 RU. (C) The highest concentration of 5 μM of 3 TCR's (TRAV22/TRBV7-9) (blue), TRAV26-2/TRBV7-9 (turquoise) and TRAV22/TRBV11-2 (yellow) as analytes run over immobilised spike glycoprotein at 150 RU.

Negative Stain Electron Microscopy of Spike Glycoprotein in Complex with TCR

The three-dimensional structure of the spike glycoprotein has previously been successfully determined with the single particle cryo-EM method to 3.5 Å resolution⁴. The spike glycoprotein forms a homotrimer and consist of two functional subunits responsible for binding to the host cell receptor (S₁ subunit, residues 14–685) and fusion with the target cell (S₂ subunit, residues 686–1273) (Fig. 2A)⁵. In the S₁ subunit, there is an N-terminal domain (NTD, 14–305 residues) and a receptor-binding domain (RBD, 319–541 residues) while the S₂ subunit harbors the fusion peptide (FP) (788–806 residues), heptapeptide repeat sequence 1 (HR1) (912–984 residues), HR2 (1163–1213 residues), TM domain (1213–1237 residues), and the cytoplasmic domain (1237–1273 residues) (Fig. 2A-B). The molecular size and structure of the spike protein makes it possible to resolve using a negative stain electron microscopy and thus we used this approach to test if a complex between the spike and the TCR could be seen. We could identify monodisperse particles, having a triangular shape, resembling that of a spike protein structure (Fig. 2C) with additional structures attached to it, which is possibly the bound TCR molecule (Fig. 2D-E). The extension is seen in close proximity to the S₁ domain of the spike glycoprotein, suggesting that the TCR binds either at the NTD or the RBD or at both domains (Fig 2). Thus, the negative stain EM data suggests that the spike glycoprotein at some instances forms a stable complex with TCR.

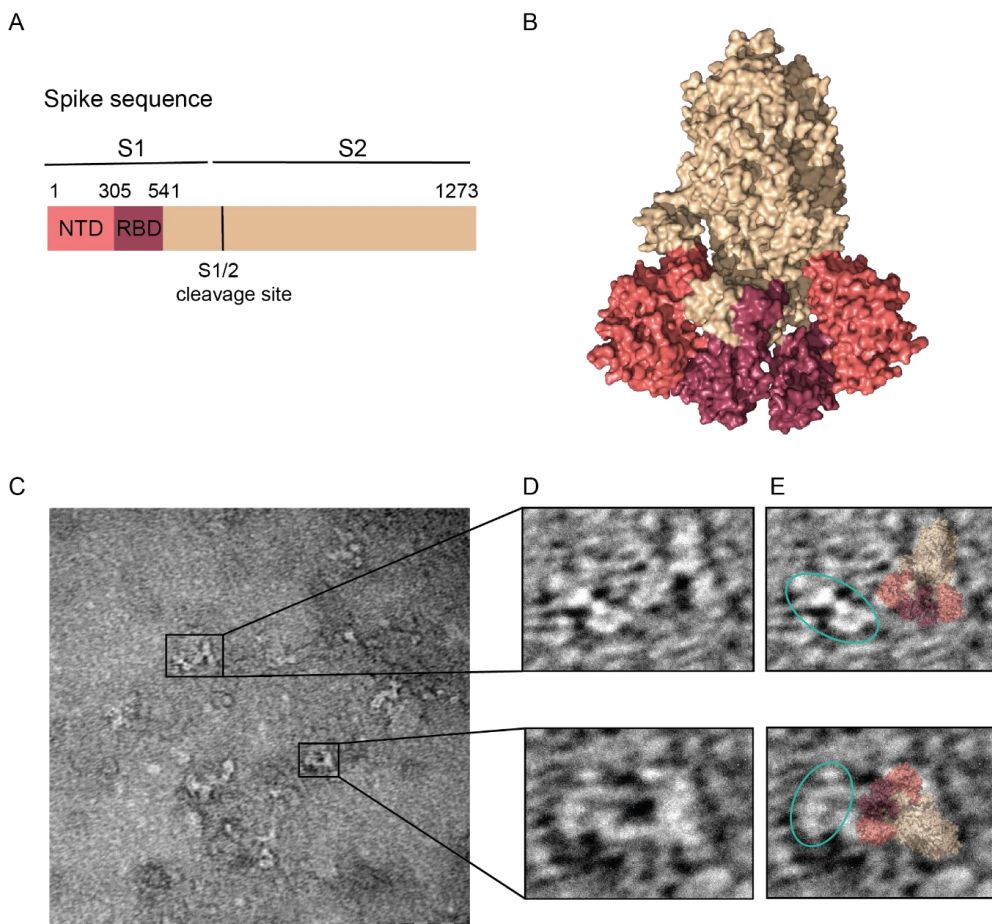


Figure 2: Negative stain showing well dispersed single particles

(A) Bar diagram of spike glycoprotein sequence highlighting NTD (salmon) and RBD (purple) domain in S1. (B) Surface presentation of spike glycoprotein (PyMOL), highlighting the NTD (salmon) and RBD (purple) domain. (C) Negative stain with TEM of spike glycoprotein and TCR (TRAV22/TRBV7-9) was mixed in 1:2 molar ratio, (D-E) zoom-in of negative stain TEM in (C). (E) Shows model of spike protein fitting shape of spike particles and visualizing a smaller particle next to it indicated in turquoise close to RBD/NTD domain.

Single Particle Cryo-EM data identifies additional Electron Density at the Spike Glycoprotein

The cryo-EM data processing resulted in clear 2D classes of well resolved spike protein (Fig 3). Subsequent Ab initio 3D reconstruction and various refinement approaches resulted in a model of 3.3 Å resolution (Fig. 3). The model of a spike protein contained extra density at the RBD/NTD, which could be a bound TCR molecule. However, the quality of the density is not good enough to conclude if that is a TCR protein at this stage and further optimizations of

sample preparation and data processing to capture a clear complex using cryo-EM are needed. Interestingly, certain attempts of Ab initio 3D reconstruction resulted in two classes – one being a spike protein and another a smaller structure, possibly free TCR, which would indicate that the ratio of spike:TCR might be further optimized to achieve an optimal sample with main particles being a complex with minimal noise. Moreover, other approaches, such as cross linking the spike and the TCR could be tried to facilitate stable complex formation on the sample grids.

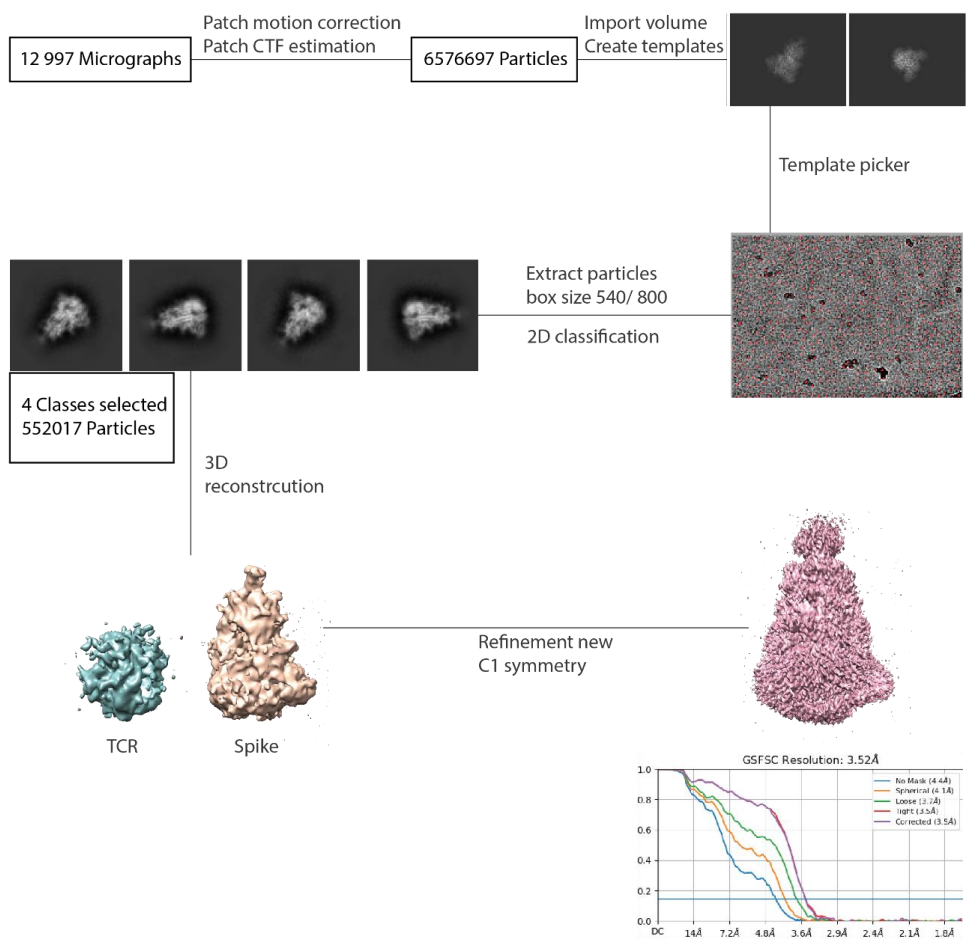


Figure 3: Single particle cryo-electron microscopy data processing workflow in cryoSPARC

Cryo-EM data processing workflow in cryoSPARC. A map of the spike glycoprotein with seemingly extra density was generated at 3.5 Å resolution.

Cross-linking Mass Spectrometry confirms the S₁ Subunit to be in close proximity of TCR

To find potential interaction sites between TRAV22/TRBV7-9 as well as TRAV26-2/TRBV7-9 and the SARS-CoV-2 spike glycoprotein, both TCRs were separately cross-linked to the spike glycoprotein using different concentrations of disuccinimidyl suberate (DSS). The cross-linked samples were either digested in solution or separated via reducing and non-reducing SDS-PAGE to enrich for complex formation (Fig. S3) with subsequent sample preparation and analysis via liquid chromatography tandem mass spectrometry (LC-MS/MS).

For TRAV22/TRBV7-9, we observe close to 2000 cross-linked spectra, the majority of which describe intramolecular cross-links (Fig. 4A, Excel Table S3). For intermolecular cross-links between TRAV22/TRBV7-9 and the spike glycoprotein, we observed 21 different cross-linked peptide pairs (Fig. 4A, Table S1) out of which 8 can be mapped onto existing models for both TRAV22/TRBV7-9 (PDB ID: 4UDT) and the spike glycoprotein (PDB ID: 6VXX) (Fig. 4C, 4E, Table S1), whereas the rest fall into regions unresolved in either PDB model. The majority of the structurally resolved interprotein cross-links map to the S₁ region of the spike glycoprotein, either in the RBD domain or in the NTD domain (Fig. 4E), and the majority of cross-linked residues from TCR maps onto the TRBV7-9 (Fig. 4C). This is in line with data derived from patient samples⁹ as well as our surface plasmon resonance data (Fig. 2) indicating that TRBV7-9 is important for spike glycoprotein interaction.

For TRAV26-2/TRBV7-9 cross-linked with the spike glycoprotein, we observe close to 800 cross-linked spectra, the majority of which describe intramolecular cross-links (Fig. 4B, Excel Table S4). The lower number of observed spectra compared to TRAV22/TRBV7-9 can in part be explained by a smaller number of samples analysed. For intermolecular cross-links between TRAV26-2/TRBV7-9 and the spike glycoprotein, we observed 6 different cross-linked peptide pairs (Fig. 4B, Table S2). Here, the structure of TRAV26-2 is not available, but on the spike

glycoprotein, the majority of these map again to the S1 domain (Fig. 4F) and to the TRBV7-9 chain (Fig. 4D). Thus, the cross-linking mass-spectrometry support the streaky density observed in the single particle cryo-EM data collection, that the spike glycoprotein and TCR interact through the S1 domain of the spike glycoprotein.

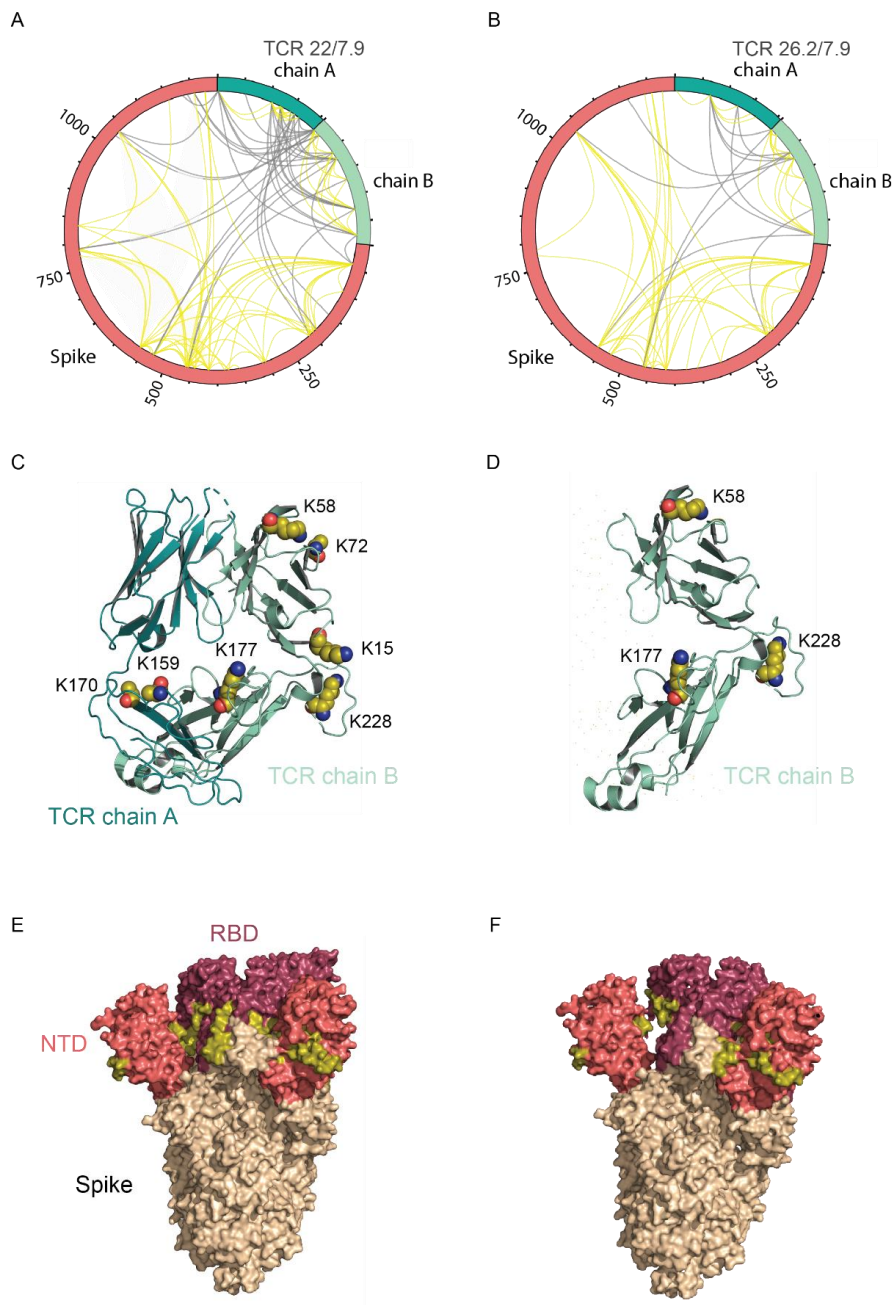


Figure 4: Cross-linking mass spectrometry identifies NTD/RBD region of spike to be important for interaction with TCR

Schematic representation of all intra (yellow)- and interprotein (grey) crosslinks identified in (A) spike glycoprotein and TRAV22/TRBV7-9 and (B) spike glycoprotein and TRAV26-2/TRBV7-9 samples. The spike glycoprotein is shown in salmon, the TRAV22/TRBV7-9 and TRAV26-2/TRBV7-9 chains A in deep teal and the chains B in green cyan. The figure was created in xVis¹. For the spike glycoprotein, locations for residues are indicated. Location of lysine residues on TRAV22/TRBV7-9 (C) and TRAV26-2/TRBV7-9 (D) central for spike glycoprotein interactions. For TRAV26-2/TRBV7-9, only chain B is shown. Surface representations of the spike glycoprotein highlighting interaction site with the TRAV22/TRBV7-9 (E) and TRAV26-2/TRBV7-9 (F) in yellow. The receptor binding domain (RBD in purple) and the N-terminal domain of the S₁ subunit (NTD in salmon) are indicated.

Conclusions

Here we present supportive evidence that the spike glycoprotein from SARS-CoV-2 forms a complex with human T cell receptors. The structural and functional analyses that was executed suggest that the spike glycoprotein binds TCR in a TRBV specific manner using its S1 domain. This specificity resembles the hallmarks of bacterial superantigens, which also binds and activates T cell in a TRBV specific manner. If SARS-CoV-2 activate T cell in a similar manner as superantigens needs to be further investigated, but the symptoms of Multisystem Inflammatory Syndrome in Children (MIS-C) caused by the SARS-CoV-2 virus share many clinical similarities with toxic shock syndrome caused by superantigens, in that both are rapidly progressive, involve multiple organ systems, and develop because of an overwhelming hyperinflammatory immune response. In addition, the fact that the symptoms of SARS-CoV-2 greatly vary on an individual basis, suggest that germline encoded parts could play an important role, supporting that the TRBV domain of TCR is involved.

Methods

Expression and Purification of Spike Glycoprotein

The used spike glycoprotein construct is the same as in Wrapp et al.⁴. Spike glycoprotein was expressed in Expi293F cells (Thermo Fisher A14527) in Exp293 expression medium (Thermo Fisher A1435101). Transfection was performed with endotoxin free DNA in Opti-MEM media (Thermo Fisher 11058021) with FectoPRO reagent (Polyplus 116-040). 500 ml flask with 250 ml at 2.8×10^6 /ml were prepared. 200 μ g DNA was added to 25 ml Opti-MEM, then 200 μ l FectoPro was added while swirling and incubated for 10 min. After 24 h 2.8×10^6 ml of 45 % glucose (Sigma G8769) and 2.8 ml of 0.3 M VPA (Sigma P4543) was added. After 72 h cells (4×10^6 viable cells/ml 40 % viability) were transfected and centrifuged at $3000 \times g$ for 15 min. The supernatant was filtered through a 0.2 μ m filter and stored at 4 °C. Then, imidazole was added to the supernatant to a final concentration of 20 mM and the supernatant was loaded (2 ml/min) onto a 5 ml HisTrap excel affinity column (GE life sciences 17371206) using Äkta system. The column was washed with a 50 ml buffer consisting of 20 mM HEPES pH 7.5, 500 mM NaCl, 20 mM imidazole and the protein was eluted with 25 ml of the same buffer but containing 400 mM imidazole. The elution fraction was concentrated in a centrifugal filter (Millipore, 50 MWCO) to a final volume of 0.8 ml and desalted using a PD10 desalting column. A final yield of 2.4 mg spike protein was obtained. Samples were frozen after adding glycerol to final concentration of 10 %.

Expression and Purification of $\alpha\beta$ -TCR

TCR was produced following published protocols¹⁰ with minor changes: *E. coli* BL21 (DE3) was used for expression and the refolding was undertaken in a buffer consisting of 100 mM Tris-HCl pH 8, 0.5 M urea, 400 mM L-arginine, 0.83 mg/l cysteamine hydrochloride and 0.73

mg/l cysteamine dihydrochloride. After refolding and dialysis, the protein was loaded on a 6 mL anion exchange Res Q column (Cytiva) and eluted with 0-400 mM NaCl over 15 CV in a linear gradient. The protein sample was concentrated and subjected to gel filtration on a Superdex 200 column (Cytiva) in a buffer containing 20 mM HEPES pH 7.4, 250 mM NaCl. A final yield of 10.4 mg TCR (22/7.9) protein was obtained. The same protocol was used for the two other TCR's (26.2/ 7.9 and 22/ 11.2). All three purified TCRs were identified with mass spectrometry.

Surface Plasmon Resonance

Surface plasmon resonance was carried out to show direct binding between the spike protein and different TCR's. The spike protein was used as a ligand by capturing it on a sensor chip while the TCR's were used as analytes by applying the different concentration solutions over the chip surface. The experiments were performed on a Biacore 3000 apparatus. For the immobilization of the His tagged spike protein, an NTA sensor chip was used (Cytiva, Sweden) and 15 µl of the 11.6 µg/ml protein solution in a running buffer of 20 mM HEPES pH 8, 150 mM NaCl, 0.01 % Tween was applied after chip preparation according to the instructions by the supplier to achieve a 150 RU of the bound protein. Then, a series of a TCR solution at concentrations of 0, 0.89, 1.25, 1.75, 2.5, 3.75 and 5 µM were applied over the chip allowing 120 s binding and 600 s dissociation time. Washing steps were performed at 20 µL/min flow rate while capture and interaction were performed at 10 µL/ min. The data was exported from the BIA evaluation software to GraphPad Prism to create sensograms (Fig. 1).

Negative Staining Electron Microscopy

To evaluate sample quality of the spike:TCR complex prior the cryo-EM experiments, negative stain EM was performed. The grids for the negative stain were prepared by applying 5 μ L of 0.02 mg/ml solution of spike:TCR at 1:2 molar ratio and incubating for 20 min. Carbon coated/ piolo term 400 mesh copper grids (Maxtaform) were used. Excess sample material was removed with blotting paper and 5 μ L of 2 % uranyl acetate staining solution was applied and incubated for 2 min followed by a washing step with 5 μ L water for 2 min. Samples were analysed with an electron microscope (TECNAI Biotwin 120 kV, FEI).

Cryo EM Sample preparation and Data Collection

Purified spike glycoprotein (1 mg/mL) and purified TCR 22/7-9 were mixed at a molar ratio of 1:1 in 20 mM HEPES, 150 mM NaCl and 0,01 % Tween. 3 μ L of the solution was deposited onto a R1.2/1.3 quantifoil grid covered with graphene oxide. Excess protein was removed by blotting for 3 seconds using vitrobot filter paper at 4 °C in 100 % humidity and then plunge frozen in liquid ethane by using a vitrobot (MarK IV, FEI). Frozen grids were screened on a Talos electron microscope and data was collected on a Titan Krios equipped with a K3 detector. Movies were collected, corresponding to a calibrated pixel size of 0.8964 Å/pixel.

Cryo EM Data Processing

The data consisting of 12997 movies was processed in cryoSPARC¹¹. After image motion correction and contrast transfer function (CTF) estimation, manual particle picking as well as blob picking functions were tried, however this did not yield any reasonable results. Instead, template picking was used. The volume of the spike protein was created in Chimera¹² using a

refined structure model (PDB ID: 6VXX) and imported into cryoSPARC to create templates. Particles were extracted with a box size of 540 and classified in 2D classes. Four 2D classes, representing a well-defined spike protein consisting of 552017 particles were selected and Ab initio 3D reconstruction was performed. The resulting model of the spike protein was then refined. Various refinement strategies have been tried including homogeneous, heterogeneous and non-uniform refinement, as well as local refinement with masking for the area at the spike protein expected to have a bound TCR. However, all the strategies tried resulted in a map of a similar quality at around 3.3-3.5Å resolution. The map was fitted to a model structure and analysed in Chimera and PyMOL.

Cross-linking Mass Spectrometry

Cross-linking was performed as previously described¹³ with some modifications. 2 µg of each TCR (TRAV22/TRBV7-9 and TRAV26-2/TRBV7-9) were separately mixed with 2 µg of spike glycoprotein and heavy/light DSS (DSS-H12/D12, Creative Molecules Inc., 001S) was added to final concentrations of 0, 0.1, 0.25, 0.5, 1.0 mM and incubated for 60 min at 25 °C, 800 rpm. The cross-linking reaction was quenched with a final concentration of 50 mM of ammonium bicarbonate for 15 min at 37 °C, 800 rpm.

Sample preparation for Mass Spectrometry

All samples for MS analysis were prepared by denaturing the proteins using an 8 M urea - 100 mM ammonium bicarbonate solution. The cysteine bonds were reduced using 5 mM Tris (2-carboxyethyl) phosphine hydrochloride (Sigma, 646547) for 60 min at 37°C, and alkylated using 10 mM 2-iodoacetamide for 30 min at 22 °C. For digestion of cross-linked samples, 1 µg of lysyl endopeptidase (Wako Chemicals, 125-05061) was added, and the

samples incubated for 2 h at 37 °C. All samples were diluted with 100 mM ammonium bicarbonate to a final urea concentration of 1.5 M, and 1 µg of sequencing grade trypsin was added for 18 h at 37 °C. The digested samples were acidified with 10 % formic acid to a pH of 3.0. Peptides were purified and desalted using C18 reverse phase columns (The Nest Group, Inc.) following the manufacturer's recommendations. Dried peptides were reconstituted in a solution containing 2 % acetonitrile and 0.1 % formic acid prior to MS analysis. The cross-linked samples were additionally separated on reducing and non-reducing SDS-PAGE, and all bands cut out and processed for MS analysis as described¹⁴.

Liquid Chromatography Mass Spectrometry

All peptides were analyzed on a Q Exactive HFX (Thermo Scientific) connected to an EASY-nLC 1200 (Thermo Scientific). The peptides were loaded onto an Acclaim PepMap 100 (ID 75µm x 2 cm, 3 µm, 100 Å) pre-column and separated on an EASY-Spray column (Thermo Scientific; ID 75 µm × 25 cm, column temperature 45 °C) operated at a constant pressure of 800 bar. A linear gradient of 4 % to 45 % acetonitrile in aqueous 0.1% formic acid was run for 50 min at a flow rate of 300 nl/min. One full MS scan (resolution 60,000@200 m/z; mass range 350 to 1600 m/z) was followed by MS/MS scans (resolution 15,000@200 m/z) of the 15 most abundant ion signals. The precursor ions were isolated with 2 m/z isolation width and fragmented using higher-energy collisional-induced dissociation (HCD) at a normalized collision energy of 30. Charge state screening was enabled, and precursors with an unknown charge state, singly charged ions as well as ions with a charge state of six or more were excluded. The dynamic exclusion window was set to 15 s and limited to 300 entries. The automatic gain control (AGC) was set to 3×10^6 for MS and 1×10^5 for MS/MS with ion accumulation times of 110 and 60 ms, respectively. The intensity threshold for precursor ion selection was set to 1.7×10^4 .

Cross-linking Data Analysis

All spectra from cross-linked samples were analysed using pLink 2 (version 2.3.9). The target protein database contained the sequence for the SARS-CoV-2 spike glycoprotein (PDB ID: 6VXX) and that for either TCR (PDB ID: 4UDT)¹⁵, respectively. pLink2 was run using default settings for conventional HCD DSS-H12/D12 cross-linking, with trypsin as the protease and up to 3 missed cleavages allowed. Peptides with a mass range of 35-8000 m/z were selected, and the precursor and fragment tolerance were set to 10 and 20 ppm, respectively. The results were filtered with a filter tolerance of 20 ppm and a 1% FDR.

References

- 1 Grimm, M., Zimniak, T., Kahraman, A. & Herzog, F. xVis: a web server for the schematic visualization and interpretation of crosslink-derived spatial restraints. *Nucleic Acids Res* **43**, W362-369, doi:10.1093/nar/gkv463 (2015).
- 2 Tay, M. Z., Poh, C. M., Renia, L., MacAry, P. A. & Ng, L. F. P. The trinity of COVID-19: immunity, inflammation and intervention. *Nat Rev Immunol* **20**, 363-374, doi:10.1038/s41577-020-0311-8 (2020).
- 3 Jackson, C. B., Farzan, M., Chen, B. & Choe, H. Mechanisms of SARS-CoV-2 entry into cells. *Nat Rev Mol Cell Biol*, doi:10.1038/s41580-021-00418-x (2021).
- 4 Wrapp, D. *et al.* Cryo-EM structure of the 2019-nCoV spike in the prefusion conformation. *Science* **367**, 1260-1263, doi:10.1126/science.abb2507 (2020).
- 5 Walls, A. C. *et al.* Structure, Function, and Antigenicity of the SARS-CoV-2 Spike Glycoprotein. *Cell* **183**, 1735, doi:10.1016/j.cell.2020.11.032 (2020).
- 6 Schultheiss, C. *et al.* Next-Generation Sequencing of T and B Cell Receptor Repertoires from COVID-19 Patients Showed Signatures Associated with Severity of Disease. *Immunity* **53**, 442-455 e444, doi:10.1016/j.immuni.2020.06.024 (2020).
- 7 Cheng, M. H. *et al.* Superantigenic character of an insert unique to SARS-CoV-2 spike supported by skewed TCR repertoire in patients with hyperinflammation. *Proceedings of the National Academy of Sciences of the United States of America* **117**, 25254-25262, doi:10.1073/pnas.2010722117 (2020).
- 8 Shomuradova, A. S. *et al.* SARS-CoV-2 Epitopes Are Recognized by a Public and Diverse Repertoire of Human T Cell Receptors. *Immunity* **53**, 1245-1257 e1245, doi:10.1016/j.immuni.2020.11.004 (2020).
- 9 Wang, P. *et al.* Comprehensive analysis of TCR repertoire in COVID-19 using single cell sequencing. *Genomics* **113**, 456-462, doi:10.1016/j.ygeno.2020.12.036 (2021).
- 10 Boulter, J. M. *et al.* Stable, soluble T-cell receptor molecules for crystallization and therapeutics. *Protein Eng* **16**, 707-711, doi:10.1093/protein/gzg087 (2003).
- 11 Punjani, A., Rubinstein, J. L., Fleet, D. J. & Brubaker, M. A. cryoSPARC: algorithms for rapid unsupervised cryo-EM structure determination. *Nat Methods* **14**, 290-296, doi:10.1038/nmeth.4169 (2017).

- 12 Pettersen, E. F. *et al.* UCSF Chimera--a visualization system for exploratory research and analysis. *J Comput Chem* **25**, 1605-1612, doi:10.1002/jcc.20084 (2004).
- 13 Hauri, S. *et al.* Rapid determination of quaternary protein structures in complex biological samples. *Nat Commun* **10**, 192, doi:10.1038/s41467-018-07986-1 (2019).
- 14 Shevchenko, A., Tomas, H., Havlis, J., Olsen, J. V. & Mann, M. In-gel digestion for mass spectrometric characterization of proteins and proteomes. *Nat Protoc* **1**, 2856-2860, doi:10.1038/nprot.2006.468 (2006).
- 15 Rödström, K. E., Regenthal, P. & Lindkvist-Petersson, K. Structure of staphylococcal enterotoxin E in complex with TCR defines the role of TCR loop positioning in superantigen recognition. *Plos one* **10**, e0131988 (2015).

Supporting information for

Structural basis for T cell receptor recognition by SARS-CoV-2 spike glycoprotein

Sibel Uzunçayır¹, Raminta Venskutonyté^{1,2}, Lotta Happonen^{3,4}, Markel Martinez Carranza¹, James Bowman⁵, Cristopher Bahl⁵, Karin Lindkvist-Petersson^{1,2}

1. Department of Experimental Medical Science, Lund University, BMC C13, 22 184, Lund, Sweden
2. LINXS - Lund Institute of Advanced Neutron and X-ray Science, Scheelevägen 19, SE-223 70, Lund, Sweden.
3. Division of Infection Medicine, Department of Clinical Sciences, BMC, Lund University, 22184, Lund, Sweden
4. Swedish National Infrastructure for Biological Mass Spectrometry (BioMS), Lund University, Lund, Sweden
5. Institute for Protein Innovation, Boston, USA.

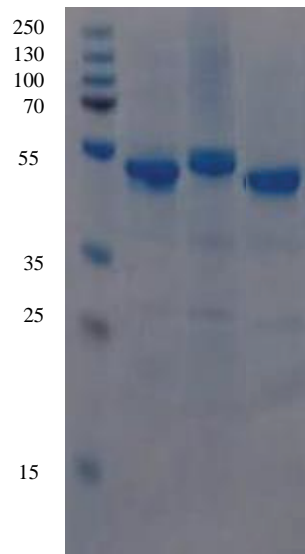


Figure S1. **Coomassie SDS-PAGE of TCR (22/7.9, 26.2/ 7.9 and 22/11.2) purification.**

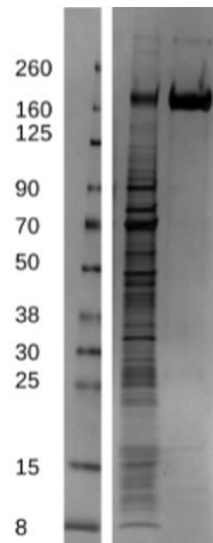


Figure S2. **Coomassie stained SDS-PAGE of spike glycoprotein purification.**

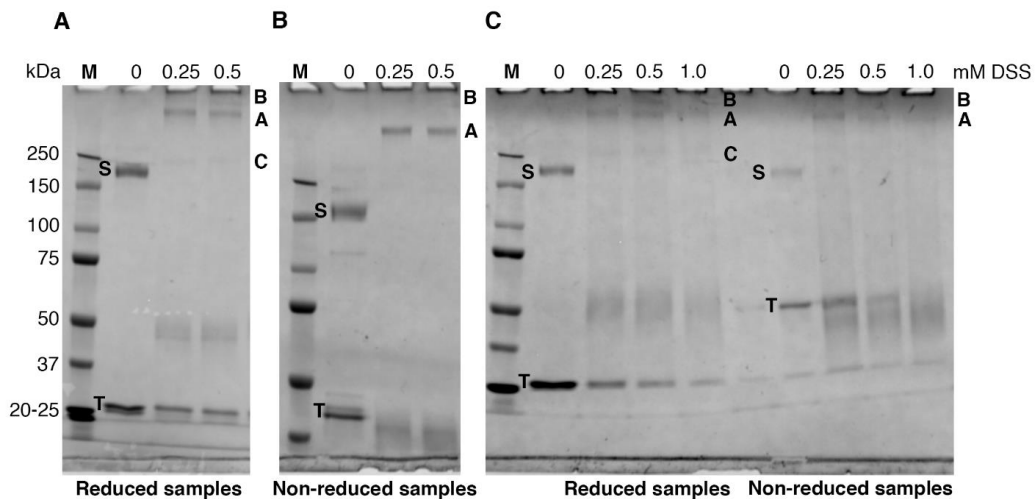


Figure S3. Coomassie stained SDS-PAGE of crosslinking spike and TCR's.

Reducing and non-reducing SDS-PAGE gels of the Spike-TCR crosslinks. (A) Reducing gel of Spike crosslinked to TCR 22/7.9; (B) Non-reducing gel of Spike crosslinked to TCR 22/7.9; and (C) Reduced and non-reduced samples of Spike crosslinked to TCR 26.2/7.9. Marker (M), Spike (S) and TCR (T) are indicated, as well as the bands excised for LS-MS/MS (A, B and C).

Table S1: **Identified cross-links between TCR 22/7.9 and spike**

Peptide	Proteins	Crosslink
AKPVTQIVSAEAWGR (2)- GYYYPDKVFR (7)	TCR_B (228)-SPIKE (41)/	TCR_SPIKE_A
DSDVYITDKCVLDMR (9)- NIDGYFKIYSK (7)	TCR_A (159)-SPIKE (202)/	TCR_SPIKE_D
DSDVYITDKCVLDMRSMDFK (9)- QIYKTPPIK (4)	TCR_A (159)-SPIKE (790)/	TCR_SPIKE_E
EFVFKNIDGYFKIYSKHTPINLVR (16)- EVHSGVCTDPQPLKEQPALNDSR (14)	SPIKE (206)-TCR_B (177)/	TCR_SPIKE_F
FSAERPKGFSFSTLEIQR (7)- GYYYPDKVFR (7)	TCR_B (72)-SPIKE (41)/	TCR_SPIKE_G
QTLGQGPEFLTYFQNEAQLEKSRLLSDR (21)- KSTNLVK (1)	TCR_B (58)-SPIKE (529)/	TCR_SPIKE_B
SMDFKSNSAWAWSNK (5)-QGNFKNLR (5)	TCR_A (170)-SPIKE (187)/	TCR_SPIKE_C
VVVLSEFLLHAPATVCGPKKSTNLVKNK (19)- ITKRGQNVTFRCDPISEHNR (3)	SPIKE (528)-TCR_B (15)/	TCR_SPIKE_H

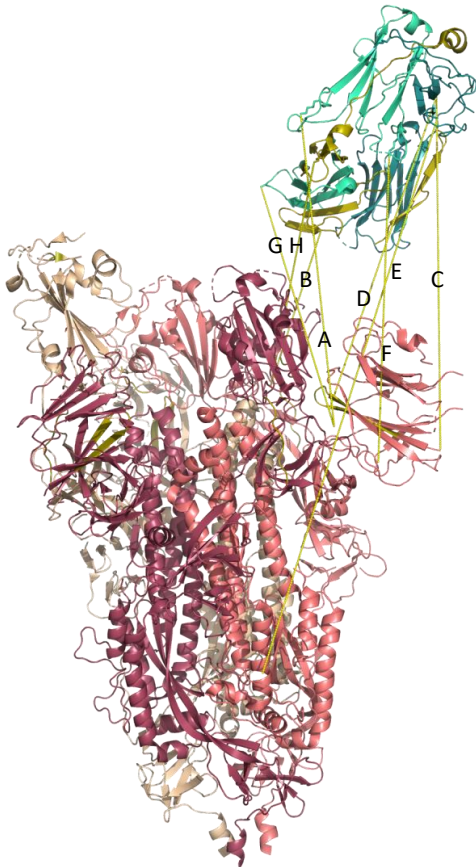


Table S2: **Identified cross-links between TCR 26.2/7.9 and spike**

Peptide	Proteins	Crosslinked peptide pair
AKPVTQIVSAEAWGR (2)- KFLPFQQFGR (1)	TCR_B (228)-SPIKE (558)/	TCR_SPIKE_C
EFVFKNIDGYFKIYSKHTPINLVR (16)- EVHSGVCTDPQPLKEQPALNDSR (14)	SPIKE (206)- TCR_B (177)/	TCR_SPIKE_A
LFRKSNLKPFER (8)- DTGVSQNPR (1)	SPIKE (462)- TCR_B (2)/	TCR_SPIKE_B
QTLGQGPEFLTYFQNEAQLEKSR (21) - MSECVLGQSKR (10)	TCR_B (58)-SPIKE (1038)/	TCR_SPIKE_D
QTLGQGPEFLTYFQNEAQLEKSRLSDR (21) - LFRKSNLKPFER (8)	TCR_B (58)-SPIKE (462)/	TCR_SPIKE_E

